PERFORMANCE ANALYSIS OF PULSATING HEAT PIPE INCORPORATED WITH TESLA TYPE D-VALVE

ANTARA MAJUMDAR
(MSc Engg., MIST)

A DISSERTATION SUBMITTED IN PARTIAL FULFILLMENT OF THE REQUIREMENTS FOR THE
MASTER OF SCIENCE IN MECHANICAL ENGINEERING

DEPARTMENT OF MECHANICAL ENGINEERING
MILITARY INSTITUTE OF SCIENCE AND TECHNOLOGY (MIST)
DHAKA, BANGLADESH

2020

CERTIFICATE OF APPROVAL

The thesis titled **"PERFORMANCE ANALYSIS OF PULSATING HEAT PIPE INCORPORATED WITH TESLA TYPE D-VALVE"** submitted by Antara Majumdar, Roll No: 1014180005, Session: October, 2014 has been accepted as satisfactory in partial fulfillment of the requirements for the Degree of Master of Science in Mechanical Engineering on 10 March, 2020.

BOARD OF EXAMINERS

1. ______________________
Lt Col Md. Faisal Kader, PhD — Chairman
Associate Professor, Department of Mechanical Engineering, — (Supervisor)
MIST (BMA Campus), Dhaka-1216, Bangladesh

2. ______________________
Dr. Dipak Kanti Das — Member
Professor, Department of Mechanical Engineering,
MIST, Dhaka-1216, Bangladesh

3. ______________________
Col Md. Humayun Kabir Bhuiyan, psc — Member
Head, Department of Mechanical Engineering, — (Ex-Officio)
MIST, Dhaka-1216, Bangladesh

4. ______________________
Dr. Mohammad Nasim Hasan — Member
Professor, Department of Mechanical Engineering, — (External)
BUET, Dhaka-1000, Bangladesh

CANDIDATE'S DECLARATION

"I hereby declare that this thesis is my original work and it has been written by me in its entirely. I have duly acknowledged all the sources of information which have been used in the thesis. The thesis (fully/partially) has not been submitted for any degree or diploma in any university or institute previously."

Signature of the Candidate

Antara Majumdar

10 March, 2020

ABSTRACT

Closed Loop Pulsating Heat Pipes (CLPHP) have emerged as a ground-breaking solution for cooling without any mechanical pumping systems for Micro sized electronics and compact packaging. The heat pipe functions on the principle of capillary effect which promotes fluid motion by interchanging liquid slugs and vapor plugs using latent and sensible heat transfer phenomenon. Incorporation of Tesla Type Valve has become the most promising option to produce larger pressure drop for the flow in reverse direction than forward which induces higher diodicity that ensures more defined fluid circulation towards a preferred direction. A special Tesla-type D-Valve design has been adopted to optimize the existing passive valve performances using methanol as working fluid. This valve has theoretically shown better diodicity mechanism against Reynolds numbers for laminar flow which leads to an increased overall heat transfer co-efficient. Moreover, it decreases minimum 15% thermal resistance than conventional heat pipes of same number of turns depending on the heat input. Although latest studies on Tesla Type D-valves were aimed at proving better diodicity and fluid circulation but limited to single turn design without having any defined mathematical correlation as a heat pipe. This thesis aims at collecting data varying different orientations and fill ratios to compare with a setup of traditional heat pipe of same turns without having any valve as well as developing empirical correlation.

ACKNOWLEDGEMENT

I would like to express my sincere gratitude to advisor *Lt Col Md. Faisal Kader, Phd, Instr Cl A*, *Department of Mechanical Engineering, Bangladesh Military Academy*, *Chattogram* for his kind supervision, guidance, encouragement and inspection throughout the entire research period.

I also express thankful gratitude to *Dr. A.J.H Frijns*, Professor, Department of Mechanical Engineering, Eindhoven University of Technology, Eindhoven, The Netherlands, who bequeathed guidelines and encouragement to her through email in this specific field of research. The author has been benefited a lot from his visionary and valuable advices at the moment of crisis of practical experiences.

I must acknowledge particular debts to laboratory employees from Bangladesh Military Academy (BMA) and Military Institute of Science and Technology (MIST) for assisting to build up the experimental setup.

I also express heartfelt gratitude to Military Institute of Science and Technology (MIST) for providing the support to complete the research.

A special appreciation goes to *SAJ Engineering and Trading Company*, who spontaneously assisted in NDT Testing of the samples.

Antara Majumdar

TABLE OF CONTENTS

NOMENCLATURE

A	Area (m^2)
a	Angle (o)
C	Chisholm parameter or constant in friction law
D	Diameter (m)
F	Convective Boiling Factor
G	Mass Flow Rate ($Kg/m^2.s$)
g	Gravitational Acceleration (m/s^2)
ID	Inner Diameter (m)
K	Thermal Conductivity (W/mK)
L	Length (m)
OD	Outer Diameter (m)
P	Pressure (Psig)
Q	Heat Input
r	Radius (m)
R	Thermal Resistance (˚C/W, K/W)
S	Suppression Factor
T	Temperature (˚C, K)
U	Shape
X	Martinelli parameter
x	Vapor mass Quality (%)

Greek Symbols

Ø	Two-phase Friction Multiplier
α	Contact Angle of Tesla Valve
β	Coefficient of Volume Expansion ($1/T_{film}$)
β	Error Band (%)
ή	Aspect Ratio
θ	Inclination Angle (Degree)
μ	Dynamic Viscosity ($N.s/m^2$)
σ	Surface Tension (N/m)
φ	Density (Kg/m^3)

Non-Dimensional Numbers

Bo	Boiling Number
B_o	Bond Number
C_O	Confinement Number
N_{CO}	Convective Number
Nu	Nusselt Number
Re	Reynold Number
We	Weber Number

Subscripts

avg	Average
ci	Condenser Inside
con	Condenser

crit	Critical
ei	Evaporator Inside
eva	Evaporator
exp	Experimental
F	Forward
fg	difference between saturated liquid and vapor
F-Z	Phase Change
g	Gaseous
i	Inner
L	Liquid
nb	Nucleate Boiling
o	Outer
php	Pulsating Heat Pipe
pred	Predicted
R	Reverse
tp	Two-Phase

Abbreviations

AC	Alternating Current
CLPHP	Closed Loop Pulsating Heat Pipe
CNC	Computerized Numerical Control
DC	Direct Current
FR	Filling Ratio
HFE	Hydrofluroether

HTC	Heat Transfer Coefficient
MAE	Mean Absolute Error
MAX	Maximum
NMP	No Moving Part
N-PHP	No Valve Pulsating Heat Pipe
OHP	Oscillating Heat Pipe
PHP	Pulsating Heat Pipe
PVC	Poly Vinyl Chloride
TV-PHP	Tesla Valve Pulsating Heat Pipe
US	United States

CHAPTER 1: INTRODUCTION

1.1 Motivation on Micro Cooling Technology

The world is advancing towards an era which is adorned by sophisticated technologies that ought to be affordable within a palm. This vision leads to a revolution of technology that integrates enormous micro and nano level electronics which have become a bulk source of heat load. As a consequence, thermal management has become a prodigious challenge to mitigate this huge demand.

1.1.1 Present status of micro cooling technology

Microprocessor data trend over 42 years including past 1970 to future 2020 has been included over several fields in the Fig. 1.1.1.1 below. The graphical representation is based on Moore's Law. The transistor density rises double each year as predicted by Moore's Law. The typical power density also follows increasing trends.

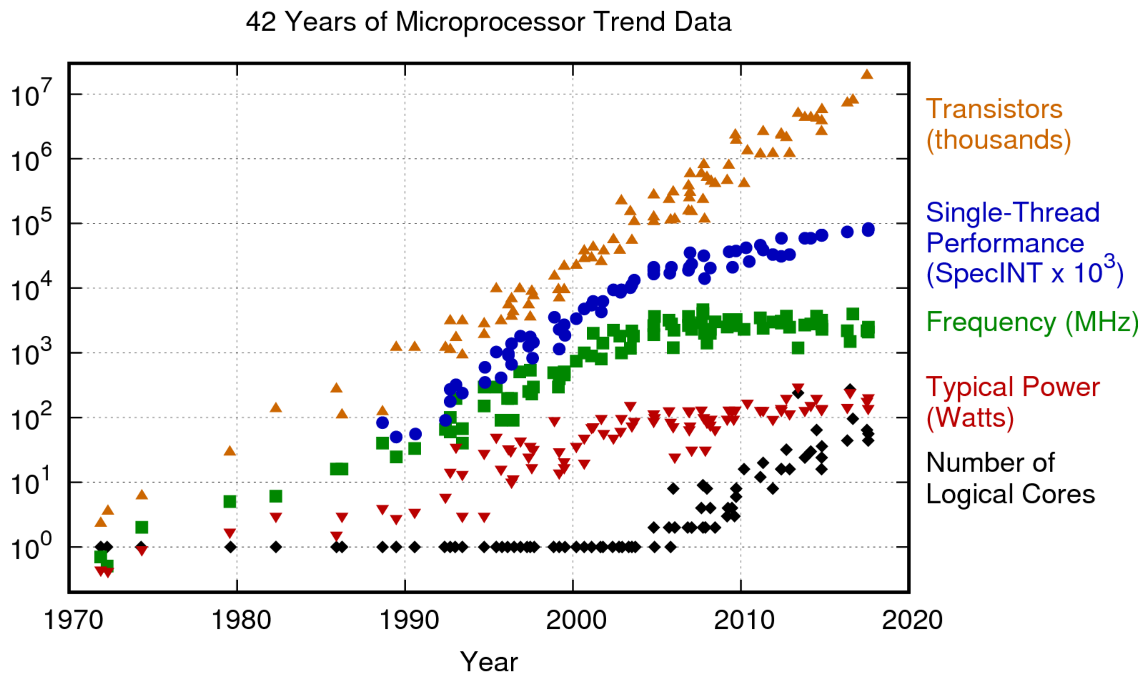

Fig.1.1.1.1: Microprocessor count over last 42 years [1]

In 2011, Patrick Gelsinger, an Intel executive, predicted that ‘unless something changed, computer chips would become hotter than nuclear reactors within a few years’[2]. The prediction is depicted in the Fig.1.1.1.2

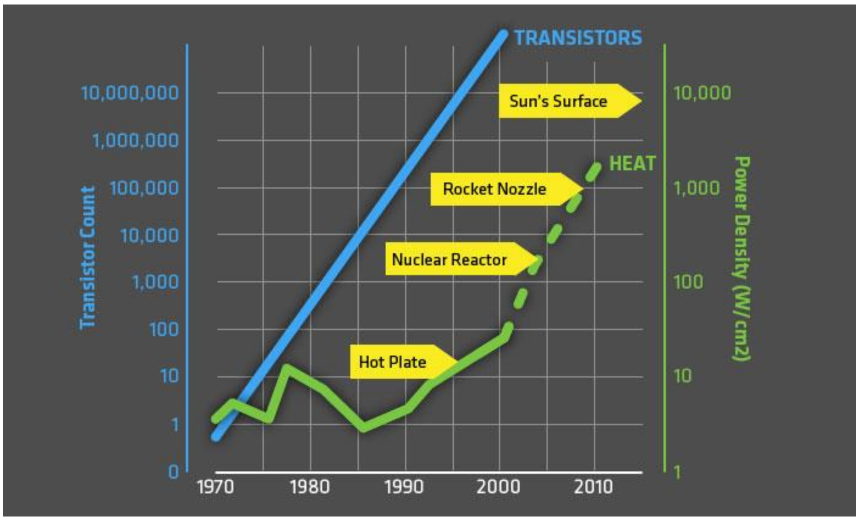

Fig.1.1.1.2: Microprocessor heat consumption illustrated by Jenna Luecke [2]

Thermal management strategies summed up by Khandekar [3] is presented below in Fig 1.1.1.3 below. It shows mainly three segments of cooling criteria of Natural Convection, Forced Convection and Phase change. Heat pipe technologies mainly falls under phase-change category.

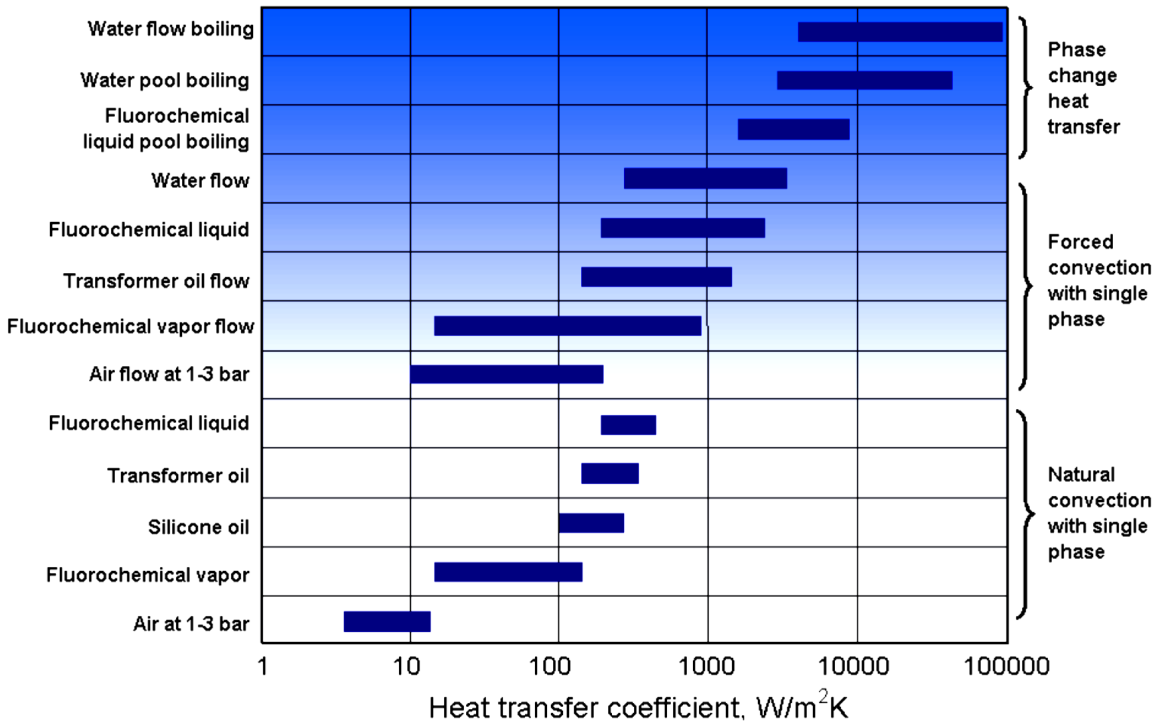

Fig.1.1.1.3: Achievable range of heat transfer coefficient by various cooling technology [3]

1.1.2 Scope of pulsating heat pipes (PHPs) on micro cooling technology

Passive heat transfer has become one of the most efficient and time demanding technology in this era. Specially cooling of microelectronics and space applications are the predominant fields. Effective use of PHPs in the field of electronic cooling for high heat input [4-5] to mobile appliances [6] have been investigated and found better thermal performances.

Space applications have become another promising field for PHP instalment. In the year 2003, Swanson [7] investigated cooling technologies feasibility specially for NASA/Goddard and NASA/JPL. They found two phase loop system as an auspicious solution for bulk heat release.

Researches on heat pipe heat exchangers using pulsating heat pipes have been conducted. They found advantages in the field of heat recovery effectiveness, compactness, light weight, complete separation of hot and liquid fluids, reliability etc. The heat exchanger is shown in the Fig. 1.1.2.1.

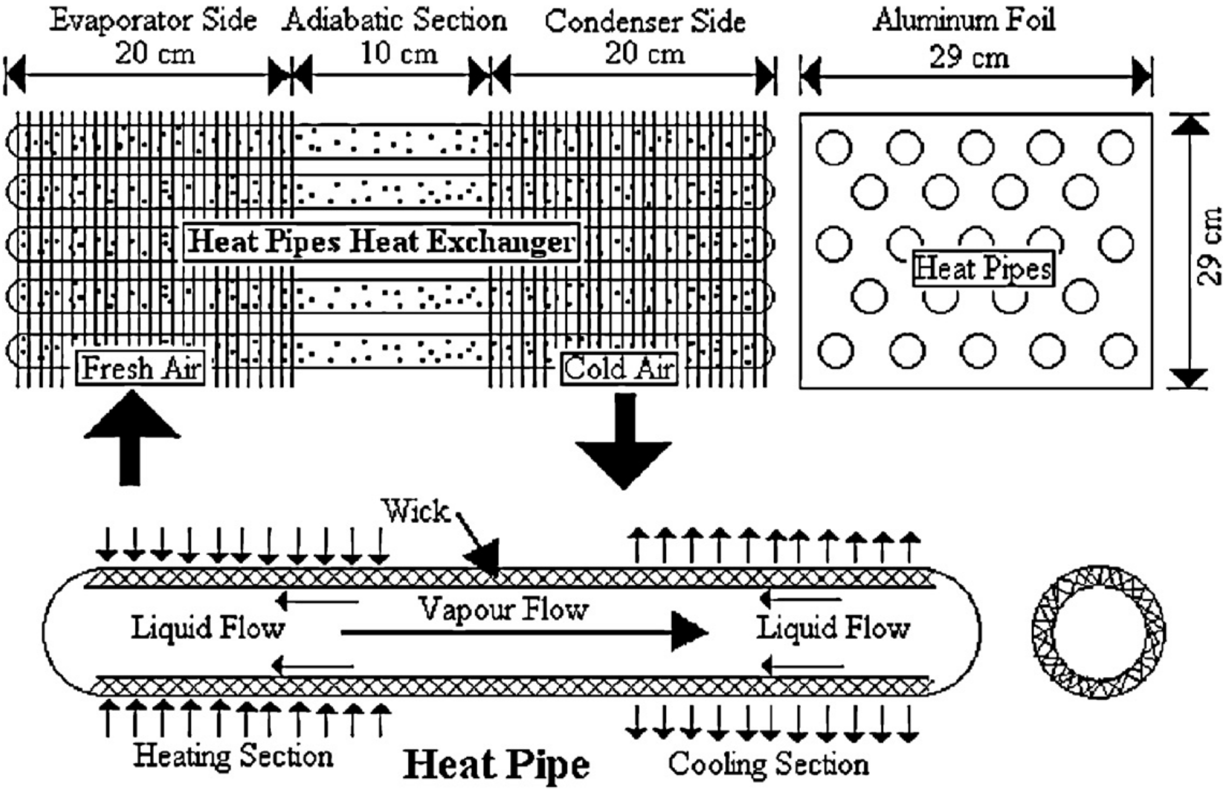

Fig.1.1.2.1: Heat recovery heat exchanger with PHP [8]

Nazari et al. [9] conducted research for finding out the usefulness of pulsating heat pipe from solar to cryogenic applications. They found PHPs as the best suitable technology for both solar and cryogenic applications. Balotaki [10] also studied over the use of PHP for photovoltaic solar panels. The research analyzes several parameters between normal solar panel with PHP incorporated solar panels. Each time they gathered better results than the traditional ones. The model is given in Fig. 1.1.2.2.

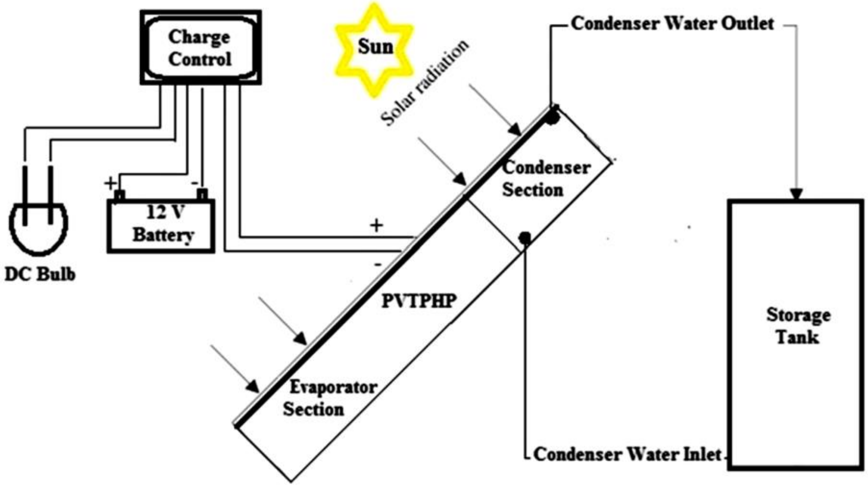

Fig.1.1.2.2: Solar collector with PHP [10]

Zuo [11-13] ran experimental studies over thermal management of automobiles for both military and civil sectors. They summarized three categories of cooling system such as heat spreader, heat transport and temperature control. Heat pipes fall under the class of heat transport and had become best suitable for space applications. Also, Burban et al. [14] presented a paper on hybrid vehicles incorporating PHP as cooling device. They found better results by changing inclination angles with four different fluids. Chi [15] developed a cooling method using closed loop pulsating heat pipe (CLPHP) for Li-Ion batteries in automobiles. The research found a lower thermal resistance for bottom cooling oscillating heat pipe using ethanol. The cooling model is shown in Fig. 1.1.2.3.

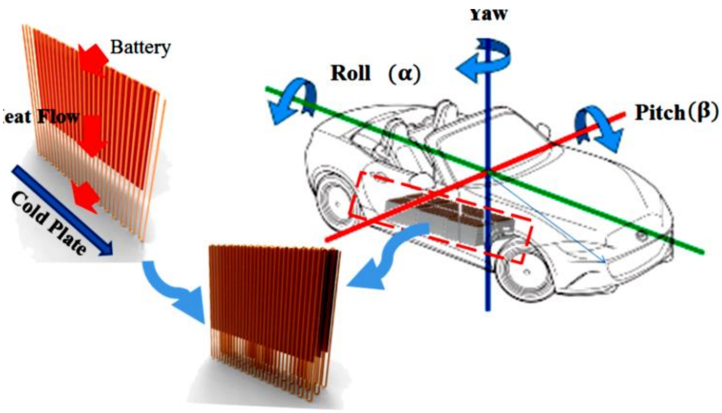

Fig.1.1.2.3: Cooling model [15]

Grinding wheels are the sectors of bulk heat production. Pulsating heat pipes are promising solution in this aspect [16]. The tube diameter of 3mm having unidirectional flow and acetone as working fluid showed the best results. This would certainly be a milestone of green energy (Fig.1.1.2.4).

Pulsating heat pipes have been also tested for cooling air conditioning units which eliminates the need of pumping system [17]. It finds the increasing of cooling effect at around 5˚C. This effort might assist for energy saving. The schematic representation is given in Fig. 1.1.2.5.

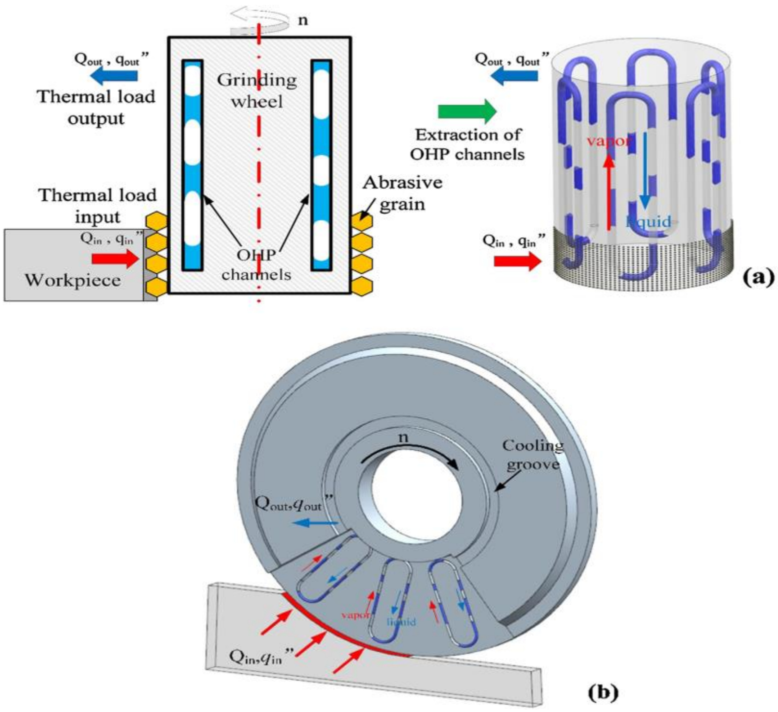

Fig.1.1.2.4: The oscillating heat pipe grinding wheel (A) Axial rotating (B) Radial rotating [16]

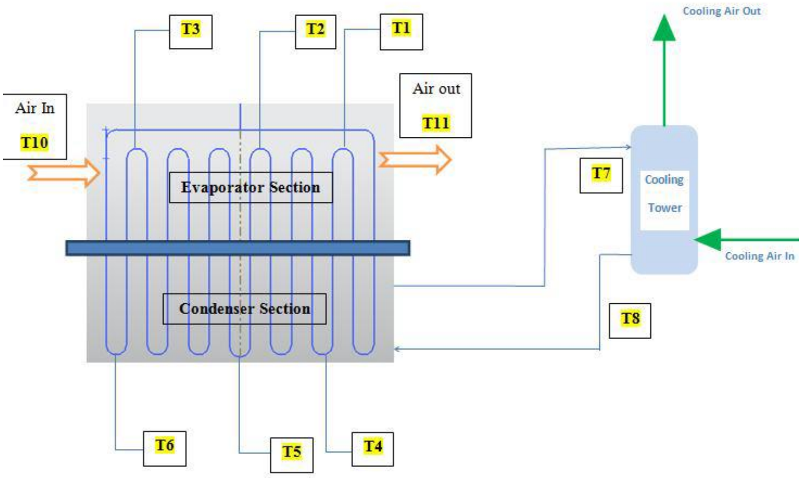

Fig.1.1.2.5: Pulsating heat pipe (PHP) incorporated air condition system [17]

1.1.3 Defense sector applications of heat pipe cooling technology

With the increase usages of electro-mechanical integrated equipment to the military devices, the heat generation has been rising at a great extent. To dissipate this heat load to the ambient, there are traditional methods as solid metal fin transformation. Connors and Zunner [18], in the year 2009, developed a model based on vapor chamber and heat pipes. They showed exemplary increase of thermal performances than the solid fin heat transfer of military embedded electronics.

In 2010, Tang et al. [19] developed a system of Loop Heat Pipe (LHP) for cooling military vehicles. They built different models based on different heat loads. The structure was mainly in-situ wick structure with passive operation. The device had high conductivity and long-distance heat transport capability. The researchers also found their device insensible to any vibration or gravitational effect of orientation.

1.2 Conventional Heat pipe

The heat pipe technology was first patented by Gaugler [20] in the year 1944. The motivation was to create a cooling technology following a cycle from evaporator to condenser without any external pumping aid. Another vision was to invent a process where the working fluid can dissipate latent heat above its saturation temperature to withstand high input load. This design had wick structure inserted within capillary tubing to absorb heat from evaporator and deliver the heat to the condenser. Again, from the condenser low temperature condensate would come to the evaporator section due to capillary wick action.

1.2.1 Operating mechanism

Heat pipe is a passive heat transfer device with capillary channel wick structures inside loops. These devices have been proven as high thermal conductive devices with two phase flow heat transfer. The working fluid takes heat away from the evaporator and delivers to the condenser through wicks instead of any external pump. After releasing heat at condenser. The condensed working fluid is getting back to the evaporator and continues the cycle repeatedly. The cross section of a heat pipe and heat transfer cycle are depicted in the Fig. 1.2.1.1 and Fig 1.2.1.2.

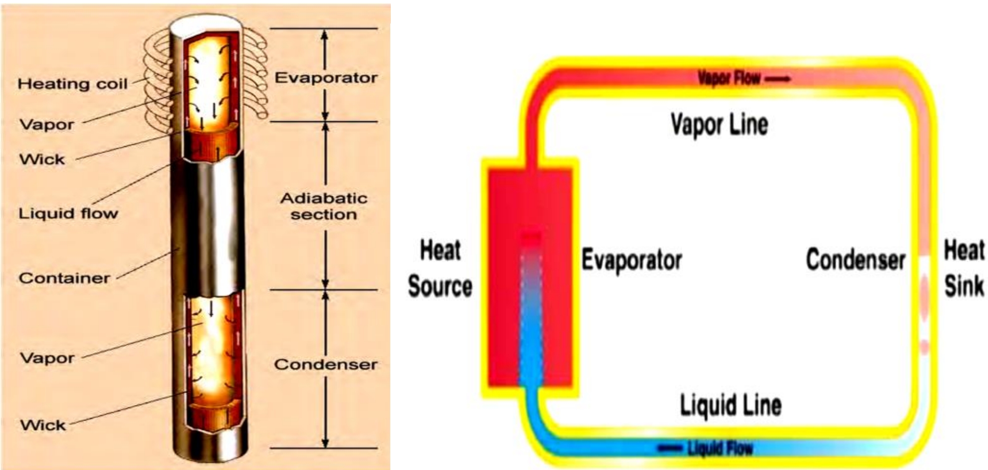

Fig.1.2.1.1: Inside construction and operating mechanism of heat pipe [3]

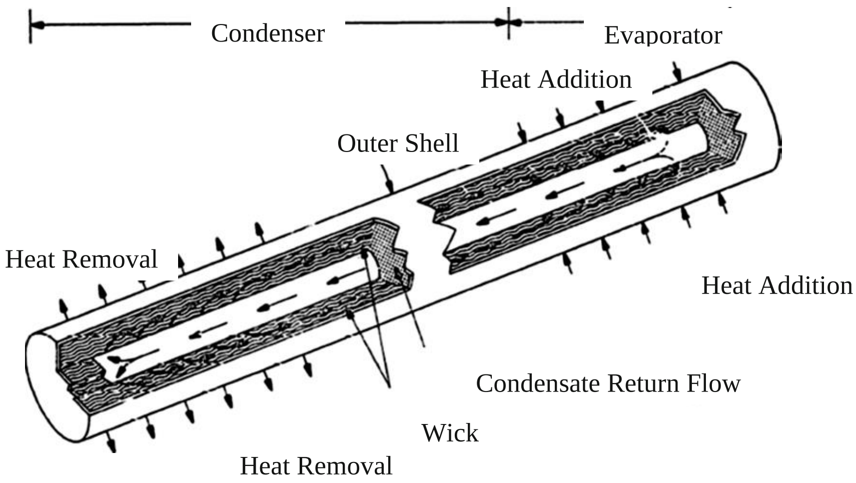

Fig.1.2.1.2: Parts and functions of basic heat pipe [21]

Different types of heat pipes are available [22] as two-phase closed thermosyphon, capillary driven heat pipe, annular heat pipe, vapor chamber, rotating heat pipe, gas-loaded heat pipe, loop heat pipe, capillary pump looped heat pipe, pulsating heat pipe, micro and miniature heat pipe, inverted meniscus heat pipe etc.

The capillary wick structures may be of different forms such as sintered powdered metal, wire screen mesh, groove tube, fiber or spring etc. The wick structures are selected depending on orientation, working fluid properties etc.

1.2.2 Limitations of conventional heat pipe

i. Complicated manufacturing process of wick structure.
ii. Complexity in construction and repair.
iii. Sizes are bigger to suit micro structures.

1.3 Pulsating Heat Pipe (PHP)

Pulsating Heat pipes are specially featured heat pipes which were developed to eliminate the limitations of traditional heat pipes. According to the connotation by Khandekar [3], pulsating heat pipes are non-equilibrium heat transfer devices driven by complex combination of various types of two-phase flow instabilities. This device operates using latent and sensible heat combinations.

1.3.1 Operating mechanism

This partially filled heat pipes are having no wick structures to transfer the working fluid from evaporator to condenser. The pulsation mechanism is fully thermally driven capillary action due to the fluctuation of pressure. To maintain this capillary action, the tube diameter is optimized by a critical value. The critical Bond number is used to define the critical diameter (D_{crit}). The Bond number is the ratio of surface tension and gravity forces and defined as follows,

$$(B_0)^2_{crit} \approx \frac{D^2_{crit} \times g \times (\rho_l - \rho_v)}{\sigma}$$

A theoretical maximum tolerable inner diameter, D_{max}, of a PHP capillary tube was derived based on the balance of capillary and gravity forces by Polasek [23]

$$D_{max} = D_{crit} = 2 \times \sqrt{\frac{\sigma}{g \times (\rho_l - \rho_v)}}$$

where σ, g, and ρ are surface tension, gravitational acceleration, and density, respectively. As the PHP tube diameter increases beyond the D_{max}, ($D >> D_{max}$ or $D \geq D_{max}$) the surface tension is reduced and all the working fluid will tend to stratify by gravity and the heat pipe will stop functioning as a PHP, and the device may operate as an interconnected array of two- phase thermo-siphons [Fig 1.3.1.1 (case A and case B)]. If $D < D_{max}$, surface tension forces tend to dominate and stable liquid slugs are formed [Fig 1.3.1.1 (case C)].

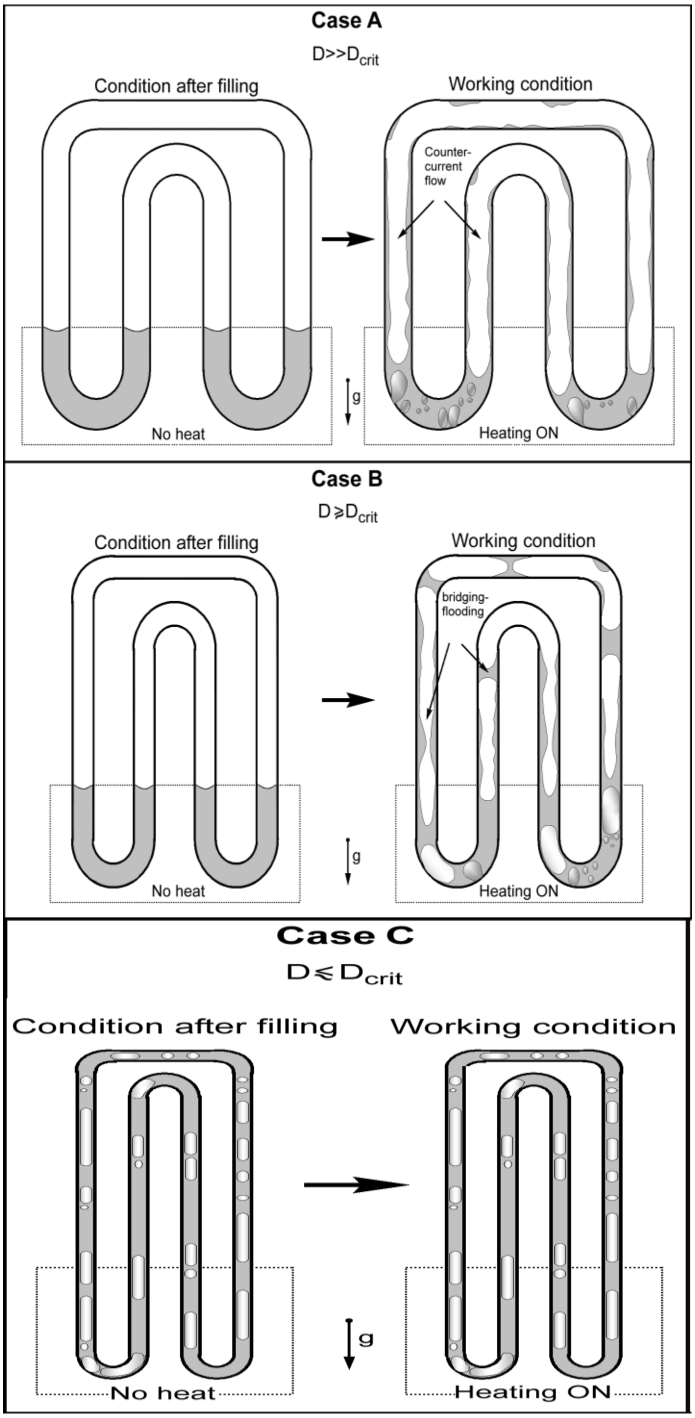

Fig. 1.3.1.1: Capillary action at optimized condition [24]

In the evaporator portion, the working fluid is absorbing heat and forming liquid slugs and vapor plugs as shown in Fig.1.3.1.2 [25]. This slug-plug mechanism caries the heat from evaporator to condenser and releases to the ambient. Internal pressure is driving this slug plug mechanism from evaporator to condenser and condenser to evaporator. This internal pressure is fully controlled by thermal instabilities which relies on the circulations of fluid inside the PHP. The flow pattern inside the PHP needs to be slug plug to annular flow for enhanced thermal performances. The transformation of flow pattern is shown in Fig. 1.3.1.3 [24]. The CLPHPs should have multiple turns to continue circulations. But there is also an optimized number of turns for a fixed condenser temperature. Because due to heat load deficiency, the internal pressure will not be sufficient to initiate circulations if there are too many numbers of turns [3].

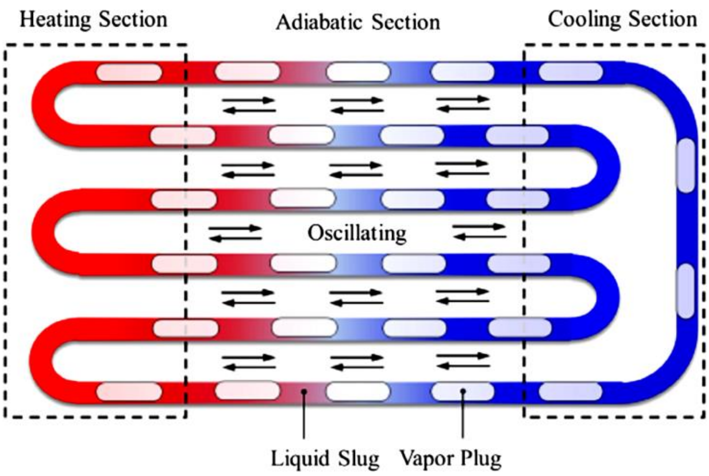

Fig. 1.3.1.2: Liquid slug and vapor plug production zones inside CLPHP [25]

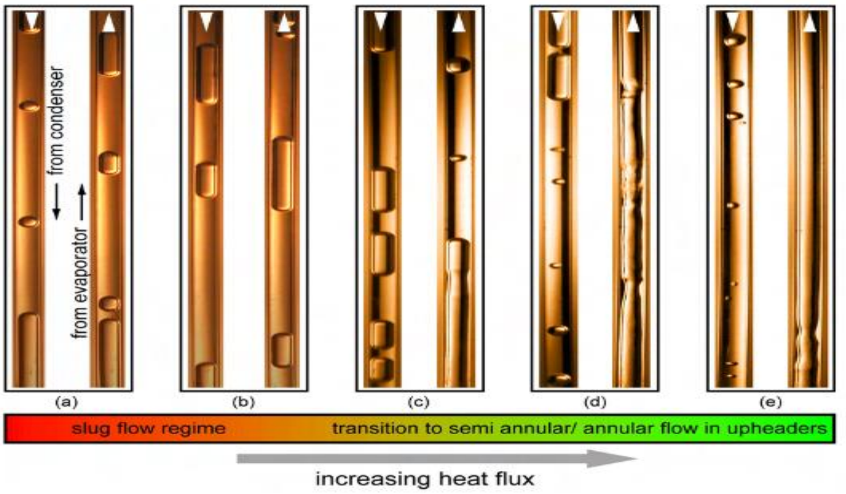

Fig. 1.3.1.3: Change of flow regimes inside a CLPHP [24]

Two types of pulsating heat pipes are available. One is Open Loop Pulsating Heat Pipe (OLPHP) and another is Closed Loop Pulsating Heat Pipes (CLPHP). OLPHPs have no connection between the starting and end point of the loop. Thus, the working fluid circulation is not same at all. This is the main difference between these two categories. Due to the closed loop and using same working fluid all over the structure, the CLPHPs are user friendly to install in a compact structure.

1.3.2 Limitations of pulsating heat pipe

i. For better thermal performances, closed loop pulsating heat pips need adequate number of turns. Thus, the size is getting increased.

ii. Due to the absence of any check valves there remains uncertainty of unidirectional flow in practical experiments.

iii. The flow should be annular for better performances. But due to the risk of burnout conditions the heat load should be deliberately below the critical value.

1.4 Tesla Type D-Valve Incorporated CLPHP

Tesla Type Valves have become the potential options among no moving part (NMP) valve designs [26-29]. This valve design is having valvular conduit with a fixed geometry that allow unidirectional flow towards a desired direction. The valve has caught attention due to the special feature called Diodicity. Mathematically Diodicity is the ratio of the reverse flow pressure drop $(\Delta P)_R$ to the forward flow pressure drop $(\Delta P)_F$.

$$D_i = \left(\frac{(\Delta P)_R}{(\Delta P)_F}\right)_Q$$

From the research of Bardell [30] this term is defined as,

‘’The figure of merit that characterizes the ability to pass flow in the forward direction while inhibiting flow in the reverse direction is the diodicity of the valve.’’

The equation of diodicity shows that, the pressure difference should be low in the destined direction than the reverse. The pressure loss is created by the inertia and viscous forces. These valves have theoretically shown better diodicity mechanism against Reynolds numbers for laminar flow [30] which leads to an increased overall heat transfer co-efficient.

Experimental and theoretical analyses on tesla type valves have been carried out both in the field of fluid mechanics and heat transfer. Among them chaotic response analysis, flow pattern analysis, flow velocity investigation, flow Restriction analysis, pressure development study, statically analysis of temperature oscillation etc. are noteworthy.

Flow restriction analysis leads to the incorporation of Tesla type valve to CLPHP. This criterion allows the maximum amount of flow in the desired direction in forward case than the reverse. Consequently D-shape Tesla Valves have been evolved for more intricate flow restriction enhancement designed by Vries at al. [31]. But there are no experimental studies available using this valve to multiturn closed loop pulsating heat pipe (CLPHP).

1.4.1 Operating mechanism

Fig 1.4.1.1 (a) shows a two-dimensional view of a Tesla type D-valve which has been collected from the research by Vries et al [31]. There is inlet, outlet, main channel, side channel, Inlet Junction (J1) and Outlet Junction (J2) in the geometry of D-valve. Tesla type D-valve enhances diodicity that ensures smaller pressure difference and elimination of flow restrictions in the promoted direction. With a view to achieving this objective, the side channel (Left side one) will have negligible fluid during forward flow while in case of reverse flow, significant amount of fluid will pass through this channel. The flow directions are shown in Fig. 1.4.1.1 (b). Theoretically around 83% flow goes through the main channel during forward flow where 56% of flow are passing through the side channel in case of reverse flow [31]. This will create more pressure differences during reverse flow than forward flow in the promoted direction which produces higher diodicity. The combination of side flow to the main channel makes more shear zone that also increases diodicity.

When the valves are assembled in a pulsating heat pipe style as shown in Fig. 1.4.1.2, it is observed unidirectionality towards clockwise (reverse) or anti-clockwise (forward) direction depending on the pressure differences. After a certain heat input to the bottom heated evaporator section, there forms liquid slugs and vapor plugs. Travelling of vapor plugs to the condenser starts circulatory motion and transfers the liquid slugs reaming in the condenser towards evaporator. If this shipment is having through right side channel of PHP then the direction is clockwise (reverse). Subsequent fast boiling in the left side of PHP forms annular flow which transports the liquid at the front part of the slug back to the condenser. This phenomenon continues until a significant bubble expansion clears the liquid slug from the evaporator. Now, whether the flow through this PHP would be clockwise (reverse) or counterclockwise (forward) will depend upon the accumulation of liquid in the channel. It is observed experimentally that, if the liquid/vapor ratio is on an average 4 in the right-side channel of PHP, accumulation of liquid is maximum in this channel. [31] This occurs clockwise (reverse) motion due to gravitational impact (as shown in Fig.1.4.1.2). Similarly, if the maximum amount of liquid is accumulated in the left side channel of PHP, counter-clockwise (forward) motion occurs. But the occurrence of counter-clockwise motion is less than reverse due to the valve diodicity. As there is less restriction in the counter-clockwise (forward) direction, significant amount of liquid accumulation occurs in the right-side channel of PHP frequently than the left. Due to gravity, the liquid transfers clock wise to the evaporator and creates reverse direction motion throughout PHP. But the velocity is almost 25% higher in counter-clockwise (forward) direction than the clock wise (reverse) direction. The circulation in the forward direction can be enhanced by decreasing the channel dimension so that diodicity-induced pressure difference can be increased over gravity induced presser difference.

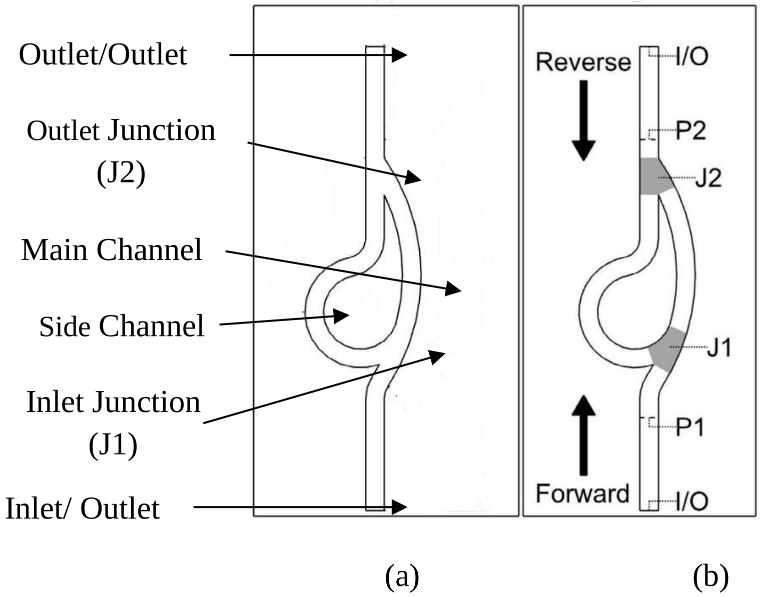

Fig. 1.4.1.1: (a) A single Tesla type D-valve with dimensions and (b) Flow direction inside a Tesla type D-valve [31]

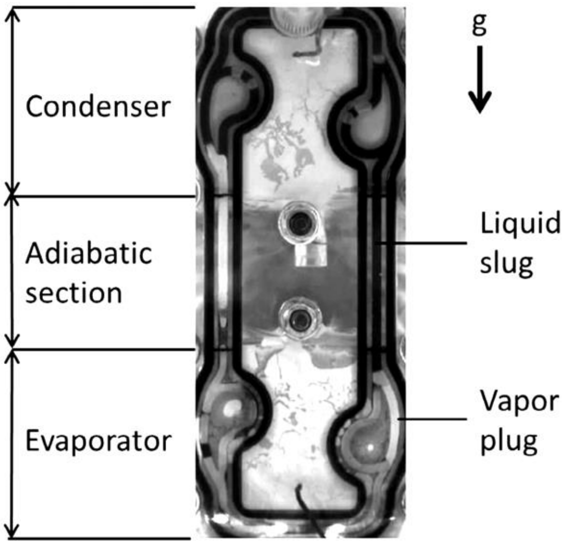

Fig. 1.4.1.2: Snapshot of clock wise circulation inside a CLPHP incorporated with Tesla type D-valve showing liquid accumulation in the right-side channel of CLPHP [31]

1.4.2 Limitations of Tesla type D-valve incorporated CLPHP

i. These researches are confined to theoretical studies.

ii. Only single turn PHP study had been carried out to visualize the flow.

iii. No specific two-phase mathematical modeling is available for the PHP application of this specially designed valve.

1.5 Present Study

Theoretically this special D-shape Tesla valve design can decrease thermal resistance at a range of 14%-25% than conventional heat pipes without having any valve of same number of turns depending on the heat input as stated by Vries et al [31]. As mentioned, there is no evidence of researches by incorporating this special valve to multiturn CLPHP structure, this research work will focus on incorporating D-shape Tesla Valve to multiturn CLPHP, collecting temperature data from evaporator, condenser and adiabatic sections and formulating empirical equations from the experimental values.

1.5.1 Prospect of present study

- A D-shape Tesla Valve incorporated CLPHP is designed for working under a wide range of heat input than the traditional heat pipes.
- Newly designed CLPHP will perform under huge pressure than the ordinary heat pipes due to more flow restrictions.
- This thesis work will focus on integrating more number for turns into the existing single turn design by Vries et al. [31] to decrease the thermal resistances.
- Additionally, this experiment will accumulate experimental data for an actual metal based multi-turn D-Valve CLPHP.
- Mathematical verification and validation can be performed from this research along with developing two phase empirical correlation using dimensionless numbers and physical parameters.

1.5.2 Objectives

1. To get higher overall heat transfer co-efficient than the conventional pulsating heat pipe of same number of turns.
2. To achieve a decrement of thermal resistance than conventional heat pipes of same number of turns.
3. To produce comparative graphs for thermal resistance and overall heat transfer co-efficient under various operational conditions (e.g. inclination angles, Fill ratios etc.).
4. To develop mathematical modelling for D-shape Tesla Valve incorporated CLPHP.

1.6 Closure

This chapter presented a compact idea about pulsating heat pipes. The inception and developments of this fields have been listed chronologically. Later, the explanation of selecting special D-shape Tesla type valves to CLPHP were provided along with specific objectives. The next section will discuss about the historical synopsis about the pulsation technology in the field of cooling.

CHAPTER 2: LITERATURE REVIEW

2.1 Historical Synopsis

Inception of pulsating heat pipes have become a revolution in the field of cooling due to its simple structure and low cost of production. The background of commercially produced pulsating heat pipes along with their chronological developments, mathematical modeling developed by researchers to express thermos-physical behavior etc. are described in the following sections. Moreover, Tesla-type valve incorporation for better performance of CLPHP and its gradual developments through ages are also noted here. Available mathematical modellings for these Tesla type valve incorporated CLPHP are provided to have idea about its behavior.

2.1.1 Pulsating heat pipes and developments

Inception of pulsating heat pipe and their further developments are listed the following paragraphs. The developments have been carried out in the field of geometry, simulation works, thermo-physical aspects etc.

<u>Patent of pulsating heat pipe</u>

in the year 1991 Hisateru Akachi [32] registered a patent on loop type pulsating heat pipe for engineering purposes. His very first patent enlisted total 24 different structures employing check valves to enhance heat transfer than the traditional heat pipes. But due to the complexity of construction and uncertain durability, in the year 1996-1997, Akachi along with other researchers developed purely capillary type pulsating heat pipe commercially known as ‘HEATLANE’ and ‘KENZAN’ fin type pulsating heat pipes [3] . The detailed photographs are provided in Fig. 2.1.1.1 (a) & (b) below.

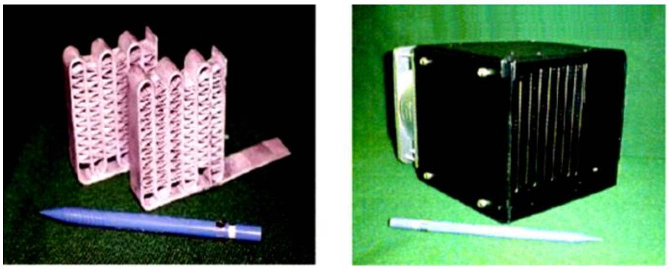

(a) HEATLANE heat pipe

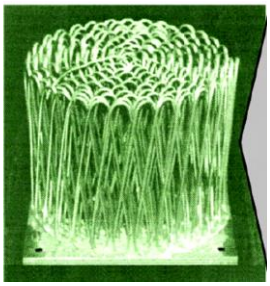

(b) KENZAN fin type heat pipe

Fig.2.1.1.1 (a) & (b): Commercially available pulsating heat pipes by Akachi [3]

<u>Variation in filling ratio and inclination angles</u>

Yang [33] investigated on 1mm and 2mm inner diameter CLPHPs and found that, 2mm inner diameter produces decreased thermal resistances than 1mm setup. Due to the enhanced capillary effect 2mm inner diameter tubes can show better performances while in vertical position. 50% filling ratio shows maximum performances for both the setups.

Varying filling ratio and inclination angles were investigated by different researches. Inclination angle gives the idea about the orientation of CLPHP structure with respect to the vertical position. Shahid et al. [34] investigated on aluminum made 3 mm uniform diameter 14 turns multiple CLPHP charged with 40%, 60% and 80% Ammonia. Individual filling ratios were examined at varying inclinations angles from horizontal to vertical. It was found that, 40% and 60% fills with 30˚ inclination would provide the best results.

Barua et al. [35] investigated over 2.2mm inner diameter CLPHP charged with Water and Methanol for different filling ratios. It could be summarized from the research that Water can be an efficient working fluid for decreased filling ratios at lower heat input. But Methanol shows higher heat transfer for all heat input for filling ratio 30% to 80%.

Jahan [36] investigated two phase behavior inside a CLPHP for varying inclination angles and found that at 70% filling ratio 75˚ inclination would give the best result.

Naik et al. [37] investigated a copper capillary CLPHP of 1.96 mm inner diameter. This research claimed that, 60% filling ratio, horizontal orientation along with acetone as a working fluid can give the best result.

Xue et al. [38] investigated using Ammonia having inner tube diameter as 2mm. the filling ratio was taken 50% having 0.02K/W thermal resistance at all orientations which shows a very high heat transfer rate.

<u>Variation in channel diameter</u>

Variations in channel diameter plays an important role for enhancing thermal efficiency of CLPHP. Chien et al. [39] ran an experiment to overcome the gravitational issue for higher heat transfer irrespective to any orientation. The research studied over two setups; one with uniform 16 channel and other with varying diameter channels of same number of tubes in total. The research found that, though the uniform diameter channel shows inclination angle depending performances, the non-uniform channel diameters can produce enhanced heat transfer at all orientation at 50% filling ratio.

Kwon et al. [40] presented a research work on varying channel diameter CLPHP and compared the result with a uniform diameter setup. The study considered glass capillary tubes 50% charged with ethanol under varying loads and inclination angles. It was found that, the asymmetric tube diameter could decrease thermal resistance up to 45% both experimentally and numerically. This happened due to the enhancement of circulatory effect. But this study recommends a range of diameter variation. Because, too large variation can cause less driving force and larger frictional losses.

Tseng et al. [41] studied over dual diameter CLPHP which shows lower thermal resistance at horizontal and vertical positions. Setup having different diameters were studied over a range of various working fluids and found that HFE-7100 produces lowest thermal resistance at lower heat input while Distilled Water can produce minimum thermal resistance at higher heat input.

Flow pattern analysis

Borkar [42] presented a research on flow pattern of a methanol charged closed loop pulsating heat pipe. The study found that, methanol can show efficient performances at a high heat load ranging from 40W to 80W.

Researchers [43-45] also investigated on CLPHP flow patterns and found that the circulation increases with the input heat load and best thermal performances could be found for annular flow patterns.

Check valve and micro grooves

Inserting ball type check valves to help the capillary action inside multi-turn PHPs have been investigated [46-47]. It was found better heat transfer but the construction of these check valves is quite difficult. that’s why these check valves had lost interest gradually. The fig. 2.1.1.2 shows the ball type check valve.

Micro groove structures inside closed loop pulsating heat pipe (CLPHP) was investigated by Qu [48], where it was found that, maximum 41.7% thermal resistances could be decreased compared to smooth tube structures. The Fig. 2.1.1.3 shows the micro grooved CLPHP structure.

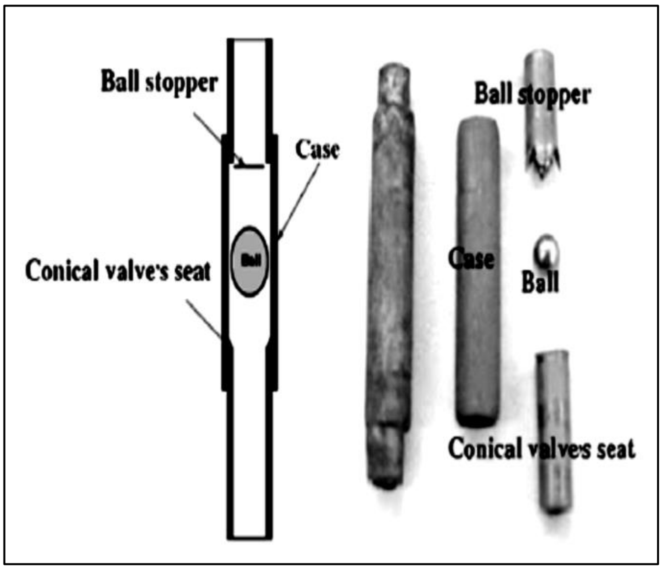

Fig.2.1.1.2: Check valves used for increased capillary action inside CLPHP [46]

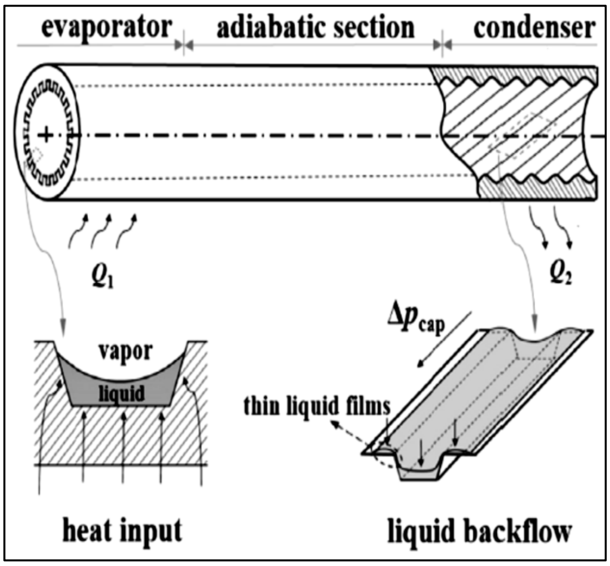

Fig.2.1.1.3: Schematic diagram of heat transfer process in a tube of the micro-grooved CLPHP [48]

<u>Micro pulsating heat pipes</u>

Yang et al. [49] investigated on micro sized pulsating heat pipes. They used Silicon as material and HFE-7100 as working fluid. The study was run for horizontal and vertical positions. For both of the positions two micro PHPs were examined. One of them was made of uniform micro channels and other was made of non-uniform micro channels. The research was to find out the pulsating oscillation behavior. It was found that, at horizontal position, the uniform micro PHP did not start up within the operating load whereas non-uniform micro channel could show oscillation after reaching at the maximum input load. But due to the advantage of gravity, both the micro PHPs showed better performances in vertical position.

<u>Numerical and simulation works</u>

Researches on computational fluid mechanics to predict numerically the thermo-hydrodynamics of pulsating heat pipes have been carried out [50-51]. Slug-plug distribution inside the capillary tubing have been simulated to predict the flow pattern inside a CLPHP. The chaotic responses [52-53] basing on different numerical correlations were studied to predict the limitations of a CLPHP in the fields of filling ratio, maximum evaporator heat input etc.

<u>Nano-fluid experiments</u>

Researchers [54-56] Studied over the use of nano-fluids as working fluid inside CLPHP. they found much increased heat transfer coefficients and lower thermal resistances than other traditional heat pipes.

2.1.2 Tesla type valve evolution

Nicola Tesla [26], developed a special type of fluid directive channel for fluid machinery. He registered the US patent in the year 1920. His primary motivation was to build a no moving part valve that would be economic, no hassle for repairing or complicated construction. The design is a channel of valvular conduit that allows fluid in a desired direction by rapid transformation of pressure and energy. In case of reverse flow, this structure can impose restrictions and turn about the surge to the forward direction by using angled restrictions. The working principle of the valve according to the patent description is as follows:

The interior of the conduit is provided with enlargements, recesses, projections, baffles, or buckets which, while offering virtually no resistance to the passage of the fluid in one direction, other than surface friction, constitute an almost impassable barrier to its flow in the opposite direction.

In the patent, it was illustrated a possible construction of valve showing eleven flow-control segments.

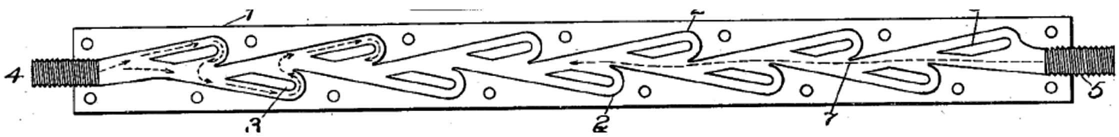

Fig.2.1.2.1: Tesla valve design by Nicola Tesla in the year 1920 [26]

2.1.3 Developments of Tesla type valves

Froster et al. [57] first incorporated Tesla Type valve for micropumps. This research shows the diodicity enhancement by comparing T45-R valve with D01-R type diffuser valve. A T45-R type Tesla valve is made up of three parts: an entrance section, a bifurcated section, and an export section. The entrance section and the export section are interchanged when the flow direction changes. The bifurcated section consists of a straight channel and an arc channel. When a fluid enters a T45-R type Tesla valve from the channel which is collinear with the straight channel of

the bifurcated section, it is called forward flow; when a fluid enters from the other end, it is called reverse flow. The D01-R type diffuser valve is etched using reactive ion etching (RIE). The geometry of the valve has been obtained from performance maps for macroscopic planar diffusers, which are based on significantly higher Reynolds numbers. It is found from the research that T45-R shows better flow restriction in the reverse direction along with lower pressure drop in the desired flow path establishes the enhanced diodicity.

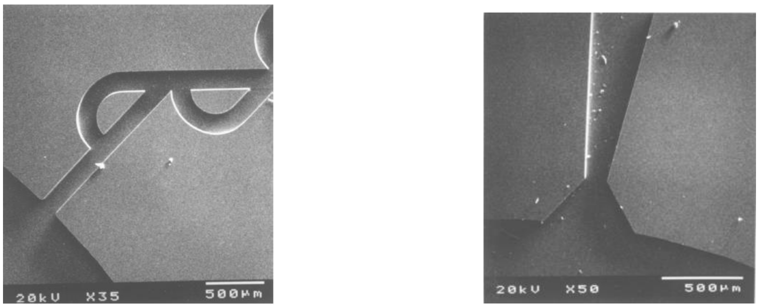

(a) (b)

Fig. 2.1.3.1: (a) Valvular conduit (T45-R) (b) Diffuser type valve (D01-R)

Bardell [30] analyzed over T45A and T45C valves for micro pumps. He also found out a process of optimum valve design. The author also applied the mechanism to rectify T45A valve and transforming it to T45A-2. Diodicity was calculated numerically by solving velocity, pressure, dissipation-rate fields, momentum and kinetic energy conservation equations into 9 regional volumes as shown in the following Fig. 2.1.3.2. T45 C valve differs from T45A by changing region 8 and 9 as shown in Fig. 2.1.3.2 (b). T45A-2 valve has been designed with much more optimization than T45A in the regions of 2,3,4,5,6,8 and 9 as depicted in Fig. 2.1.3.2 (c).

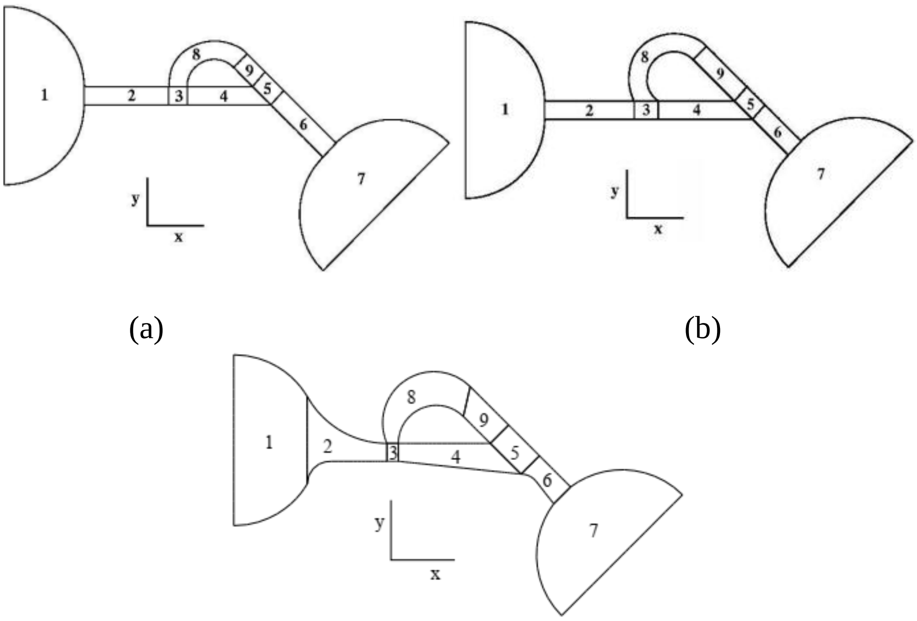

(a) (b)

(c)

Fig. 2.1.3.2: (a) Division of the T45A valve into regional control volumes (b) Division of the T45C valve into regional control volumes (c) Division of the T45A-2 valve into regional control volumes [30]

Truong and Nguyen [58] studied finding out a suitable method for optimum valve design correcting optimum angle α and optimum straight segment L of a typical Tesla type valve design (Fig. 2.1.3.3) which are inversely proportional and proportional to the Reynold number respectively.

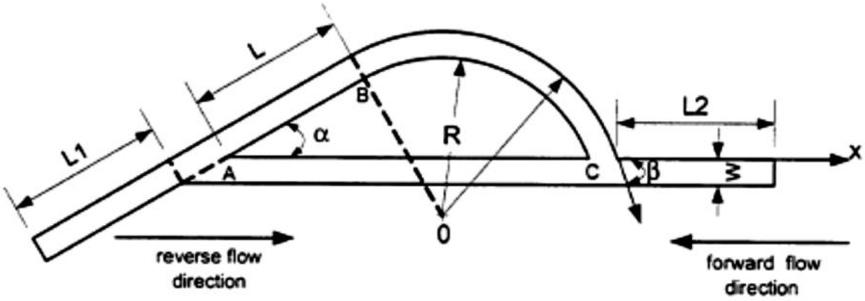

Fig. 2.1.3.3: Geometry of a typical Tesla type valve [58]

Morris et al. [59] investigated the optimization of Tesla type valve by determining optimal parameters with a low order linear model based on first principal and finding out the best valve shape for a desired Reynolds number range.

Gamboa et al. [28] tried to optimize the design used by Morris et al. The optimization was carried out over typical Tesla Valve that was termed as Tesla Valve I. Total six independent non dimensional design parameters were analyzed for valve design optimization as described in Fig. 2.1.3.4. The result shows that, 25% higher diodicity can be achieved by an average over a range of Reynolds number 0 to 2000. The motto of this research was to optimize valve shape, predicting pump resonant behavior with a linear dynamics model and developing a system optimization technique irrespective of all geometrical parameters.

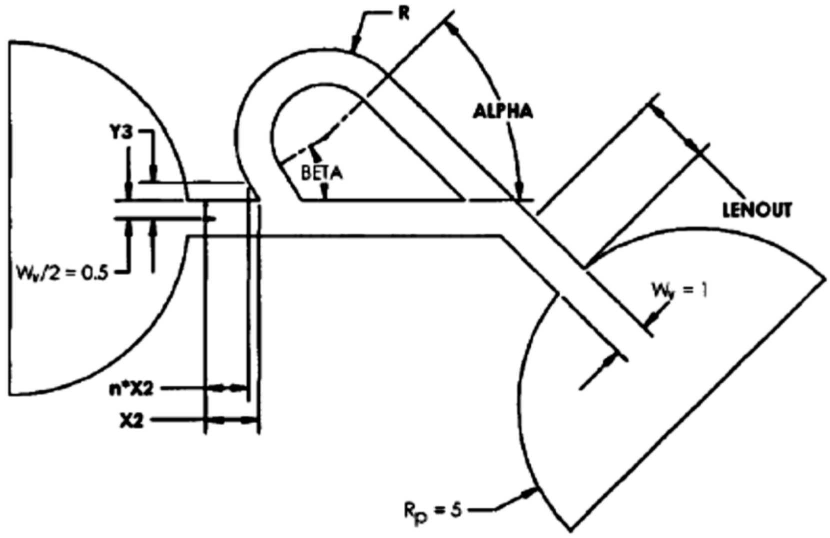

Fig. 2.1.3.4: Design variables for the Tesla-type valve: 1. the length of the inlet segment in forward flow X2, 2. scale factor n yielding the coordinate nX2, and 3. coordinate Y3 that defined the outer tangent location of the return section of the loop segment, 4. loop outer radius R, 5. outlet segment length LENOUT, and .6. outlet segment angle a [28].

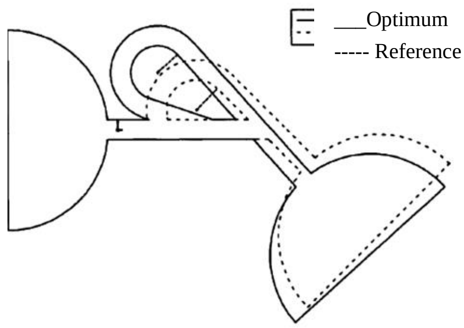

Fig. 2.1.3.5: Optimization with the Tesla type valve I [28]

Valve	X_2	n	Y_3	LENOUT	R	α	β	Average Di
Optimized	1.60	0.797	0.608	2.94	2.35	41.9°	71.7°	1.50
Reference	1.50	0.990	0.600	2.00	2.50	45.0°	8.53°	1.21

Table 2.1.3.1: Optimized and reference Tesla-type valve parameters [28]

Qian et al. [60] investigated numerically the diodicity and flow rectification over T45R valve using Al_2O_3-water nano fluid. It was found that most of the nanofluids flow into the straight channel of the bifurcated section when flowing forward, and into the arc channel when flowing reversely. This situation shows increased diodicity.

D-shape Tesla Valve has been proposed by Vries [31]. The necessity of optimization was to develop more efficient thermally efficient Tesla valve that would create enhanced diodicity than the previous designs specially T45A-2. A generic sketch is presented here to compare the geometrical reconstructions that have been made for D-shape Tesla Valve to enhance the diodicity in the following Fig 2.1.3.6.

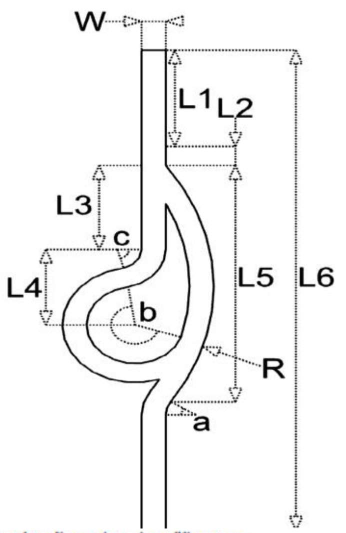

D-valve dimensions in millimetres.

Parameter	Value in mm
W	2
L1	10
L2	2
L3	8.75
L4	7.85
L5	24.65
L6	50
R	Radius 22
a	Radius 2.5 (Angle $\alpha = 33°$)
b	Radius 4 (Angle $\beta = 243.5°$)
e	Radius 2 (Angle $\epsilon = 75°$)

(a) D Valve design with dimension table [31]

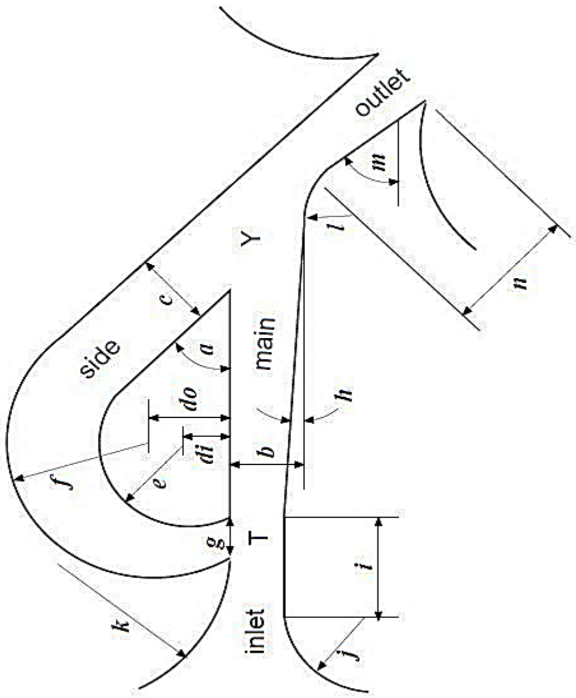

(b) Sketch of generic Tesla-type NMP valve with dimensioning per design rules for high diodicity [30]

Fig. 2.1.3.6 (a) & (b): Geometrical comparison of D-shape Tesla type valve with generic Tesla valve

The developments in the regular design of Tesla valve by Vries et al. [31] for optimized design of D-shape are provided herewith.

1. Angle between main and side channel

- T45A-2 design [30] suggests that, by increasing the angle **α** between the main and side channel the flow can be delivered at a large scale through the side channel. In D-shape design this angle has been made wider.
- In correspondence to that, for reducing the diffusion flux, the side channel is reconnected with the main channel after covering certain length along with the outlet.
- T45A-2 suggest that, increased path length at inlet helps increasing the momentum of the reverse flow so that it can reach the opposite wall of the main channel. In D-shape design, this suggestion has been taken into consideration.

2. Main channel geometry

- By keeping the suggestion of h and b dimension from T45A-2 design, the main channel was built at a radius 22mm to help the diffusion of main channel flow before reaching junction 2 to lessen the energy losses. Additionally, it enhances diodicity by increasing the acceleration of the main channel reverse flow in the inlet.

3. Inlet channel geometry

- T45A-2 suggests that the dimension K should be large enough to allow a gradual acceleration of the forward flow in the inlet channel. D-shape valve has taken this into consideration and minimizes the forward-direction dissipation rate by avoiding high velocity-gradient near the wall.
- Radius J was suggested to keep small at a range of 50% to 100% of dimension b in case of T45A-2. But in case of D-shape valve, it was kept 125% of b due to make the radius 22mm for main channel.

4. Outlet channel geometry

- From the design of T45A-2, The radius l should be large enough and in case of D-shape it has been made 180 degree to make the inlet and out let aligned.

- Abiding by the suggestion of T45A-2 the mouth of the outlet has been made sharp for further inhibit the reverse flow.
- To maintain direction dependent dissipation the value of n has been reduced further than T45A-2 for D-shape design

The diodicity against Reynolds number obtained from D-shape Tesla valve is shown in Fig. 2.1.3.7. Vries et al. [31] claims that, the 2D forward case does not converge for Re > 650, while the reverse case is still converging. With only the forward case of the 3D model not converging for Re > 200, this phenomenon is believed to result in transitional flow behavior causing the non-convergence of the laminar model.

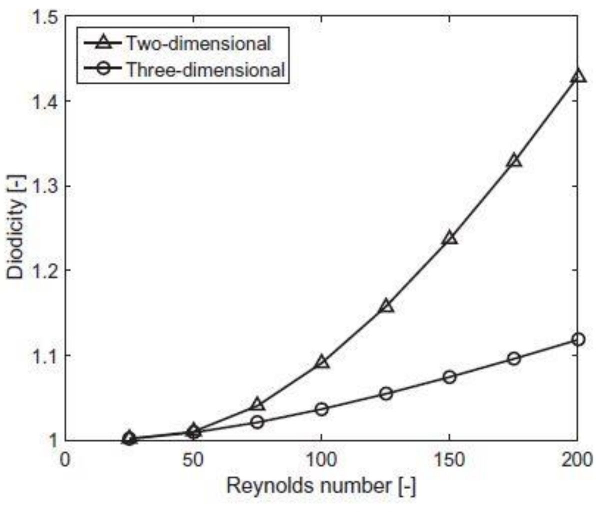

Fig. 2.1.3.7: Plot of the single-phase diodicity against the Reynolds number computed by the 2D and 3D model for the D-valve design [31]

T45A is the traditional Tesla Valve, T45C and GMF are improved by Bardell [30] where these two valves are optimized by Gamboa [28]. The graphical comparisons are provided below in Fig. 2.1.3.7 (a) & (b). From the Fig. 2.1.3.7 (a) it is evident that, D-shape Tesla valve shows much higher diodicity against increased Reynolds number than TMW valve and a uniformly increased diodicity curve which is almost similar to T45C valve. The pressure difference between forward and reverse flow is also showing a uniformly increased plot against Reynolds number for D-shape Tesla valve which is almost overlapping with the T45C valve.

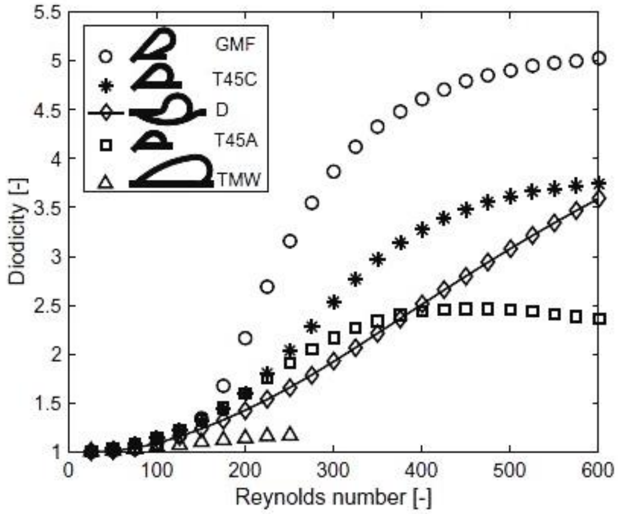

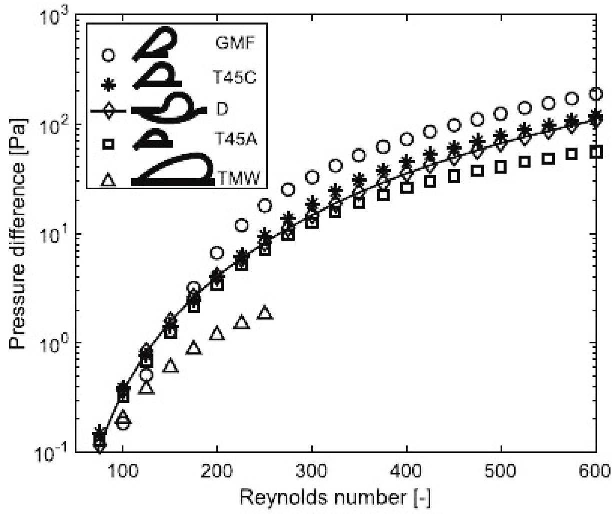

(a) (b)

Fig. 2.1.3.8: (a) Plot of the single-phase diodicity against the Reynolds number computed with the 2D model for the GMF, T45C, the proposed D, T45A and TMW valve as indicated in the legend from top to bottom respectively

(b) Plot of absolute single-phase pressure difference between forward and reverse flow against the Reynolds number computed with the 2D model for the GMF, T45C, the proposed D, T45A and TMW valve as indicated in the legend from top to bottom respectively [31]

2.1.4 Applications of Tesla type valve to CLPHP

Heat transfer through a closed loop pulsating heat pipe may vary depending geometrical, chemical, ambient conditions etc. Geometrical variables may be listed as inclination angles, internal tube diameter, filling ratios, implementing no moving part valves, surface tension etc. viscosity of working fluid, variations of working fluid etc. are the influencing parameters in the chemical sector. Temperature rise, latent and sensible heat are variables related to ambient. From geometric point of view, Tesla type valve incorporation can be a milestone in the field of CLPHP. But application of Tesla valve to closed loop pulsating heat pipes are not extensively available.

Thompson [27] ran an experiment on flat plate oscillating heat pipe with Tesla-type check valves. A pair of Aluminum flat plates are engraved with Tesla valve geometry are attached to form a CLPHP. The evaporator section was covered with an aluminum block through cartridge heaters. Four Tesla valves are located in the evaporator while another four were in the condenser section by operating with heat load not exceeding 150W. The investigation proved that using Tesla valve gives flow uniformity. This phenomenon enhances diodicity that increases thermal performances. Hence, the thermal resistance decreased 15%-25% by implementing Tesla valve to the CLPHP as shown in Fig.2.1.4.1. This thermal enhancement attributes as supplying more fluid to the evaporator turns, fewer periods of static fluid motion and increased fluid velocities occurring in the non-promoted flow direction.

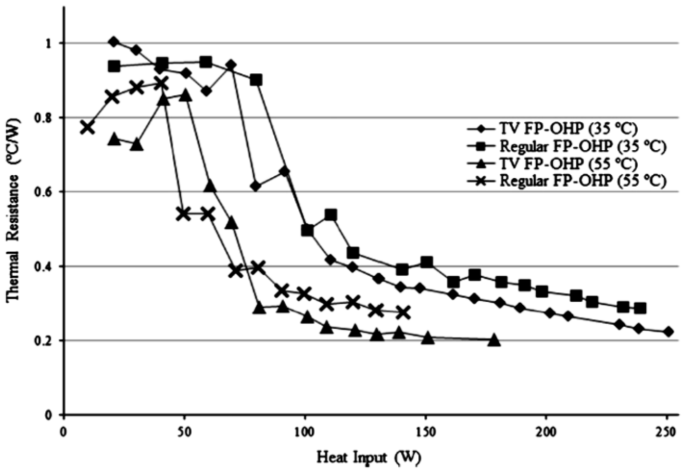

Fig. 2.1.4.1: Thermal resistance vs. average heat input for TV FP-OHP and regular FP-OHP at 35 ˚C and 55 ˚C cooling temperatures [27]

Incorporation of Tesla type D-valve

Vries et al. [31] proposed this D-shape Tesla valve from their research in the year 2017. They investigated using single loop polycarbonate (PC) CLPHP. There were two models. One was without having any valve (N-PHP) and other was with the incorporated Tesla Valve (TV PHP). Their intention was to validate the numerical simulated data with the experimental values. The working fluid was taken as Water. As PC is transparent, the visual analysis had been carried out of finding uniform circulation throughout the CLPHP and the slug-plug zones. This research also showed a comparative graph of thermal resistance between N-PHP and TV PHP. This graph executed their one of the mottos to reduce the thermal resistance up to 14%-25% using TV to the CLPHP. Though the experiment was not purely for observing heat pipe action, but it gives a comparative evaluation with traditional PHP with Tesla type D-valve incorporated PHP. Fig. 2.1.4.2 illustrates the two models of traditional PHP without any valve channels along and a PHP having Tesla type D valve. In the design both PHP the evaporator and condenser are having same length. The total setup was confined with a vacuum chamber to prohibit heat loss. Fig. 2.1.4.3 and Fig. 2.1.4.4 depicts the flow pattern and thermal performances respectively [31]. The left image of Fig. 2.1.4.3 shows masking procedure used for image registration, where 1 indicates the inlet channel section and 2 the side channel section. The right image shows the applied masks for determining the air ratio in the main (A) and side (B) valve channel. An individual grey-scale frame of a reverse flow case with and average inlet velocity of 0.21 m/s is shown on top and below the corresponding binary image. Fig. 2.1.4.4 shows that, Tesla type D-valve shows much lower thermal resistance than empty and partially filled no valve incorporated PHPs.

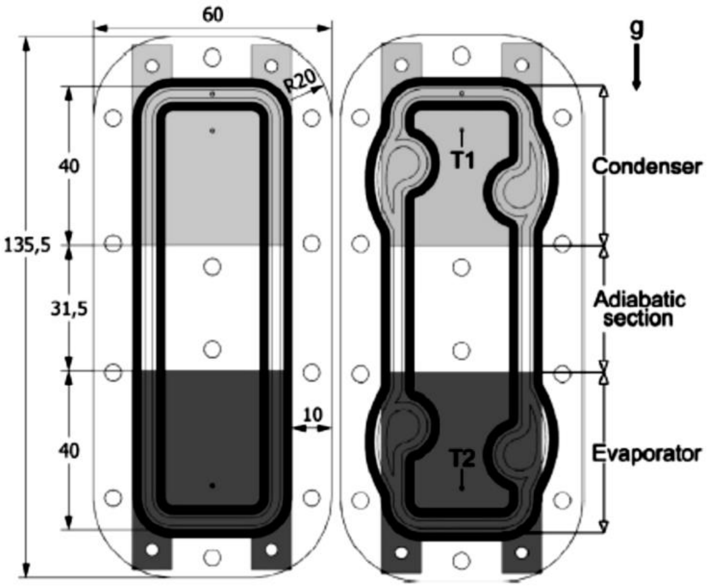

Fig. 2.1.4.2: Illustrative image of N-PHP and TV-PHP with dimension [31]

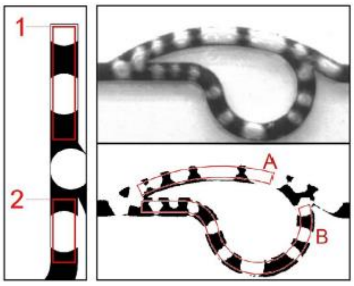

Fig. 2.1.4.3: Masking procedures used for the two-phase experiment. [31]

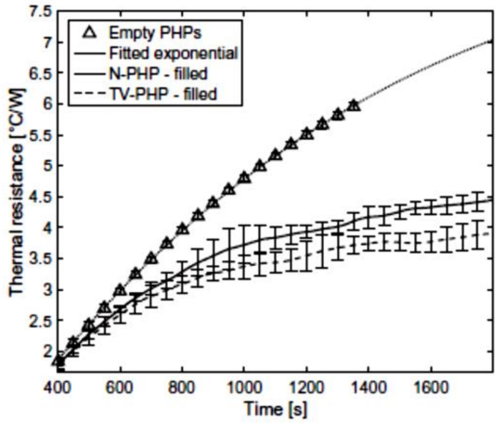

Fig. 2.1.4.4: Thermal resistance comparison [31]

Chandavar [61] investigated on D-shape Tesla valve incorporation to CLPHP for decay heat removal in nuclear power plants. The author adopted the design from the research published by Vries [31] The study was purely based on simulation using ANSYS Workbench. This study compared the results of mass flow rate, unidirectionality of flow and stability between a loop using D-shape Tesla Valve and without any valve. It was found that, incorporating this special valve produces unidirectional flow through the loop which enhances heat transfer.

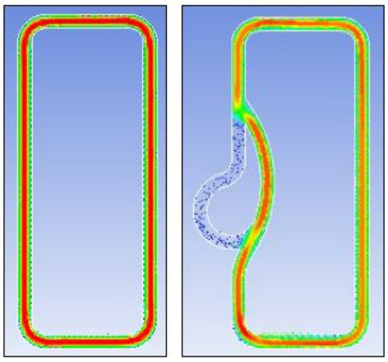

Fig. 2.1.4 5: Unidirectional 2-D velocity vector plot [61]

Fig. 2.1.4.5 shows the simulation output for velocity vector. It is also evident that the incorporation of D-shape Tesla valve can operate at horizontal position efficiently Moreover, this valve incorporation saves 100s more than the loop without any check valve to reach steady state [61].

2.2 Closure

This chapter gives a clear demonstration of historical transformation of CLPHP to Tesla-type valve incorporated CLPHP. The necessity of dissipating more heat from condenser section, there needed to increase more fluid flow through the channels. This requirement urges the need of newly designed efficient valves. Thus, the evolution of Tesla type D-valve valve incorporation to CLPHP came under concentration. The next chapter will carry forward the demand of this special valve design by providing detailed about experimental setup and procedures.

CHAPTER 3: EXPERIMENTAL ANALYSIS

3.1 Experimental Setup

A closed loop pulsating heat pipe (CLPHP) incorporate with D-type Tesla Valve have been fabricated and set up as shown in the following Fig: 3.1.1. The setup and accessories descriptions along with some NDT test, experimental procedure and data collection are discussed in the following sections of this chapter.

The CLPHP structure is a combination of alternating copper tubing welded with copper bars. The alternate tubing is a capillary pipe of 2mm ID and 3mm OD. The copper bars are used to engrave the special D-shape Tesla valve design. This design has been produced using CNC Milling machine from copper plate of 3mm thickness. After milling operation, symmetric pair of plates (each plate: 50mm×26mm) for 16 valves (evaporator section: 8 Valves, condenser section: 8 Valves) were brazed together with 8 copper pipes of internal and external diameter as 2mm and 3mm respectively. These 8 pipes (each pipe: 56mm long) forming adiabatic section of CLPHP is covered by glass wool and insulating tape. The height of the evaporator, adiabatic and condenser section are 63mm, 56mm and 63mm respectively as shown in Fig. 3.1.2 below. Evaporator turns are coiled with Ni-Chromium heating wire over mica tape wrapping to connect with voltage variac. Wooden movable holder is holding the CLPHP connected with temperature data logger. The orientation angles could be changed by moving the wooden shaft of the holder. The temperature readings from K type thermocouples will be taken at an interval of 1 second. After reaching steady state, different readings of thermal resistance, pressure, heat flux etc will be observed against various filling ratios (40%, 50%, 60%, 80%) and orientations (0°, 10°, 20°, 30°, 45°, 60°, 90°, 180° etc). the detailed description of each individual are described in the following sections. The geometrical specifications are given in Table 3.1.1.

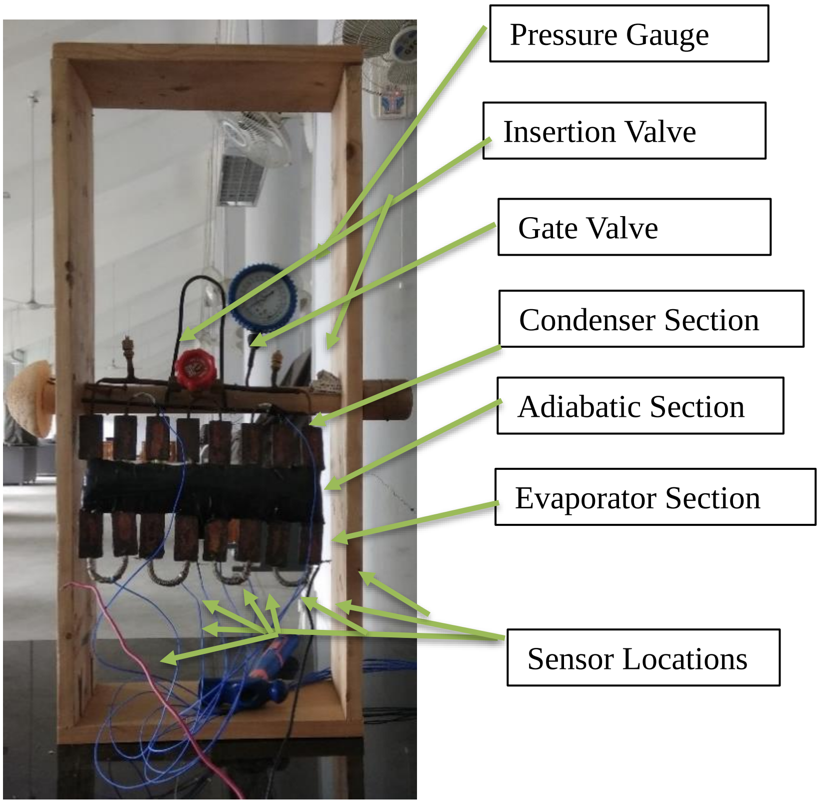

Fig.3.1.1: D-type Tesla valve incorporated CLPHP with wooden holder

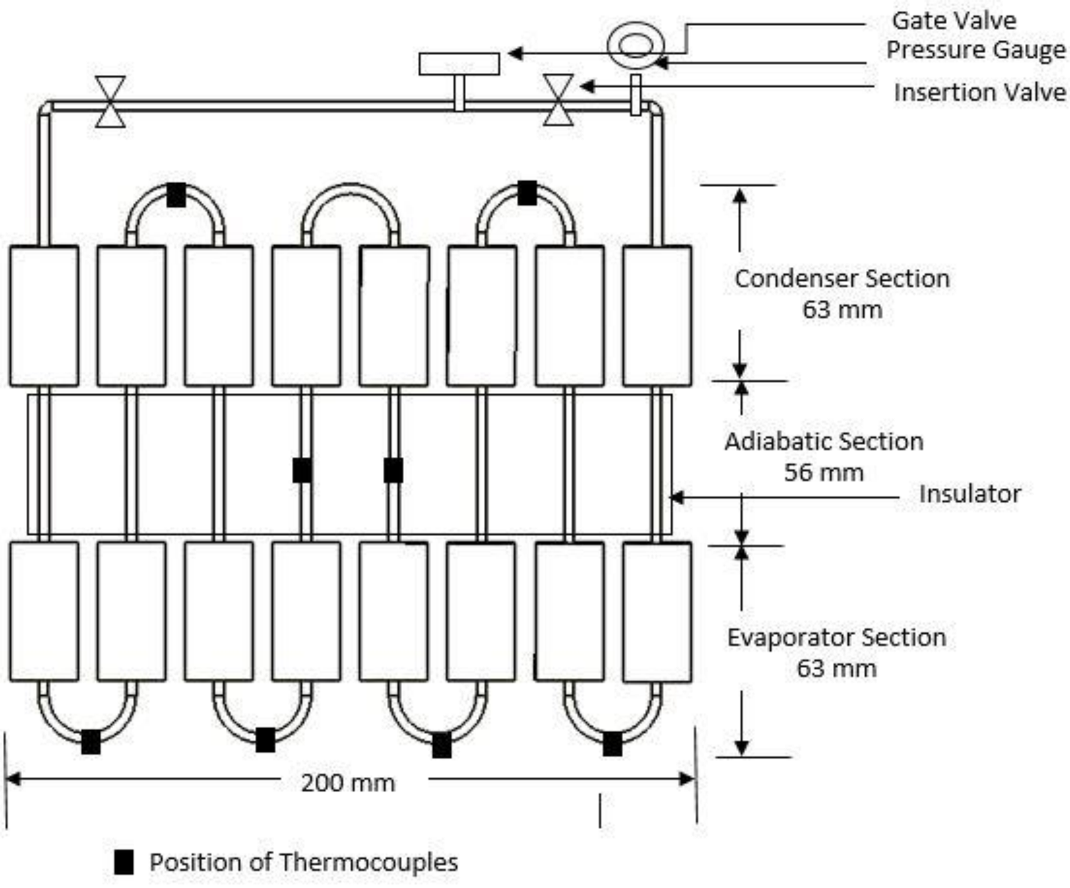

Fig.3.1.2: Schematic diagram of the Tesla type D-valve incorporated CLPHP system

Section	Vales	Dimension
Total Internal Volume of Evaporator	3.75×10^{-6}	m^3
Total Internal Volume of Condenser	3.567×10^{-6}	m^3
Total Internal Volume of Adiabatic Section	1.40×10^{-6}	m^3
Total Internal Volume of PHP	8.73×10^{-6}	m^3
Area of Evaporator Section	6.08×10^{-3}	m^2
Area of Condenser Section	5.70×10^{-3}	m^2
Inner diameter of the tube	2×10^{-3}	m
Outer Diameter of the tube	3×10^{-6}	m
Length of Evaporator Section	0.9712	m
Length of Condenser Section	0.912503	m

Table 3.1.1: Geometrical specifications of Tesla type D-valve incorporated CLPHP

Thermo-physical influencing parameter:

Thermophysical parameters that influence the performance of CLPHP are listed and optimized in the following segments.

1. Internal tube diameter In the year 2017, Drolen and Smoot [62] found out that the critical diameter for capillary action best suits for 2.4mm to 2.7mm range. But traditionally the critical diameter is determined by the following equation,

$$D_{crit} = 2 \times \sqrt{\frac{\sigma}{g\times(\rho_l-\rho_v)}} \qquad [24]$$

Referred to the critical diameter equation, it is taken 2 mm as the internal diameter of the CLPHP which can best suit for capillary action.

2. Number of turns Increasing number of turns to the CLPHP, increases the thermal performance. But there is an optimization criterion. Excess number of turns in evaporator section will create lack of bubble production and reduction of evaporator temperature [3]. Another study shows that for a desired temperature difference between evaporator and condenser, evaporator length should be minimized as possible [62-63]. In this research, the evaporator and condenser lengths are designed almost same and the total number of turns are seven to accommodate 16 valves CLPHP design. Increasing a greater number of turns increases the amount of valve incorporation. This phenomenon increases the total size and weight of the CLPHP. That's why to keep minimum size and weight as well as decreased thermal resistances seven turns have been designed for this research.

3. Working fluid As mentioned by Bardell [30,64], Fluids having a large saturated pressure gradient coupled with a low dynamic viscosity would best suit for the working fluid inside a CLPHP. Methanol has satisfactorily a large saturation pressure gradient as its saturation pressure at atmospheric temperature is 2 psi. It is also having very low dynamic viscosity at atmospheric pressure. That's why methanol is considered one of the best suitable working fluids.

4. Filling ratio The more bubbles (lower filling ratios) mean higher degree of freedom but simultaneously there is less liquid mass for sensible heat transfer. Less bubble (higher filling ratios) mean less perturbations and the bubble pumping action is reduced thereby lowering the performances.

It is shown by Khandekar [3] that pulsation action along with heat load best starts from 30% filling ratio and best suits up to filling ratio of 80%. In this experiment, data have been taken at 60% and 80% filling ratios.

5. Pressure inside CLPHP After fully evacuating the device, the pressure indicates the saturation pressure. Due to the valve design as well as the milling operation to engrave the valve over copper plate, there imposes some degree of excess flow restrictions in the desired direction. Thus, a large pressure gradient is required between evaporator and condenser. The average pressure inside the CLPHP was found 14 psi gauge pressure.

6. <u>Working fluid distribution inside the CLPHP</u>

After just filling, the fluid cannot reach to every portion inside the CLPHP. Thus, the productions of slug –plug become hampered. After filling the device, it was heated at a very high heat flux so that all the fluid can be vaporized and after cooling, liquid deposited over all the internal portions of the evaporator section.

7. <u>Limitation of heat load</u>

Oscillating motion does not initiate before reaching a certain range of heat input. Moreover, thermal performances increase with the increase of heat loads [33]. The flow pattern at this peak performance becomes annular flow. But there is highest limit above which input heat can cause burn out of the devices. The safe heat load limit for this research has been taken 40W to 90W.

3.1.1 Copper tubing and copper bars

<u>Copper tubing</u>

The alternate copper tubing is covering both condenser and evaporator sections while there are separate copper pipes of 2mm inner diameter (ID) and 3mm outer diameter (OD) forming the adiabatic section. Each U bend tube is 78.7 mm long (Fig. 3.1.1.1). It has two legs of 15 mm length each. Its 10 mm of length is inserted through the 3.5 mm hole of copper bar. Finally, each leg is brazed with the copper bar separately.

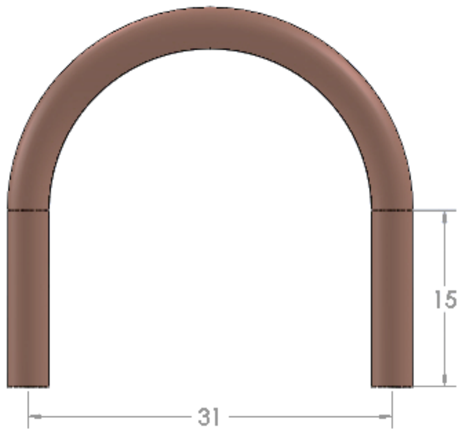

Fig.3.1.1.1: Copper U bend tubing

Copper pipes

Total eight copper pipes of 76mm long each having 2mm internal and 3mm outside diameter are forming the adiabatic sections (Fig. 3.1.1.2). The pipes are brazed with the copper bars. This section is insulated so that no heat can pass out to the surrounding.

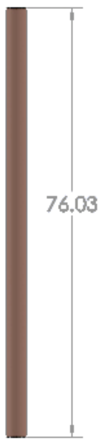

Fig.3.1.1.2: Copper straight pipe

Copper bars

These bars are mainly holding the D-type Tesla valve for the CLPHP. As it is very tough to casting the cylindrical D-shape, it was symmetrically divided into two parts that are producing a single copper bar together. Thus, each bar consists of two symmetrical copper plates (each plate: 49.15mm×24mm×3mm). The CAD design as shown in Fig.3.1.1.3 (c) was engraved over the plates by using five axes CNC milling machine. Total 32 copper pates consisting of 16 symmetrical with the other 16 plates are producing 16 copper bars. The valve was designed using SolidWorks 2016 version. Then it was loaded to MasterCAM software through which automatic milling operation procedures are designed. The file is saved as .NC extension and sent to CNC control unit for converting to G Code. Each symmetric part of D shape channel is cut by using 1mm diameter 2 flute Tungsten-Carbide ball mill cutting tool. The inlet and outlet channels are cut out by using 2 mm cutting tool. The operation procedure was designed as it could cut 16 homologous valves at a single operation from 12 inches long and 20 inches wide copper plate of 3mm uniform thickness. The MasterCAM operation screen shot for cutting the design as well as the final output of milling operation over copper plates are shown in the Fig. 3.1.1.3 (a) and 3.1.1.3 (b) respectively.

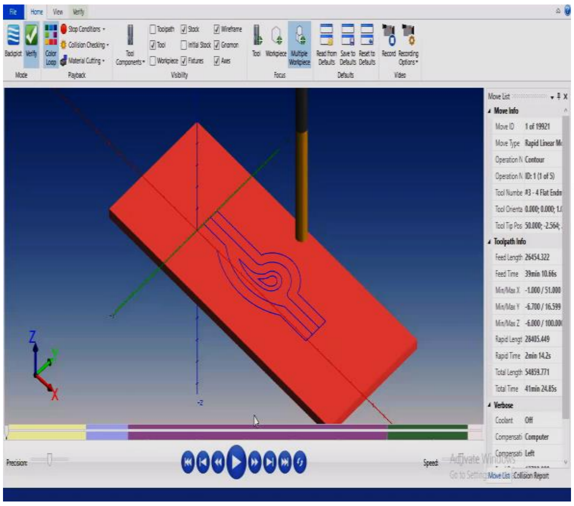

(a)

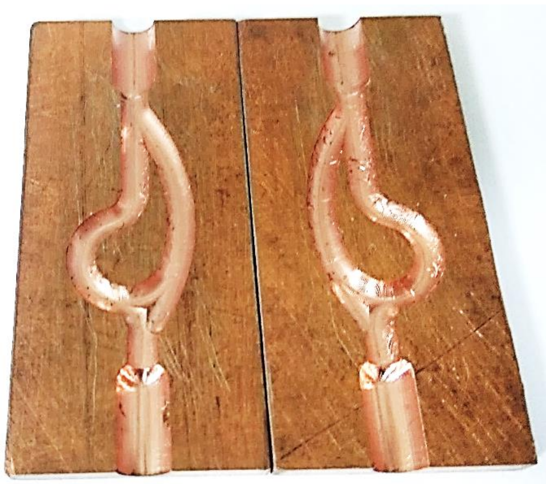

(b)

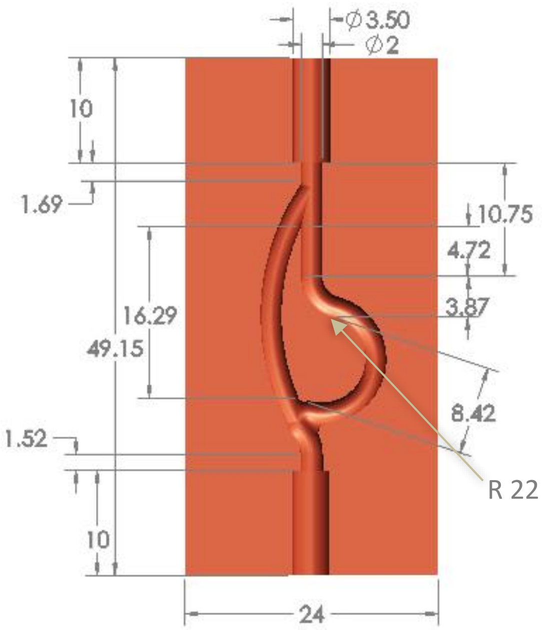

(c)

Fig.3.1.1.3 (a) MasterCAM operation screen shot (b) Copper plates before brazing

(c) CAD drawing of Tesla type D-valve with dimension in mm.

Fluid pipe:

A fluid pipe of 6mm diameter was brazed at the top to insert the working fluid (Fig.3.1.1.4). There are two small valves to pour the liquid by using plastic syringe through the fluid pipe to reach to the evaporator section. These two valves help to consume working fluid maintaining closed vacuum. There is a gate valve to control the fluid motion through the CLPHP while inserting. During the input, the gate valve remains closed so that the fluid can pass only one side of the CLPHP. Same process happens for the input through the other valve. After pouring desired amount of working fluid through the CLPHP, the gate valve was kept open.

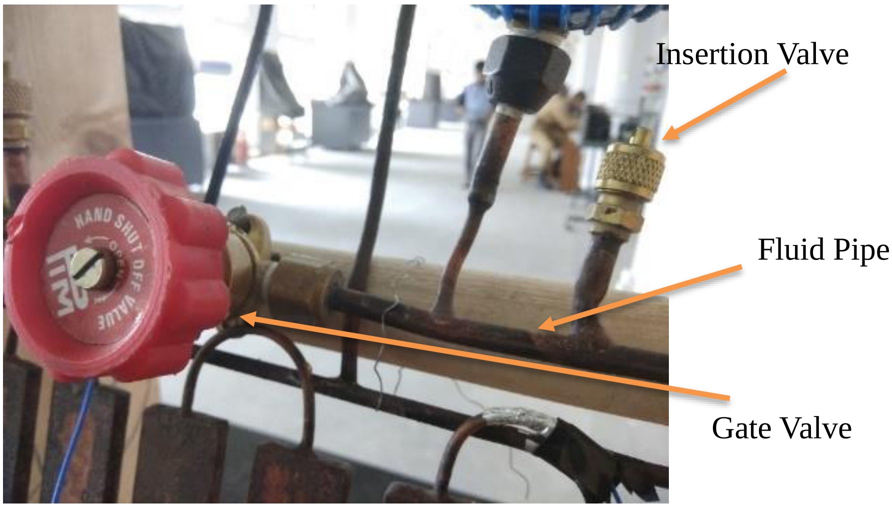

Fig.3.1.1.5: Fluid pipe and valves

3.1.2 Insulation

The adiabatic section supplies heat load from the evaporator to condenser without any losses. Strong insulation is needed for heat resistance. The adiabatic section covers 200 mm wide and 56 mm long insulated area between evaporator and condenser section (Fig. 3.1.2.1). Under this insulation there are eight straight copper pipes of 2 mm internal diameter and each pipe is 56 mm long. Heat seal gel is pasted over these copper pipes to resist moisture and heat transfer. These pipes are covered with aluminum heat insulating tape over which 1 cm thick glass wool layer has been stacked firmly. Finally, PVA tape has been wrapped all over the section to bind the layer of insulation with the CLPHP structure.

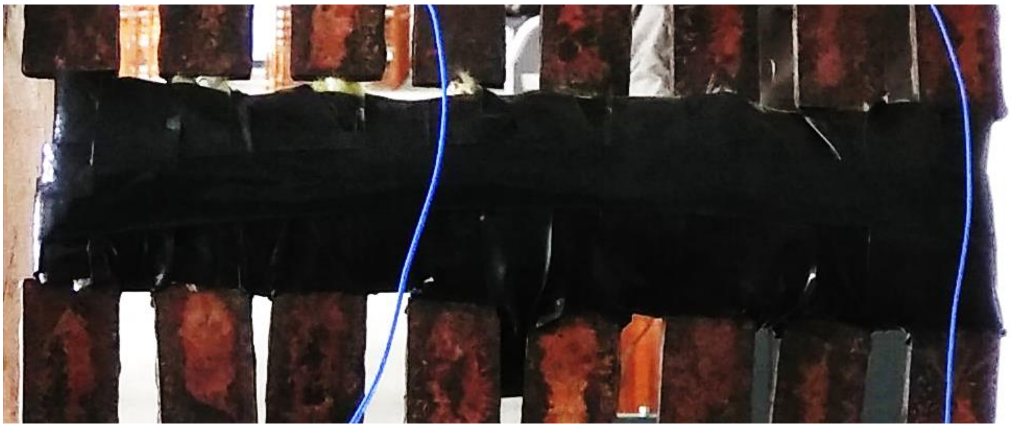

Fig.3.1.2.1: Insulation over adiabatic section

3.1.3 Wooden movable holder

The whole setup has been fixed upon a wooden holder which is having a shaft that can move 360° rotations (Fig. 3.1.3.1). The setup is having a screw system to be attached with the shaft. By the help of protractor various orientation angles were selected. It was chosen wooden holder to avoid electrical short circuits.

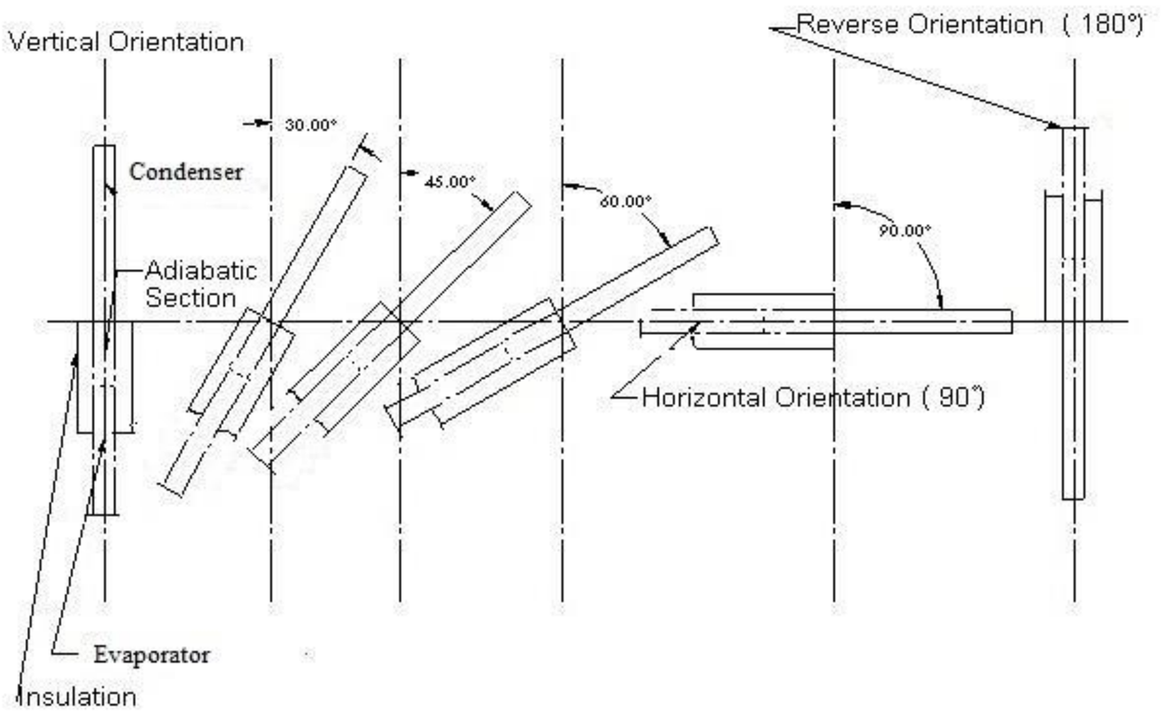

Fig.3.1.3.1: Wooden movable holder and changing of orientation angles

3.1.4 Power source and heating coil

An AC voltage variac is used to regulate input single phase line voltage. It is needed to experiment the operations of CLPHP under various input heat fluxes. It can operate through a range of 0-250V output from single phase 220V source. The line voltage is stabilized by using an UPS. The variac is connected with two input wires and two output wires. Among the four wires of input and output side, two are neutral connections. The output wires are connected with two ends of heat coil winding. The specification of the voltage variac is given in the Table No: 3.1.4.1 below.

Fig.3.1.4.1: Voltage variac

Specification	
Model No.	GGG
Input Voltage	220 V
Output Voltage	0-250V
Output current	4A
Frequency	50 Hz
Capacity	1KVA
Country of Origin	China

Table 3.1.4.1: Voltage variac specification

The output voltage is measured by multimeter where the current is measured by using clamp-on meter for user benefits. The collected voltage and current readings are used for calculating the input power.

(a) Multimeter (b) Clamp-on meter

Fig.3.1.4.2 (a) & (b): Temperature measuring instrument

For supplying the heat load, a continuous winding of nicrome wire of 0.25mm diameter is used at an interval of 1.5mm (Fig. 3.1.4.3). The wire coil is wrapped around the evaporator section U bend tubing. Each U shape bend is holding 35 turns. Two ends of the coil are connected with voltage variac connecting cables.

Fig.3.1.4.3: Heating coils at evaporator section

3.1.5 Temperature measurement

AT4208 Multi-Channel Temperature Data Logger along been used to measure and record the temperature. It has total eight K-type thermocouples to collect temperature readings at 8 different locations. In the setup, there are four thermocouples placed in evaporator section. Among the rest four, adiabatic and condenser section both are holding two thermocouples each. The thermocouples are attached by using heat seal gel and secured by PVC tape. The meter displays the temperature readings on a display panel. It records the data at an interval of 1 second and stores as excel file. The compilation is done by AT42X software which is provided with the instrument package. In the screen, serial number 1 and 2 are indicating condenser section temperatures, serial number 3 and 4 are for storing adiabatic section temperatures and serial number 5 to 8 are for recording evaporator temperatures. The detailed description of the temperature meter is given below in Table No: 3.1.5.1.

Fig.3.1.5.1: Temperature data logger.

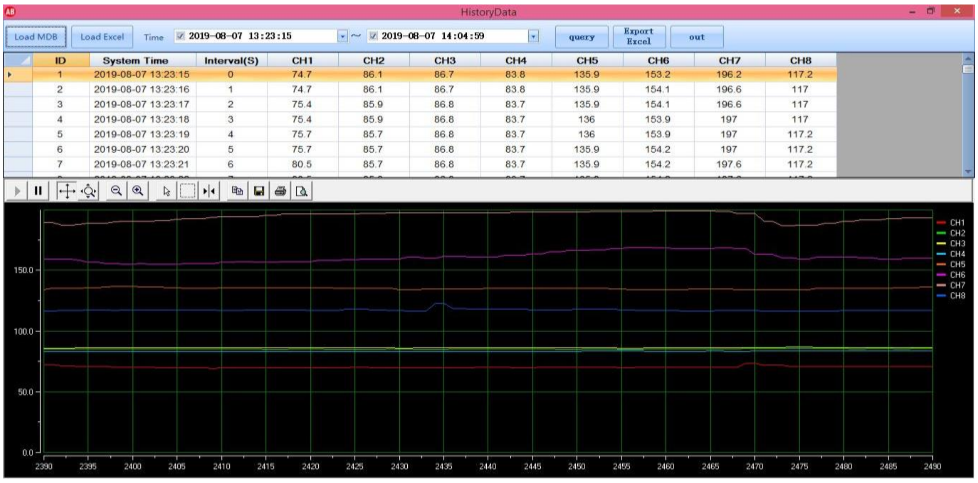

Fig.3.1.5.2: AT42X software

Specification	
Brand Name	Applent Instruments
Model No	AT4208
Thermocouple Type	K Type
Temperature Range	-100°C-1350°C
Resolution	0.1°C
Accuracy	±1.2°C
Interface	USB High Speed mode: 48MHz, USD-HID Protocol, ASCII Transi
Battery	Li
Country of Origin	China

Table 3.1.5.1: Temperature data logger specification

3.1.6 Pressure measurement

To monitor the system pressure, a pressure gauge has been installed over the fluid supply pipe. The gauge is inserted using a copper pipe of 6mm diameter and brazed together with the fluid supply pipe. The detailed specifications are given in Table: 3.1.6.1 below.

Fig.3.1.6.1: Pressure gage

Specifications	
Manufacturer	HAWK
Working fluid	Methanol
Lowest pressure	14.7 psi
Highest pressure	300 psi

Table 3.1.6.1: Pressure gage specifications

3.1.7 Evacuation system

The setup must be fully vacuum for perfect pulsating behavior. If vacuum is not maintained properly, trapped air creates obstacles to the circulations of slug plug. Thus, reduces the performance of CLPHP. Moisture also creates damage to the inside surfaces.

Compressed air is passed inside the empty CLPHP structure to blow any liquid or hard particles from inside channels. Then it is taken to vacuum pump to fully suck all the air from inside. After evacuation, the insertion valves are made closed vary cautiously.

3.1.8 Working fluid

Methanol has been chosen as the working fluid here because of having satisfactorily a large saturation pressure gradient as its saturation pressure at atmospheric temperature is 2 psi. It is also having very low dynamic viscosity at atmospheric pressure. Moreover, methanol can be sourced with a lower cost from the local market.

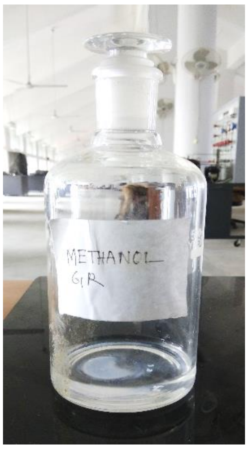

Fig.3.1.8.1: Methanol in a glass container

3.2 NDT Test of a Single D-Type Tesla Valve and CLPHP

Nondestructive sample X-ray test was performed for a single tesla valve bar after brazing. The intention was to identify any welding defects or leakages. But the result was found absolutely positive having no defects or leaking zones. There also found no clogging through the valve channel. The X-ray test had been done for both of the top and bottom flat surfaces. The X-ray reports are attached in Appendix A.

The CLPHP setup was checked for any internal leakage or clogging by passing compressed air from air compressor. The check valve remains open and the compressed air is passed through one of the input valves. The other input valve keeps open. The compressed air passes all through the tubing, pipes and channels and exits out through the open input valve. This indicates no leakages or clogging inside the structure.

3.3 Experimental Procedure

There are various researches on Closed Loop Pulsating heat pipe specially by changing orientation angles, Filling Ratios, working fluids, inserting check valves, asymmetrical heating, variation in channel diameter, inserting no moving parts pumping system etc. In this research, no moving parts D-shape Tesla type valve incorporation has become one of the distinctions among other researches. Besides, changing of orientation angles and variation in filling ratios are also done for different system conditions. The experiment has been run at an average ambient temperature of 33˚C. The setup was placed in thermodynamics laboratory at Bangladesh Military Academy, Bhatiary, Chittagong. There were free spaces inside the room and natural air was flowing all around. No mechanical cooling systems were used for releasing heat from the condenser to the environment other than natural air circulation inside the room.

Analyzing the experimental data, pulsation mechanism showed steady state behavior at an average tenure of 3 hours and 30 minutes. The average evaporator and condenser temperature have been taken after steady state condition. Experimental analysis was carried out on varying loads to find out the critical heat flux. The detailed procedures to collect and store data are described in the following sections. The process diagram is shown in Fig. 3.3.1 below.

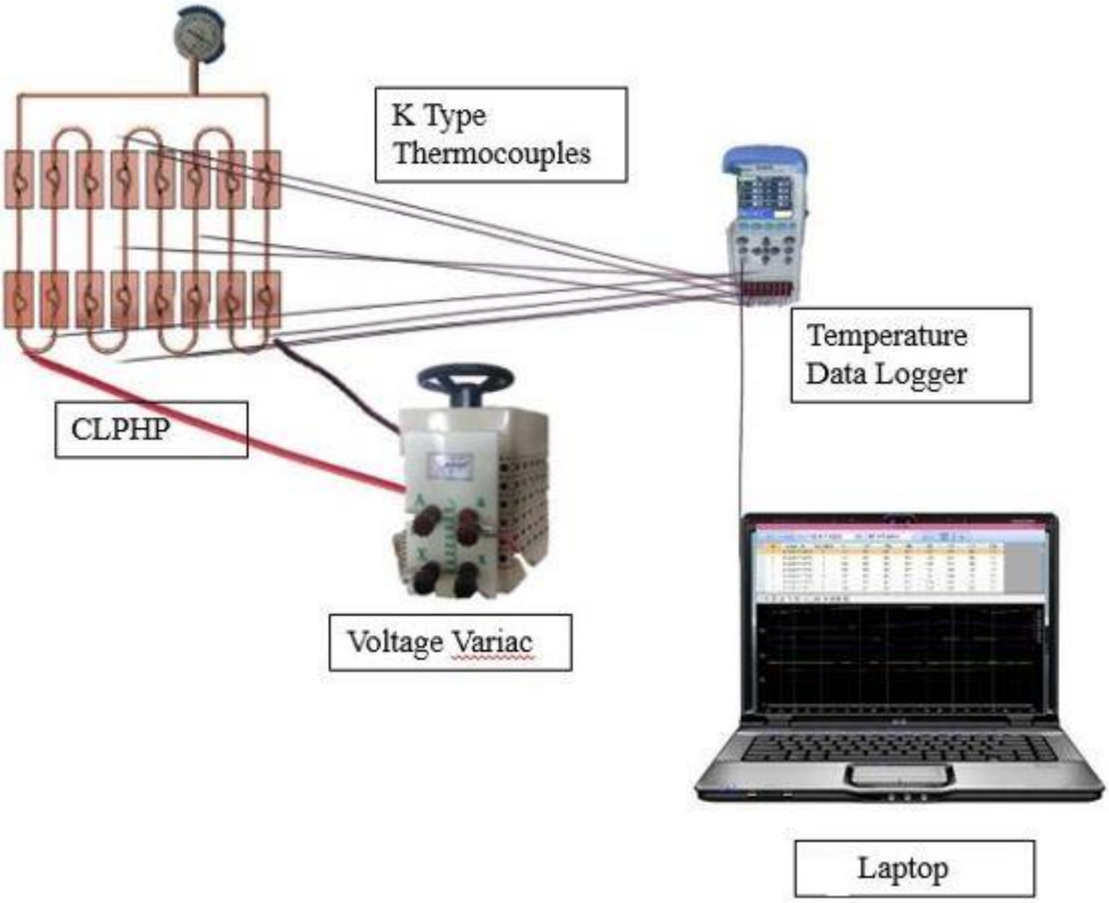

Fig.3.3.1: Process diagram of data collection from D-shape Tesla valve incorporated CLPHP

3.3.1 Heating and data storing procedures

1. After assembling the full setup, the CLPHP is evacuated fully to make perfect vacuum by using vacuum pump.
2. Then desired amount of working fluid is inserted by using syringe through the insertion valves while the gate valve is kept closed. The process is done with great concern keeping the system fully vacuum. The total volume inside CLPHP is

calculated as 8.7 CC. When it is 60% filling ratio, there inserted 5.2 CC working fluid through a syringe.

3. After partially filling the CLPHP, it is heated with high heat input to deliver the working fluid to make it fully vaporized. By sudden stopping the heating produces deposition of fluid all over the volume of evaporator.
4. Data has been collected by changing the setup orientation angles. By using a protractor orientation angles are being changed as reference to the vertical.
5. The AC power supply is provided to the voltage variac which is changing the voltage with a desired value of DC supply.
6. With the help of a multimeter and clamp on meter, output voltage from the variac as well as the current supply to the heating coil are measured.
7. The temperature data logger is executing the results from different thermocouples from the designated locations. There execute eight continuous curves for eight thermocouples over the screen of AT42X Software.
8. At the beginning there shows a sharp increase of temperature in the graph area for all of the thermocouples. Before reaching to steady state, there are fluctuating behaviors found from the graph. After steady state condition, all the lines of each thermocouple become almost straight lines.
9. At this situation, the data collection is stopped and stored as excel files.
10. In case of changing the filling ratios, compressed air is passed through insertion valve. After removing the liquid, the CLPHP setup is brought to vacuum pump and follows the same process as mentioned in serial 1 and 2.

3.4 Closure

This chapter has provided detailed description about the experimental apparatus used. The products are having been sourced from Bangladesh and China. The experiment was conducted at an average ambient temperature 33˚C. The working procedures are also described in this chapter. The data acquisition had been taken after steady sate condition reached. The experimental data are stored in Appendix B. The Appendix C will provide the uncertainty propagation from this experimental data.

CHAPTER 4: RESULT ANALYSIS

This section is arranged with four sub sections. In section 4.1 the experimental data will be analyzed in terms of temperature rise, overall heat transfer co-efficient and thermal resistance. The calculated results are given in the form of data tables and graphs. Next section 4.2 represents the verification of the experimental data with established theoretical equations in the field of CLPHP. The results are verified by calculating Mean Absolute Error (MAE) and error band. Section 4.3 provides the validation of data from D-type CLPHP with that of traditional CLPHP without any valves. The mathematical correlations from experimental data are analyzed in section 4.4. At the end, there will be an enclosure to provide a summery on this analysis.

4.1 Experimental Result Analysis

Experimental data have been collected for total 36 different cases (six different inclination angles, θ and six different heat loads, Q) at 60% fill ratio. Temperature data were collected from these 36 experiments within 280 minutes run time of each case. After reaching steady state condition, the average data for four evaporator thermocouple readings and average of readings from two thermocouples in condenser and two in adiabatic section have been calculated. Total inside surface area of evaporator and condenser section are 6.1×10^{-3} m^2 and 5.7×10^{-3} m^2 respectively. The equation for calculating overall heat transfer co-efficient and thermal resistance from experimental data are based on the convection heat transfer by the working fluid. The equations are described below [27]:

Experimental Thermal Resistance calculations:

After reaching steady state,

$$\Delta T_{avg} = (T_{eva} - T_{con}) = \frac{1}{4}\left(\sum_{m=5}^{8} T_{avg,m}\right)_{eva} - \frac{1}{2}\left(\sum_{m=1}^{2} T_{avg,m}\right)_{con}$$

R = (T_{eva} - T_{con})/Input Heat Load (Q)

Here,

R = Thermal Resistance

T_{eva} = Average Evaporator Section Temperature (˚C)

T_{con} = Average Condenser Section Temperature, (˚C)

In the evaporator section, heat is transferred from the PHP tube wall to the working fluid and it may be determined by the Newton's Law of Cooling. [24]

$$Q_e(W) = hAdT = h_{fe}\, A_{ei}\, (T_{eva} - T_{fe}) \qquad (4.1.1)$$

Where, A_{ei} = Inner surface area of the evaporator (m^2) = $\pi d_i L_{eva}$

T_{eva} = Average evaporator temperature (˚C)

T_{fe} = Average temperature of fluid in the evaporator (˚C)

h_{fe} = Convective heat transfer coefficient between the evaporator inner surface and the working fluid ($W/m^2\,^oC$)

Assuming no addition or loss of heat in the adiabatic section, the heat absorbed by the working fluid in the evaporator section should be completely transferred to the condenser section. In the condenser section, heat is transferred from the working fluid to the condenser wall and it may again be determined by the Newton's Law of Cooling.

$$Q_c(W) = hAdT = h_{fc}\, A_{ci}(T_{fc} - T_{con}) \qquad (4.1.2)$$

Where, A_{ci} = Inner surface area of the condenser (m^2) = $\pi d_i L_{con}$

T_{con} = Average condenser temperature (˚C)

T_{fc} = Average temperature of fluid in the condenser (˚C)

h_{fc} = Convective heat transfer coefficient between the condenser inner surface and the working fluid ($W/m^2\,^oC$)

Equation 4.1.1 shows that the thermal resistance in the evaporator section is $1/(hA_{ei})$. Similarly, equation 4.1.2 shows that the thermal resistance in the condenser section is $1/(hA_{ci})$. So, the overall thermal resistance from evaporator inner wall to the condenser inner wall is $1/(hA_{ei})+ 1/(hA_{ci})$. So, it can be written

$$Q = \frac{(T_{eva} - T_{con})}{\frac{1}{hA_{ei}} + \frac{1}{hA_{ci}}} = h\frac{(T_{eva} - T_{con})}{\frac{1}{A_{ei}} + \frac{1}{A_{ci}}} \qquad (4.1.3)$$

In steady state, considering the overall heat flow path from the evaporator to the condenser via the working fluid, one may write,

$$Q_e = Q = Q_c$$

Rearranging equation 4.1.3, we get,

$$h = \frac{Q}{(T_{eva} - T_{con})}\left[\frac{1}{A_{ei}} + \frac{1}{A_{ci}}\right] \tag{4.1.4}$$

The overall heat transfer coefficient, h in equation 4.1.4 involves heat transfer by both convection and phase change. Hence, to differentiate it from the convective heat transfer coefficient between the working fluid and the solid wall, the overall heat transfer coefficient is denoted by U and equation 4.1.4 is rewritten as,

$$U(\frac{W}{m^2}{}^{\circ}C) = \frac{Q}{T_{eva} - T_{con}}\left(\frac{1}{A_{ei}} + \frac{1}{A_{ci}}\right) \tag{4.1.5}$$

Here,

Q = Heat Transfer throughout the CLPHP, W

A_{ei} = Inner surface area of the evaporator (m^2) = $\pi d_i L_{eva}$

A_{ci} = Inner surface area of the Condenser (m^2) = $\pi d_i L_{con}$

L_{eva}= Length of the Evaporator Section (m)

L_{con}= Length of the Condenser Section, (m)

The results are listed the Table 4.1.1 below. Highest value of overall heat transfer coefficient is found 614.99 W/m^2˚C for 10˚ inclination angle at 80 W. Lowest thermal resistance 0.55 ˚C/W can be obtained from 10˚ inclination angle at 80 W. But it is observed that beyond 60 W it surpassed the critical heat load. Critical heat load is a peak point. After surpassing critical heat load, the system becomes unstable and cannot achieve steady state condition. Increasing more heat input to the device beyond critical heat load may cause burnout of the system. So, the stable values should be taken 60 W or below 60 W.

In the following sections 4.1.1, 4.1.2 and 4.1.3 temperature rise effects, overall heat transfer coefficient and thermal resistances are discussed through graphical representations.

FR	Inclination Angle (Degree)	Q	T_{eva} (˚C)	T_{con} (˚C)	Ae (m^2)	Ac (m^2)	U ($W/m^{2}°C$)	R, (˚C/W)
60%	0 Degree	40	94.83	53.07	6.1×10^{-3}	5.7×10^{-3}	325.38	1.04
		50	110.95	62.79	6.1×10^{-3}	5.7×10^{-3}	352.58	0.96
		60	112.98	62.50	6.1×10^{-3}	5.7×10^{-3}	403.70	0.84
		70	131.55	83.24	6.1×10^{-3}	5.7×10^{-3}	492.13	0.69
		80	160.58	88.36	6.1×10^{-3}	5.7×10^{-3}	376.26	0.90
		90	144.05	92.09	6.1×10^{-3}	5.7×10^{-3}	588.33	0.58
	10 Degree	40	106.41	64.38	6.1×10^{-3}	5.7×10^{-3}	323.21	1.05
		50	109.49	63.71	6.1×10^{-3}	5.7×10^{-3}	371.00	0.92
		60	117.97	65.09	6.1×10^{-3}	5.7×10^{-3}	385.44	0.88
		70	151.24	80.43	6.1×10^{-3}	5.7×10^{-3}	335.79	1.01
		80	124.10	79.91	6.1×10^{-3}	5.7×10^{-3}	614.99	0.55
		90	147.93	85.16	6.1×10^{-3}	5.7×10^{-3}	486.99	0.70
	20 Degree	40	97.33	61.42	6.1×10^{-3}	5.7×10^{-3}	378.36	0.90
		50	105.96	65.67	6.1×10^{-3}	5.7×10^{-3}	421.57	0.81
		60	121.34	79.52	6.1×10^{-3}	5.7×10^{-3}	487.31	0.70
		70	134.84	67.39	6.1×10^{-3}	5.7×10^{-3}	352.52	0.96
		80	137.80	84.16	6.1×10^{-3}	5.7×10^{-3}	506.55	0.67
		90	168.84	90.78	6.1×10^{-3}	5.7×10^{-3}	391.65	0.87
	30 Degree	40	94.58	49.24	6.1×10^{-3}	5.7×10^{-3}	299.66	1.13
		50	109.07	63.81	6.1×10^{-3}	5.7×10^{-3}	375.20	0.91
		60	119.15	63.04	6.1×10^{-3}	5.7×10^{-3}	363.19	0.94
		70	161.92	72.74	6.1×10^{-3}	5.7×10^{-3}	266.61	1.27
		80	137.66	80.62	6.1×10^{-3}	5.7×10^{-3}	476.38	0.71
		90	194.79	83.31	6.1×10^{-3}	5.7×10^{-3}	274.22	1.24
	60 Degree	40	107.10	47.48	6.1×10^{-3}	5.7×10^{-3}	227.90	1.49
		50	120.59	53.43	6.1×10^{-3}	5.7×10^{-3}	252.87	1.34
		60	130.29	64.86	6.1×10^{-3}	5.7×10^{-3}	311.47	1.09
		70	157.39	67.73	6.1×10^{-3}	5.7×10^{-3}	265.18	1.28
		80	175.03	68.55	6.1×10^{-3}	5.7×10^{-3}	255.20	1.33
		90	187.74	69.15	6.1×10^{-3}	5.7×10^{-3}	257.78	1.32
	90 Degree	40	115.94	42.21	6.1×10^{-3}	5.7×10^{-3}	184.28	1.84
		50	130.11	44.10	6.1×10^{-3}	5.7×10^{-3}	197.46	1.72
		60	154.61	48.76	6.1×10^{-3}	5.7×10^{-3}	192.54	1.76
		70	167.46	49.59	6.1×10^{-3}	5.7×10^{-3}	201.72	1.68
		80	187.98	52.64	6.1×10^{-3}	5.7×10^{-3}	200.79	1.69
		90	207.76	57.01	6.1×10^{-3}	5.7×10^{-3}	202.78	1.68

Table 4.1.1: Experimental result

4.1.1 Temperature rise

To study the temperature rise effect of different heat load at different inclinations graphical comparisons have been provided below. These graphs will provide the information about the nature of temperature curves due to the input of various loads. The safe heat load idea will be established from this study at different inclinations. The steady state conditions were achieved at different time for different heat input. That's why the following Temperature Vs Heating Time curves for various inclination angles for evaporator, condenser and adiabatic sections are ending at different times.

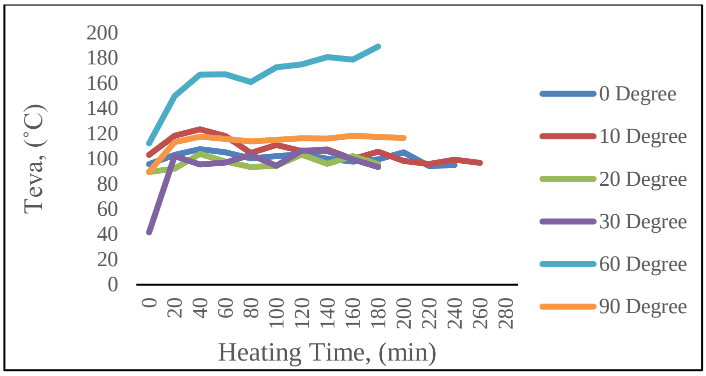

Fig.4.1.1.1: Time variation of evaporator temperature at different inclinations for 40 W heat input at 60% fill ratio.

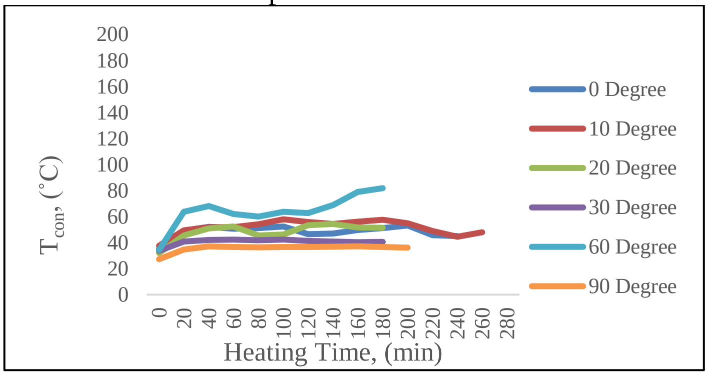

Fig.4.1.1.2: Time variation of condenser temperature at different inclinations for 40 W heat input at 60% fill ratio.

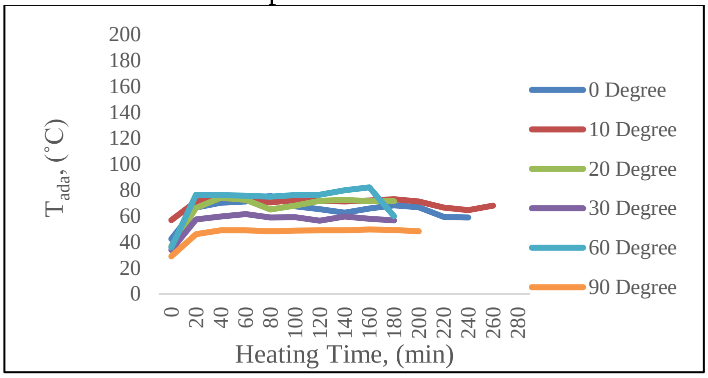

Fig.4.1.1.3: Time variation of adiabatic section temperature at different inclinations for 40 W heat input at 60% fill ratio.

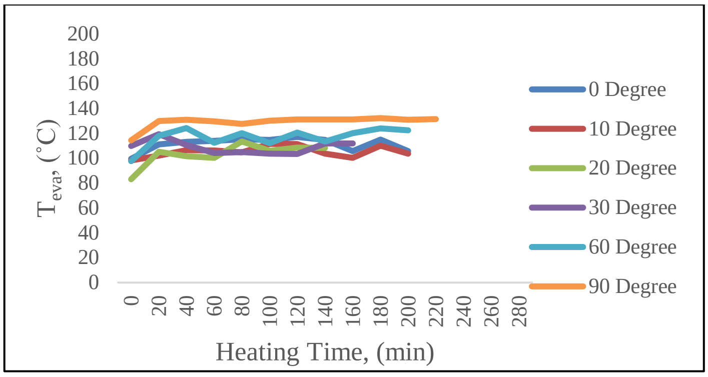

Fig.4.1.1.4: Time variation of evaporatortemperature at different inclinations for 50 W heat input at 60% fill ratio.

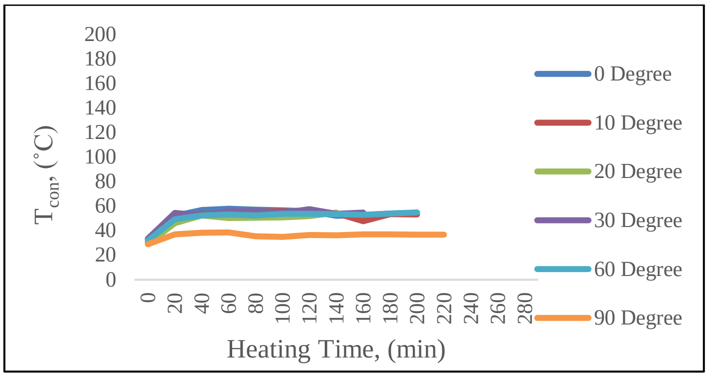

Fig.4.1.1.5: Time variation of condenser temperature at different inclinations for 50 W heat input at 60% fill ratio.

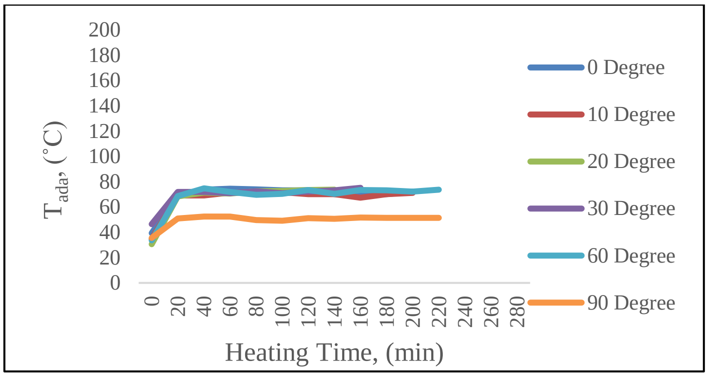

Fig.4.1.1.6: Time variation of adiabatic section temperature different inclinations for 50 W heat input at 60% fill ratio.

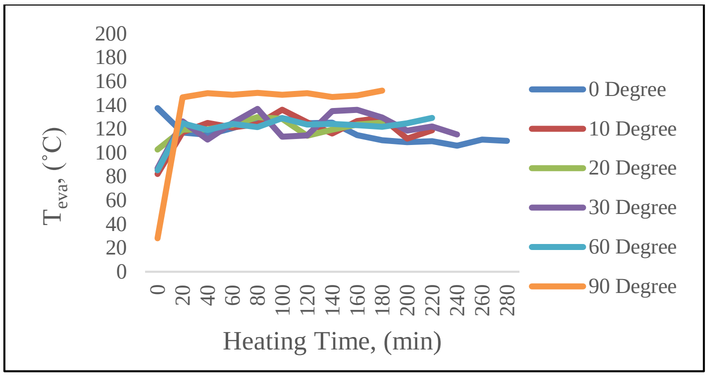

Fig.4.1.1.7: Time variation of evaporator temperature at different inclinations for 60 W heat input at 60% fill ratio.

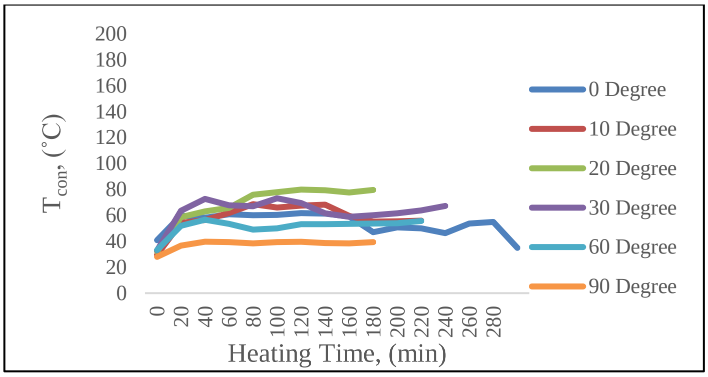

Fig.4.1.1.8: Time variation of condenser temperature at different inclinations for 60 W heat input at 60% fill ratio.

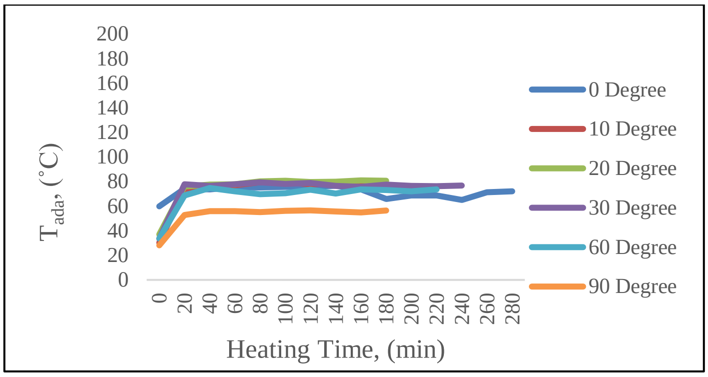

Fig.4.1.1.9: Time variation of adiabatic section temperature at different inclinations for 60 W heat input at 60% fill ratio.

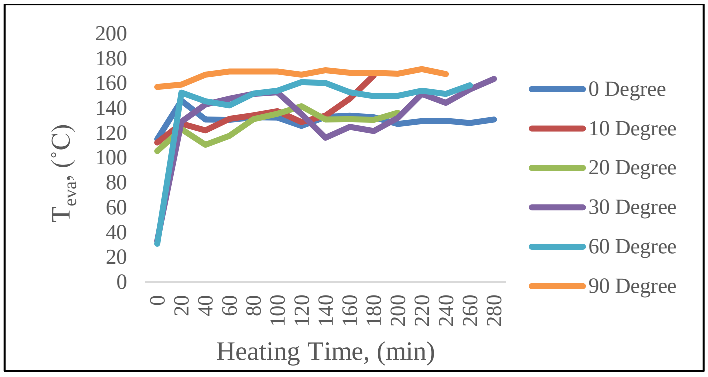

Fig.4.1.1.10: Time variation of evaporator temperature at different inclinations for 70 W heat input at 60% fill ratio.

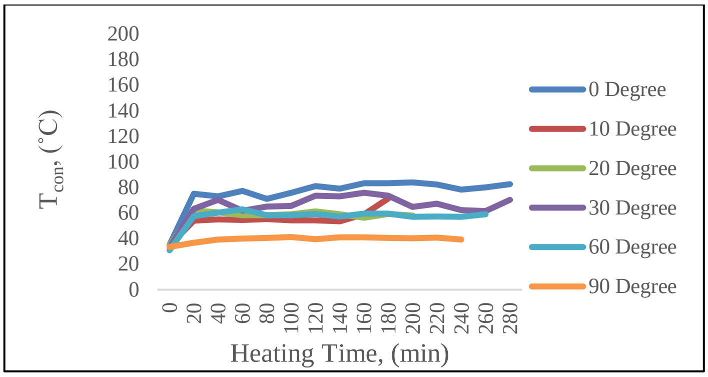

Fig.4.1.1.11: Time variation of condenser temperature at different inclinations for 70 W heat input at 60% fill ratio.

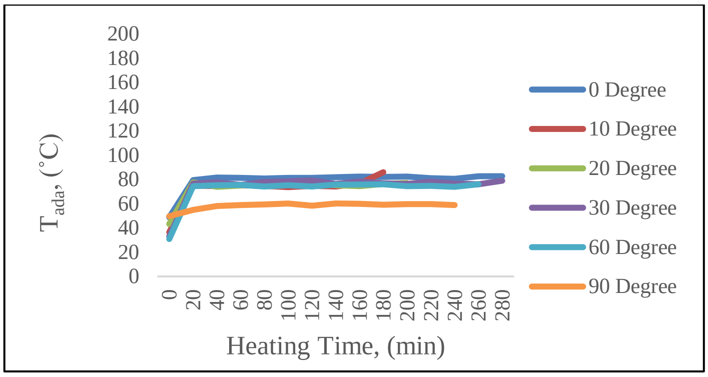

Fig.4.1.1.12: Time variation of adiabatic section temperature at different inclinations for 70 W heat input at 60% fill ratio.

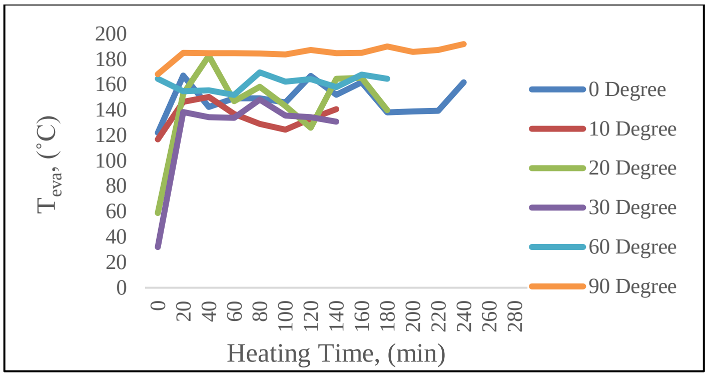

Fig.4.1.1.13: Time variation of evaporator temperature at different inclinations for 80 W heat input at 60% fill ratio.

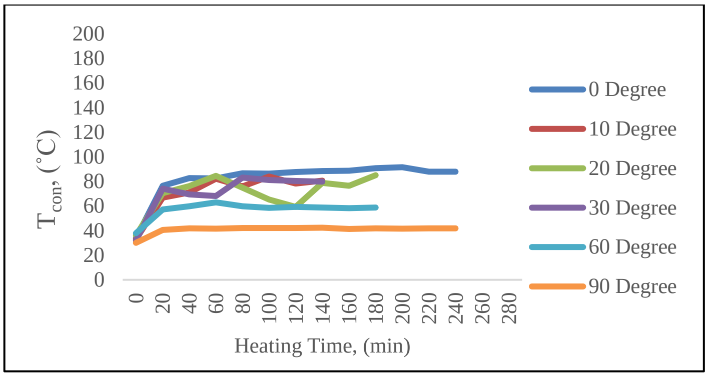

Fig.4.1.1.14: Time variation of condenser temperature at different inclinations for 80 W heat input at 60% fill ratio.

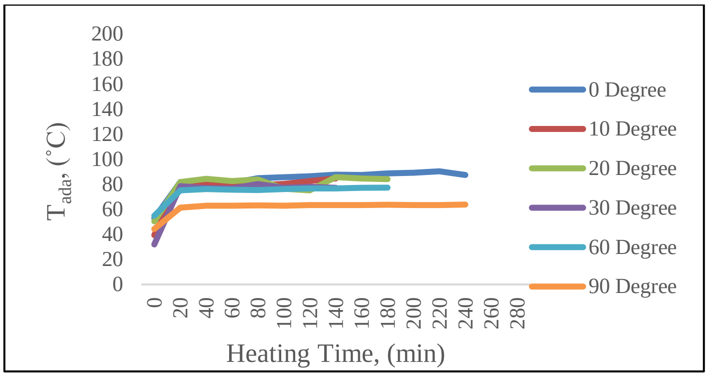

Fig.4.1.1.15: Time variation of adiabatic sectiontemperature at different inclinations for 80 W heat input at 60% fill ratio.

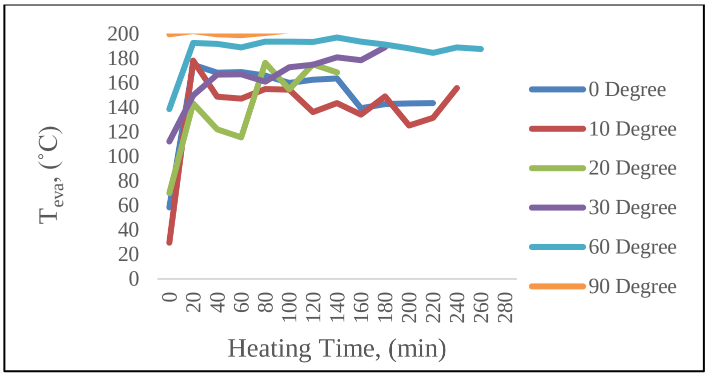

Fig.4.1.1.16: Time variation of evaporator temperature at different inclinations for 90 W heat input at 60% fill ratio.

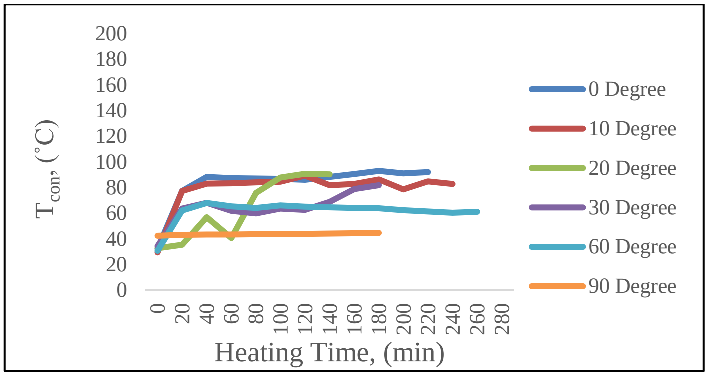

Fig.4.1.1.17: Time variation of condenser temperature different inclinations for 90 W heat input at 60% fill ratio.

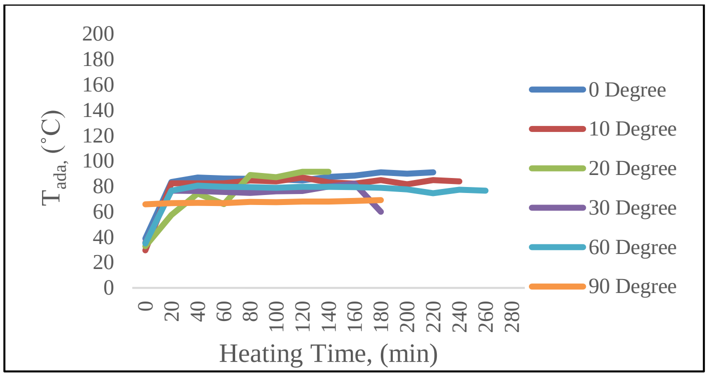

Fig.4.1.1.18: Time variation of adiabatic section temperature at different inclinations for 90 W heat input at 60% fill ratio.

Investigating the graphs from Fig. 4.1.1.1 to Fig. 4.1.1.18, it is found that at very high inclinations, for all the heat loads, the temperature difference between evaporator and condenser sections are very large. This produces lower overall heat transfer coefficient and higher thermal resistances. It is seen that, the temperature curves for lower inclination angles up to 30 Degree are almost adjacent to each other for all heat loads.

There are frequent fluctuations of temperatures in the three sections for higher heat loads crossing 60W. This means, 60W is the critical heat load and beyond 70 W, the system does not come to a steady state condition and there prevails the risk of burning out of the structure. Moreover, it is found that, the three sections temperatures are not straight line or smooth curves. It indicates rapid circulation of fluid throughout the CLPHP.

Graphs for different inclination angles at various heat loads for three sections will be showed in the following figures from Fig. 4.1.1.19 to Fig. 4.1.1.24. The focus of this representation is to find the best suitable inclination angle which can help to enhance diodicity against the gravity.

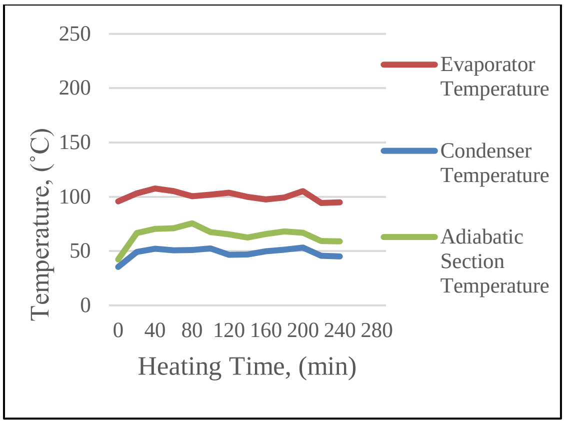

(a) 40W

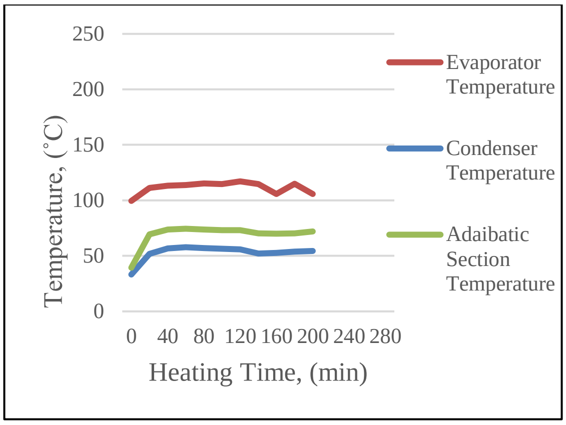

(b) 50 W

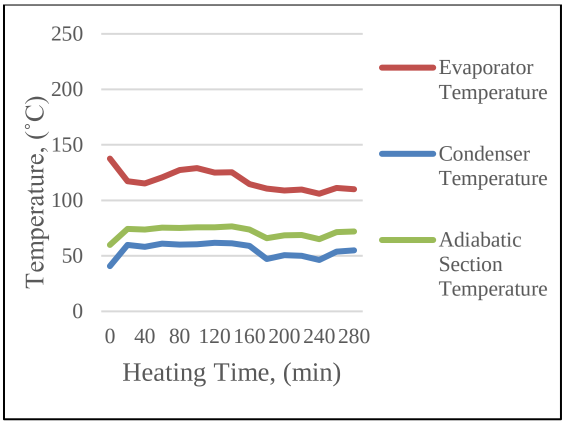

(c) 60W

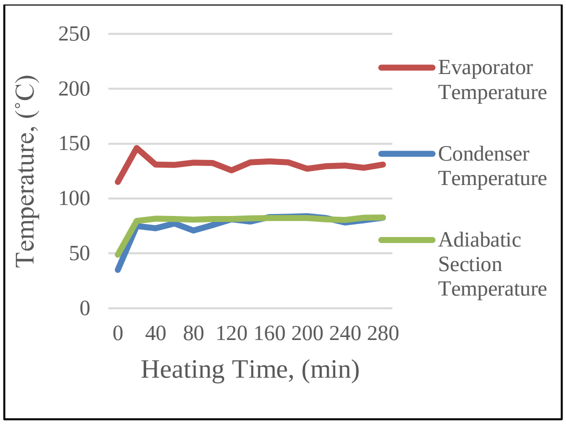

(d) 70 W

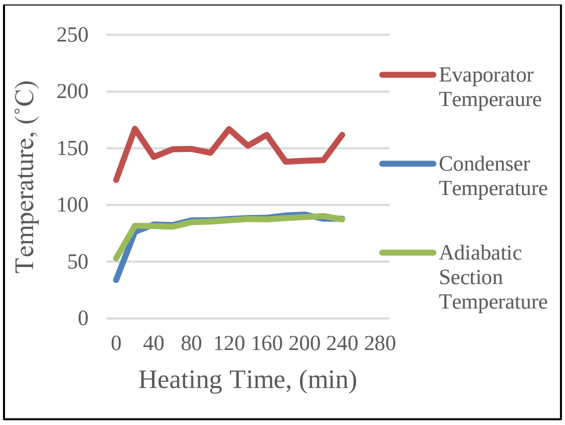

(e) 80W

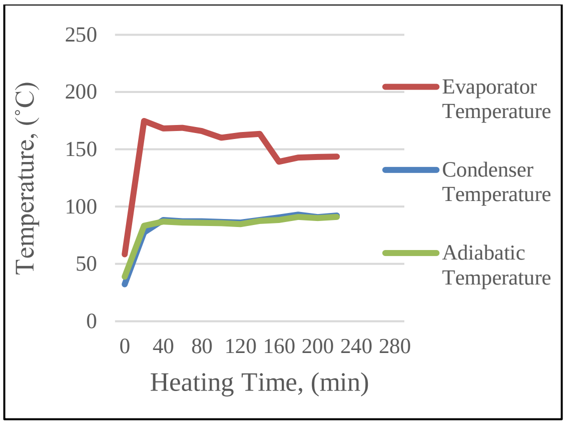

(f) 90 W

Fig.4.1.1.19: Temperature vs heating time of evaporator, condenser and adiabatic section for inclination angle, θ = 0 degree of various heat load at 60 % FR

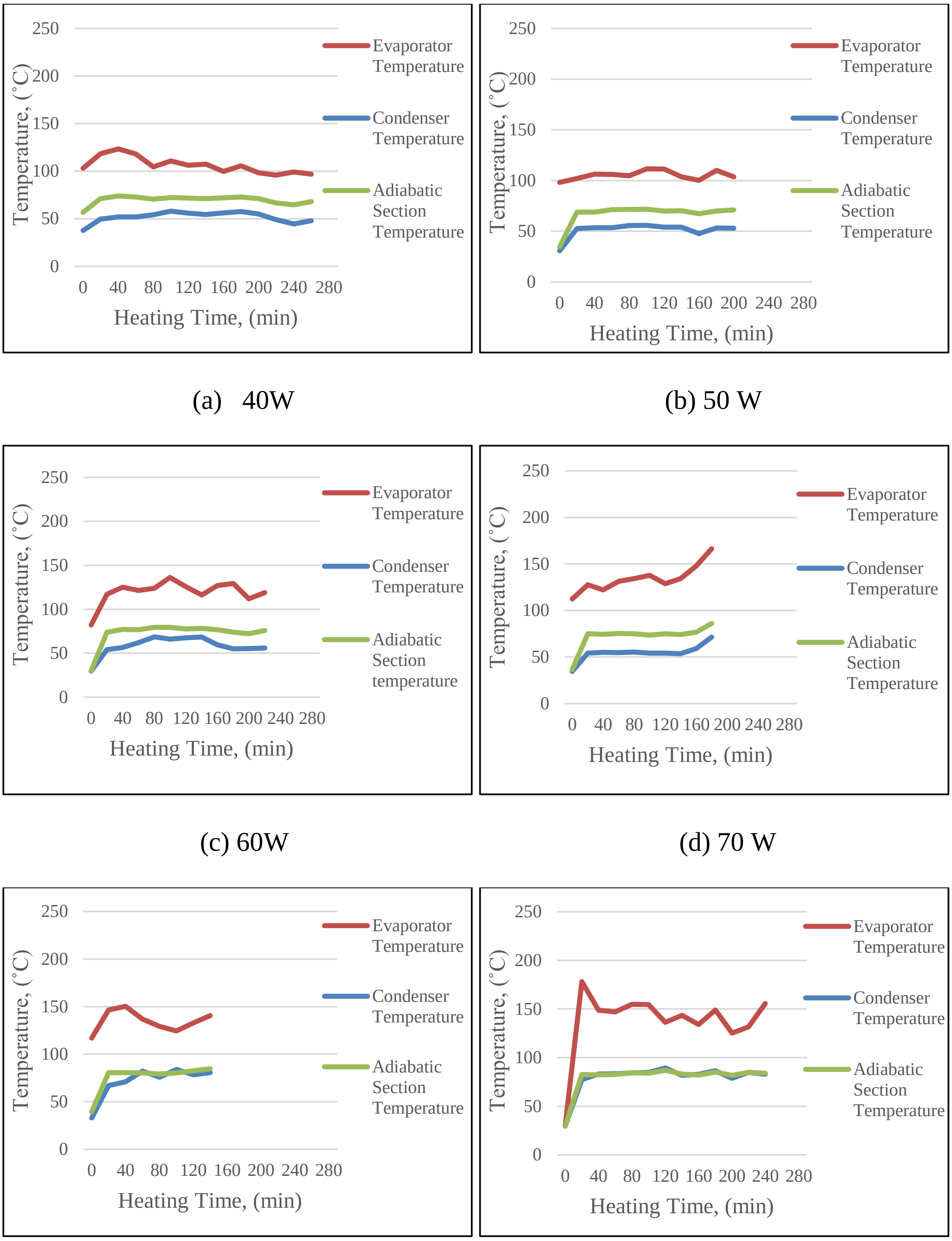

(a) 40W (b) 50 W

(c) 60W (d) 70 W

(e) 80 W (f) 90 W

Fig.4.1.1.20: Temperature vs heating time of evaporator, condenser and adiabatic section for inclination angle, θ = 10 degree of various heat load at 60 % FR

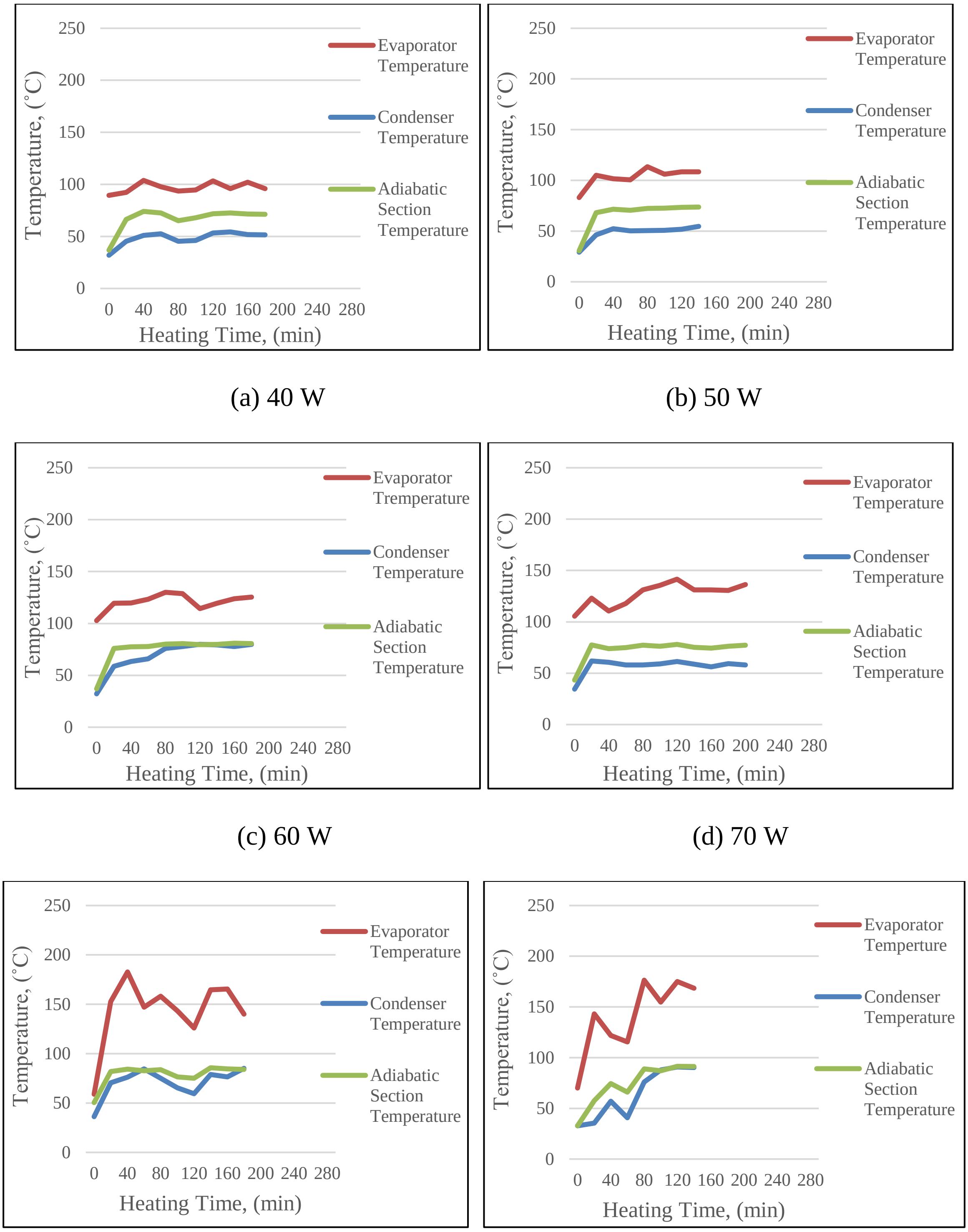

(a) 40 W

(b) 50 W

(c) 60 W

(d) 70 W

(e) 80 W

(f) 90 W

Fig.4.1.1.21: Temperature vs heating time of evaporator, condenser and adiabatic section for inclination angle, θ = 20 degree of various heat load at 60 % FR

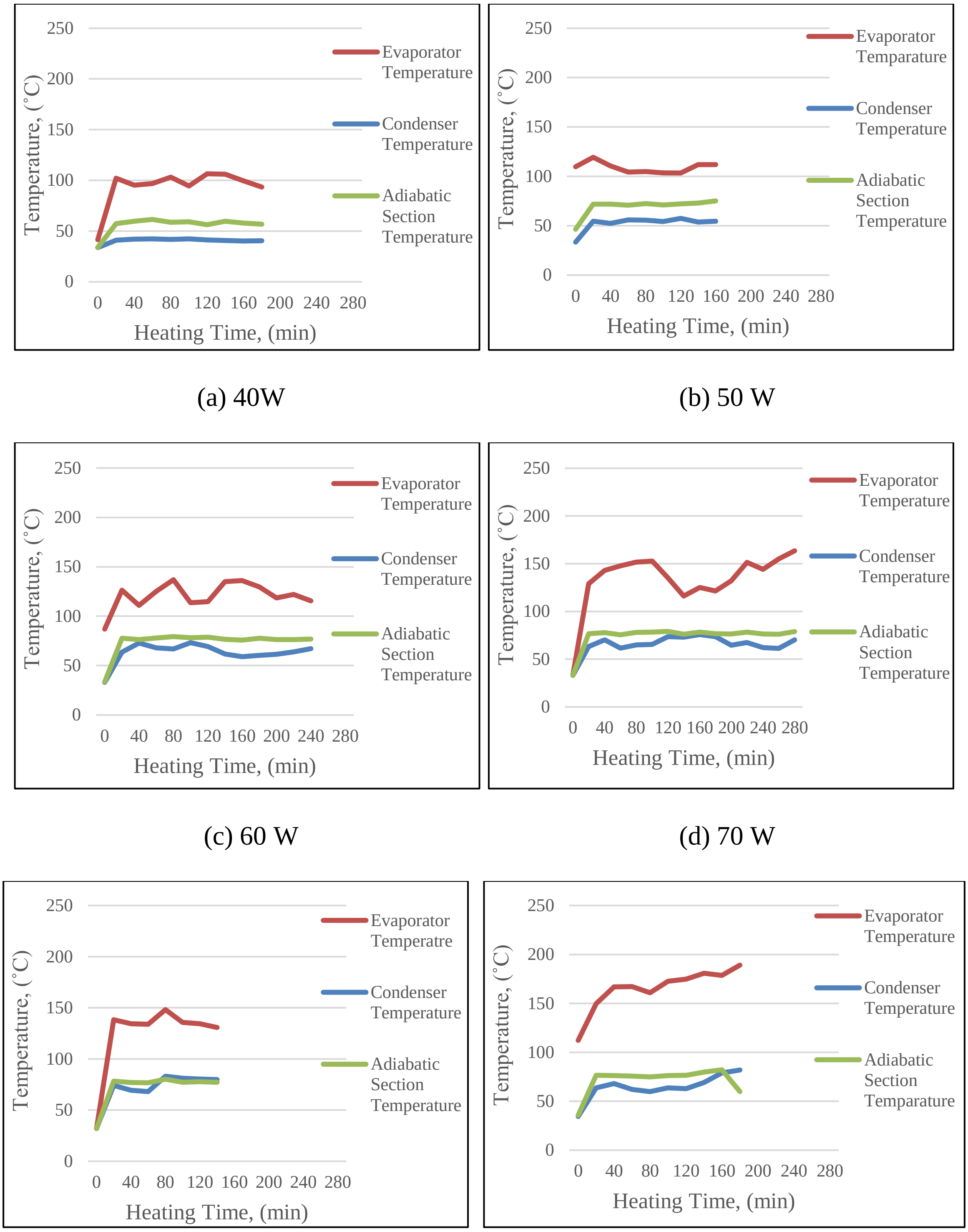

(a) 40W (b) 50 W

(c) 60 W (d) 70 W

(e) 80 W (f) 90 W

Fig.4.1.1.22: Temperature vs heating time of evaporator, condenser and adiabatic section for inclination angle, θ = 30 degree of various heat load at 60 % FR

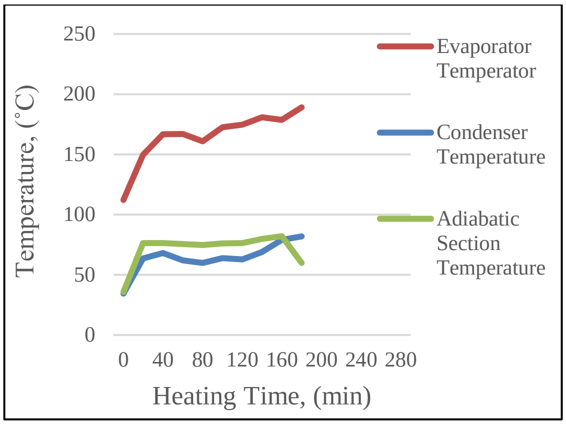

(a) 40 W

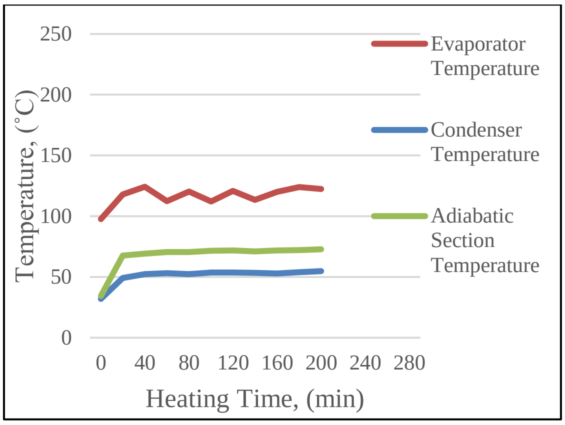

(b) 50 W

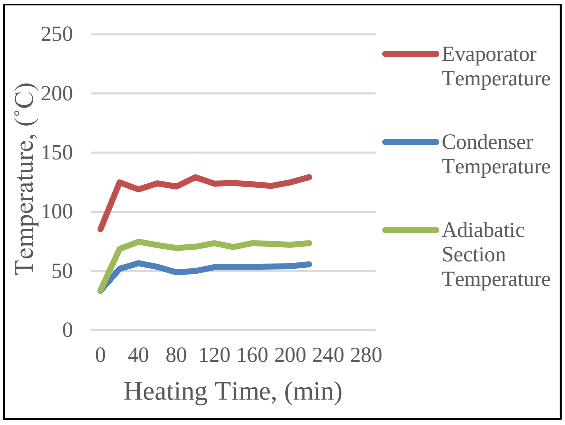

(c) 60 W

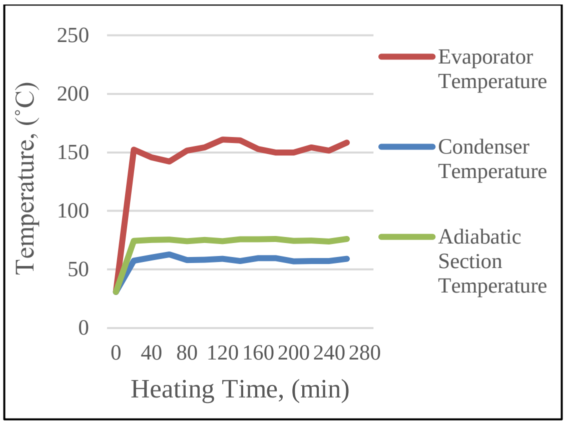

(d) 70 W

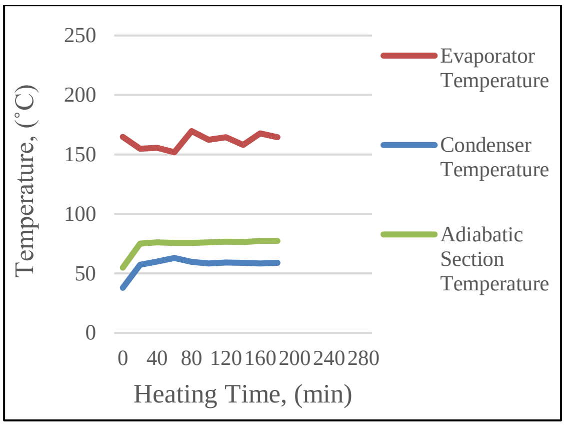

(e) 80 W

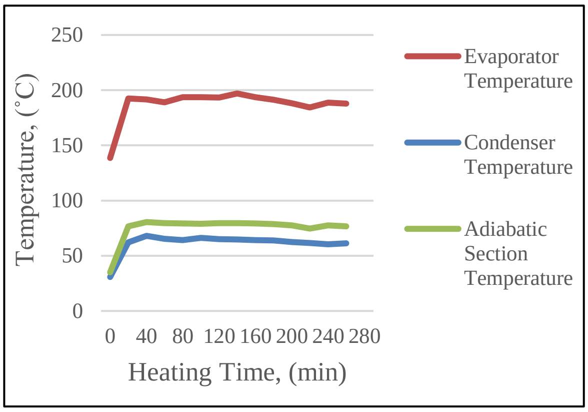

(f) 90 W

Fig.4.1.1.23: Temperature vs heating time of evaporator, condenser and adiabatic section for inclination angle, θ = 60 degree of various heat load at 60 % FR

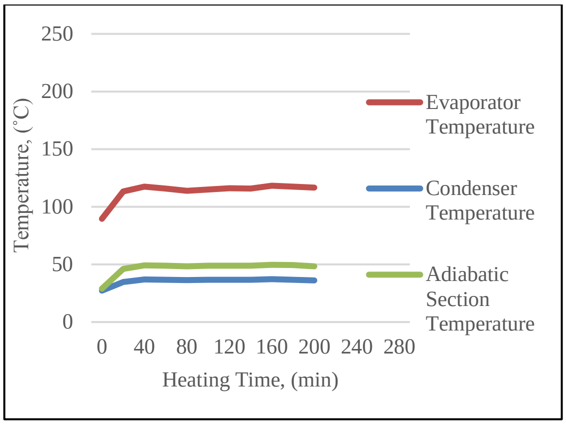

(a) 40 W

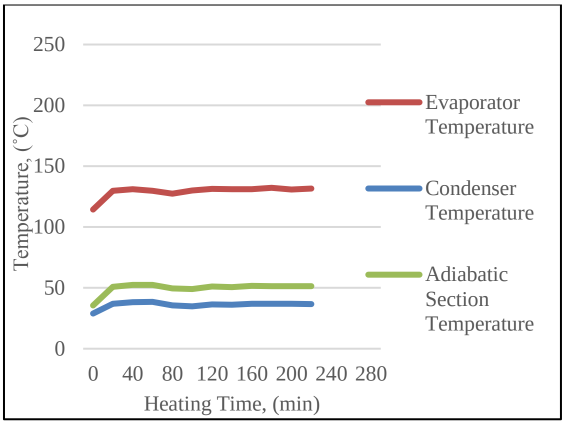

(b) 50 W

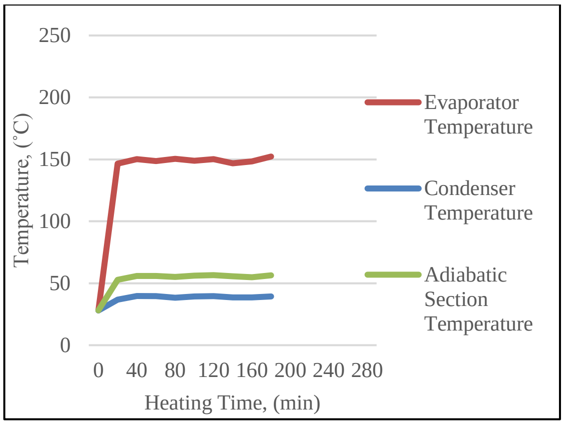

(c) 60 W

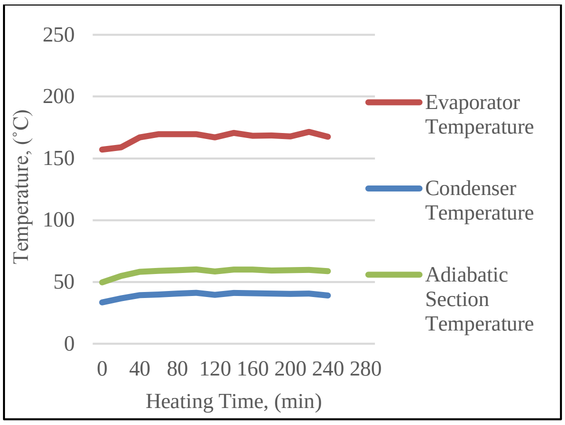

(d) 70 W

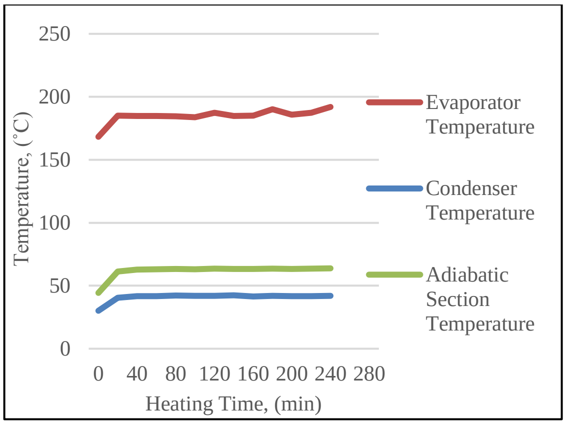

(e) 80 W

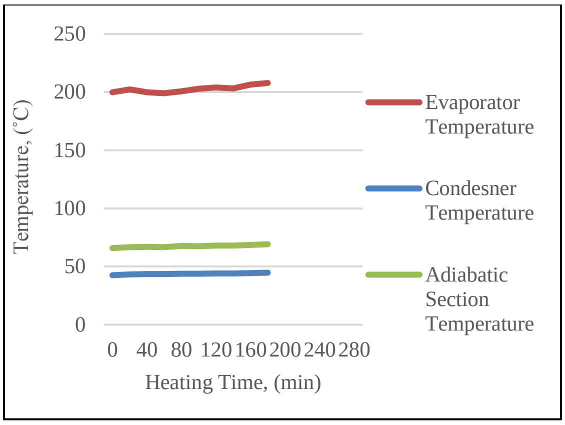

(f) 90 W

Fig.4.1.1.24: Temperature vs heating time of evaporator, condenser and adiabatic section for inclination angle, θ = 90 degree of various heat load at 60 % FR

Form Fig. 4.1.1.19 to Fig. 4.1.1.24 it is evident that, the temperature difference between evaporator and condenser is larger for higher inclinations over 30 Degree. As a result, over

30 Degree inclination, lower overall heat transfer coefficients and higher thermal resistances are found from the experimental data.

It is clearly understandable that, the adiabatic and condenser section temperature curves are adjacent to each other for the cases of lower inclinations up to 30 Degree. For 20 Degree inclination, the graph for 60 W shows almost overlapping of curves of adiabatic and condenser section temperatures.

Analyzing the graphs, it is found that 20 Degree inclination angle produces lowest thermal resistance at the input heat load of 60 W before dry out. The adiabatic and condenser section temperature curves are overlapping each other and it becomes almost continuous straight lines. Inclination angle higher than 30 Degree, almost doesn’t show overlapping tendency of adiabatic and condenser sections. This means, there creates hindrances of transferring heat to the condenser due to the easy mobility of slug-plug flow. As there are more flow restrictions for Tesla type D-valve incorporated CLPHPs than traditional CLPHPs, gravity implies more obstacles with the higher inclinations.

4.1.2 Overall heat transfer coefficient

Overall heat transfer coefficient (HTC) is calculated from individual heat transfer coefficient of evaporator and condenser sections. Due to the increased diodicity, the overall heat transfer coefficient increases which provides better heat transfer from heat source to sink. From the idea of pool boiling regimes against various heat loads, it is found that the curve increases exponentially with the increased heat input as shown in Fig.4.1.2.1 [65]. After reaching a certain heat load, there is a sudden decrease of the overall heat transfer coefficient. This happens due to the phenomenon of dryout. The inside working fluid becomes almost mist. After that, it again starts to increase rapidly and at a very high heat load burnout occurs.

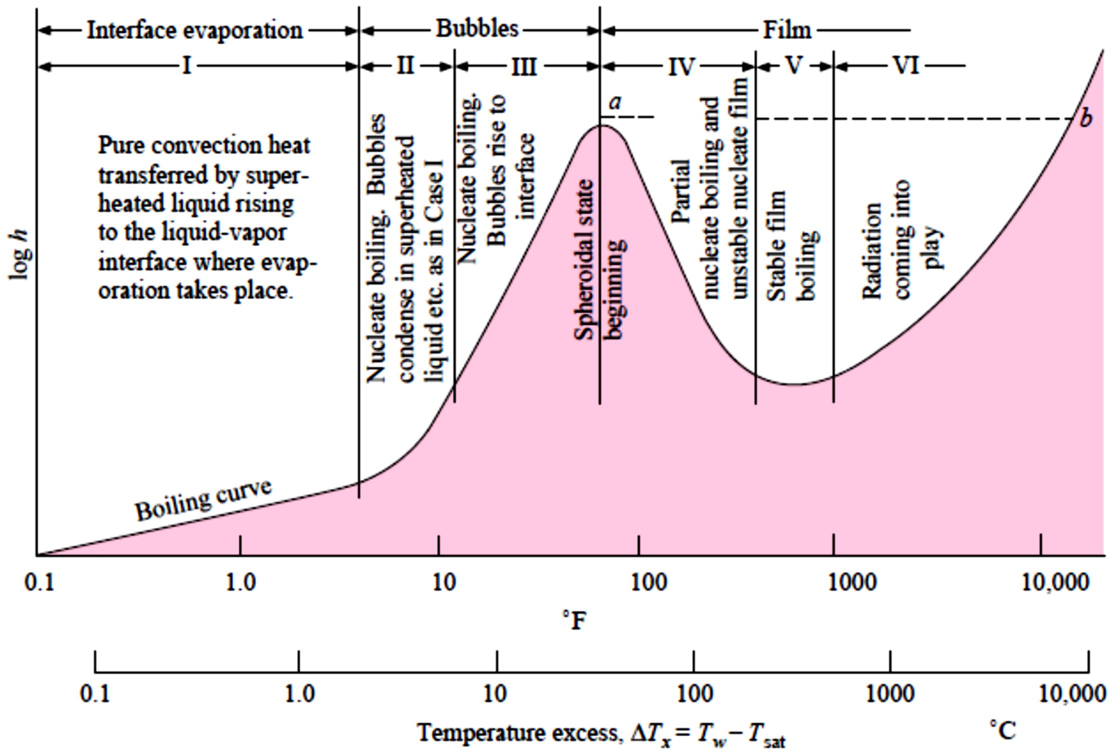

Fig.4.1.2.1: Pool boiling regimes [65]

Following Fig. 4.1.2.2 and Fig. 4.1.2.3 are shown to study the nature of the curves for variation of Overall Heat Transfer Co-efficient (U) with input heat load (Q). From these graphical representations, where founds indications about critical heat load and best suitable inclination angle.

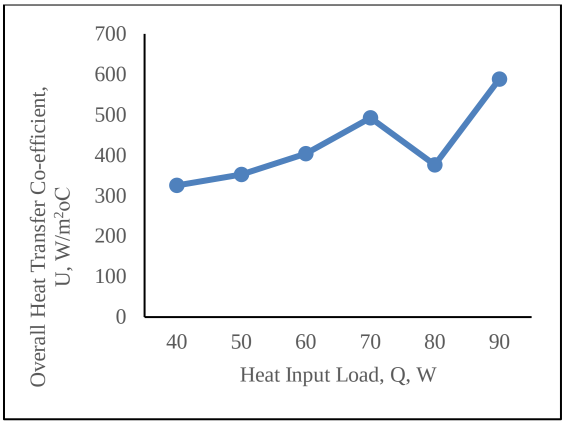

(a) 0 degree inclination angle

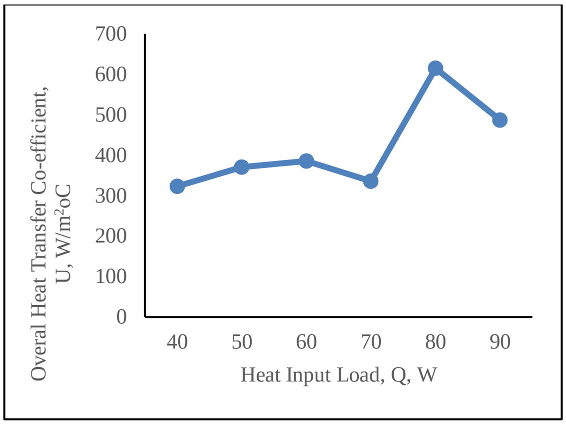

(b) 10 degree inclination angle

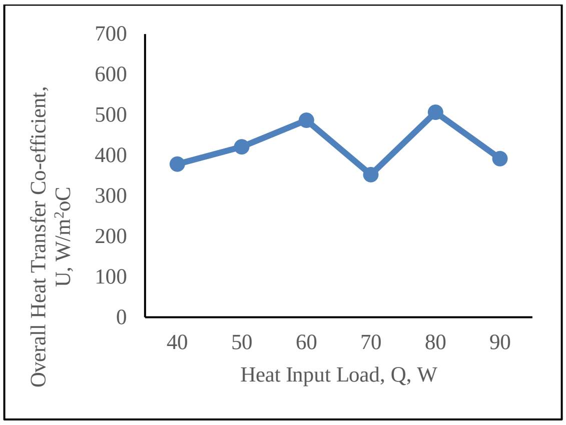

(c) 20 degree inclination angle

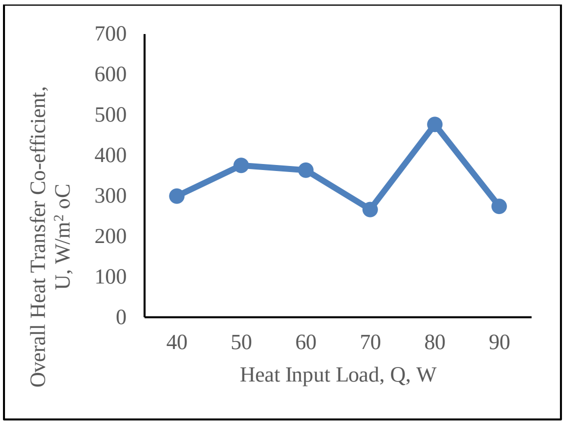

(d) 30 degree inclination angle

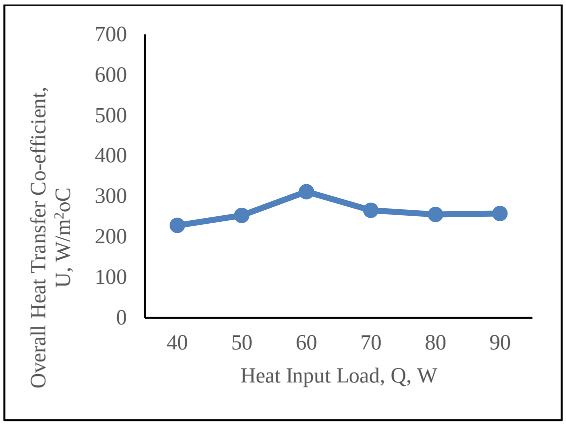

(e) 60 degree inclination angle

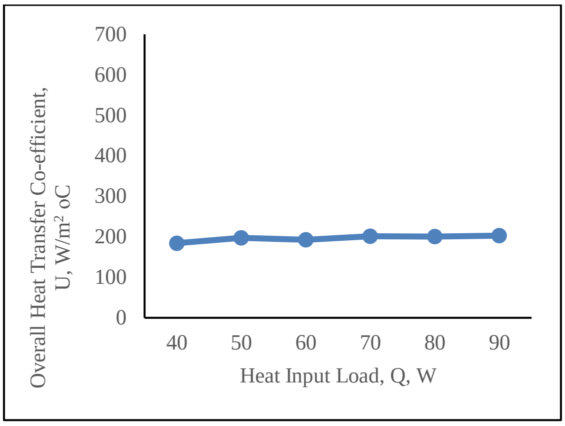

(f) 90 degree inclination angle

Fig.4.1.2.2: Overall heat transfer coefficient, (HTC) vs heat input load (Q) at different inclination angles for 60% fill ratio

From Fig. 4.1.2.2 (a) to (f) it is evident that the curves are following the trend of boiling heat transfer curve. At vertical condition (0˚), the critical heat input is 70 W. When it is fully horizontal (90˚), the critical value is found at 50 W. In case of vertical position (inclination angle = 0 Degree), almost all the fluid remains in the evaporator section that it can produce large critical heat flux to vaporize bulk mount of fluid. Contrary to this, at the horizontal position (inclination angle = 90 Degree), there creates a deficiency of liquid working fluid and dryout occurs at a comparatively lower heat input. In between these two positions, 60 W has been proven as the critical heat input load condition.

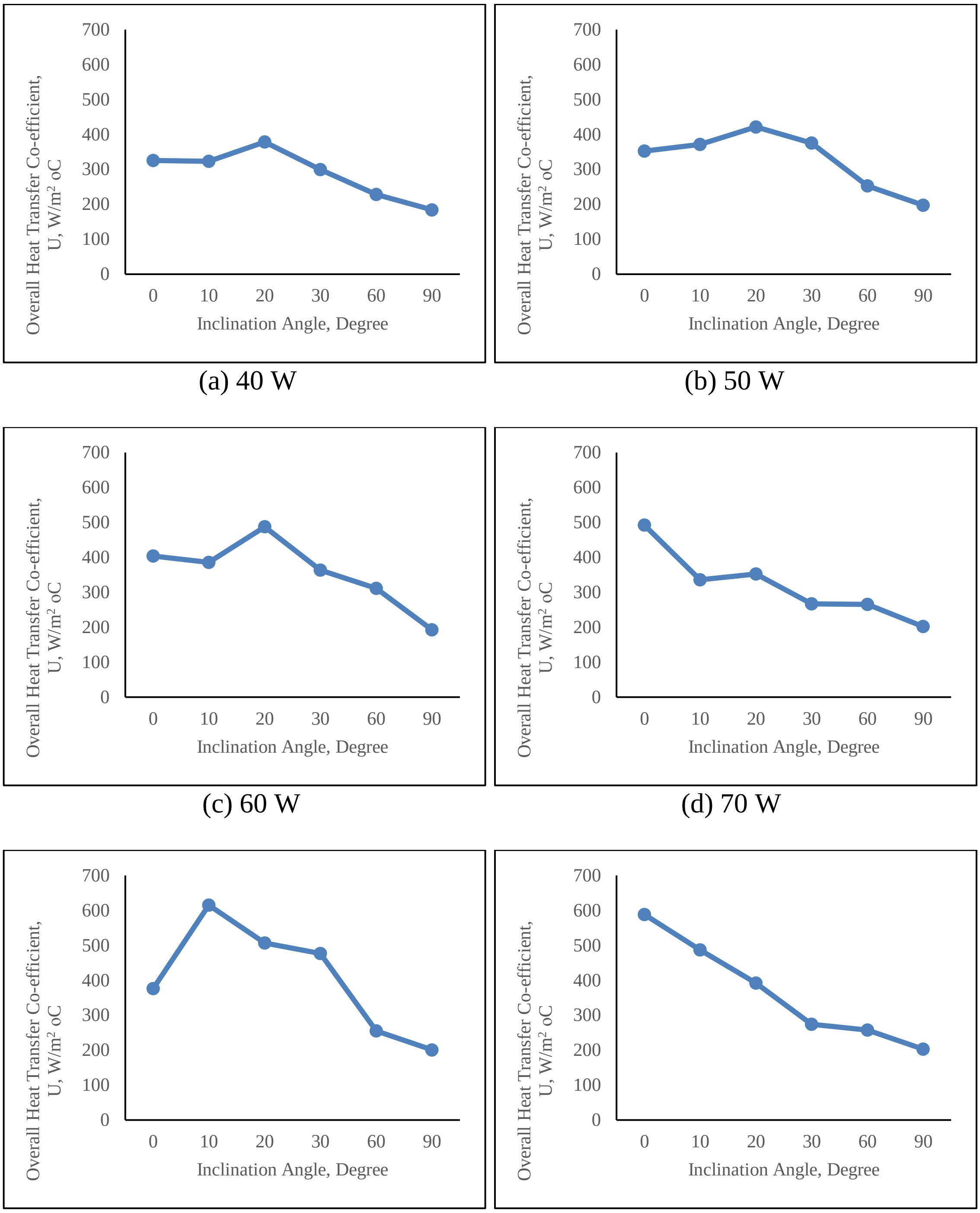

(a) 40 W (b) 50 W

(c) 60 W (d) 70 W

(e) 80 W (f) 90 W

Fig.4.1.2.3: Overall heat transfer coefficient (HTC) vs inclination angles at different heat load for 60% fill ratio

Fig.4.1.2.3 (a) to (f) shows the graphs for Overall Heat Transfers Coefficient against various inclination angles. These graphs give the information that, below 70 W, 20 Degree inclination provides the maximum Overall Heat Transfer Coefficient. Beyond 20 Degree inclination, there produces more restrictions in the flow due to gravity as well as geometrical shape of Tesla type D-valve. Thus, the value of Overall Heat Transfer Coefficient (HTC) decreases. At 70 W, vertical position (inclination angle = 0 Degree), shows maximum value of HTC than all other positions. As described in the above paragraph, at vertical position, presence of maximum working fluid in the evaporator can produce larger critical heat flux. Also, it is visible that, in between horizontal and vertical position, 20 Degree inclination can produce maximum Overall Heat Transfer Co-efficient at 60 W. After 60 W, there prevails a condition of excess chaos which leads no steady state condition inside the CLPHP. At 90 W, it finds a higher value of HTC at vertical position because due to this large value of heat load, the bulk fluid can acquire mobility. Contrary to this, as there is a deficiency of working fluid in the evaporator in horizontal position (inclination angle = 90 Degree), the evaporator surface had to take excess heat load that creates very poor value of Overall Heat Transfer Coefficient.

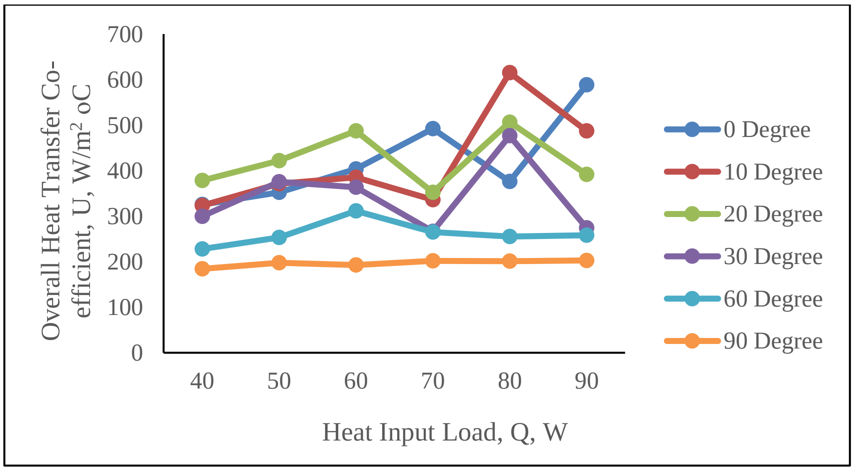

Fig.4.1.2.4: Overall heat transfer coefficient (HTC) vs various heat input load at various inclination angles for 60% fill ratio

Fig. 4.1.2.4 shows a comparison of Overall Heat Transfer Coefficient against various heat loads for different inclination angles. From the behavior of temperature values, it was found that beyond 70 W the temperatures do not provide steady state result. This is why 60 W and below input heat loads are safer options for this CLPHP setup. From the Fig. 4.1.2.4, it is visible that 60 W is producing maximum Overall Heat Transfer Co-efficient within safer limit. It is also evident from the Fig. 4.1.2.4 that, after surpassing 30 Degree inclination angle, there produces poor results for Overall Heat Transfer Coefficient. This phenomenon indicates 60W and 20 Degree inclination angle can produce best result.

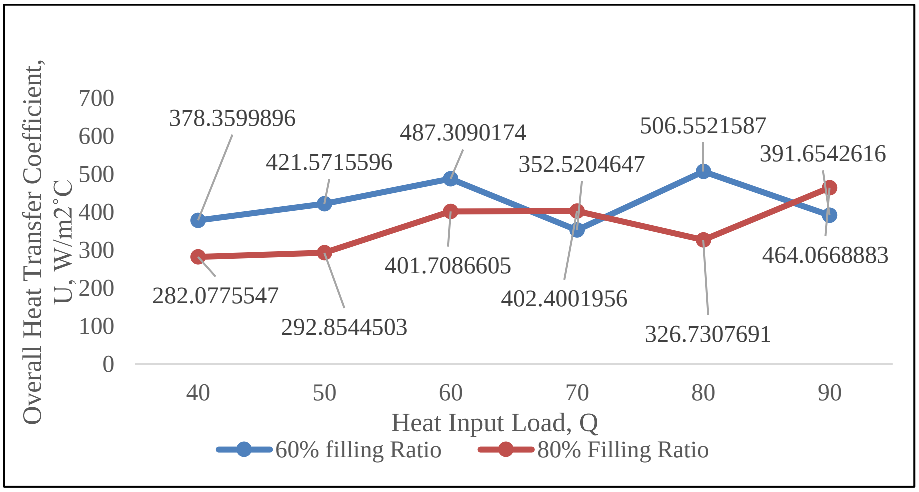

Fig.4.1.2.5: Comparison of overall heat transfer coefficient vs heat input load at 60% and 80% filling ratios at 20-degree inclination angle.

The Fig. 4.1.2.5 shows that, 60% filling ratio can produce maximum overall heat transfer coefficient than 80% filling ratio. This means, 60% filling ratio can deliver more amount of heat from evaporator to condenser.

4.1.3 Thermal resistance

Thermal resistance (R) is the ratio between temperature difference of evaporator and condenser sections and the input heat load. Higher thermal resistance indicates lower performance of a CLPHP. Because it creates hindrances to deliver the heat from evaporator to condenser section. This parameter can be increased due to the increased flow restrictions, production of excess vapor bubble, deficiency of vapor bubble, gravitational impacts etc.

The following Fig. 4.1.3.1 and Fig. 4.1.3.2 will show graphs depicting the curves showing thermal resistances against various heat load and thermal resistance compared to different inclinations respectively. Analyzing these figures, the decision about critical heat input and best suited inclination angle can be reestablished for lowest thermal resistance obtained from the present study.

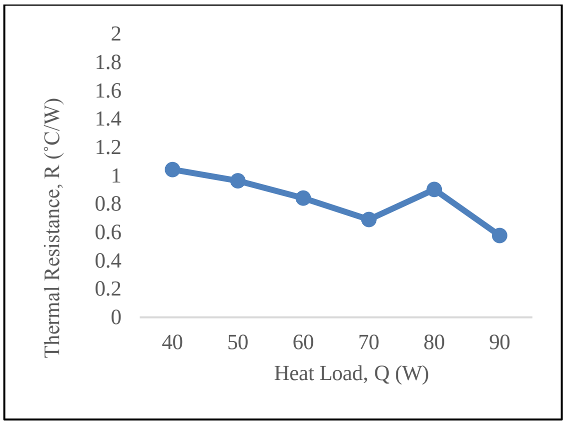

(a) 0 degree inclination angle

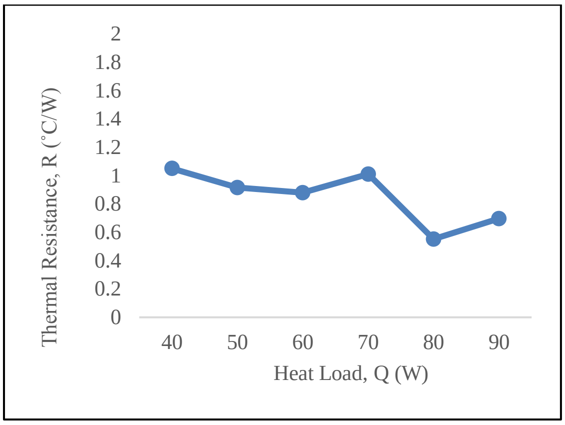

(b) 10 degree inclination angle

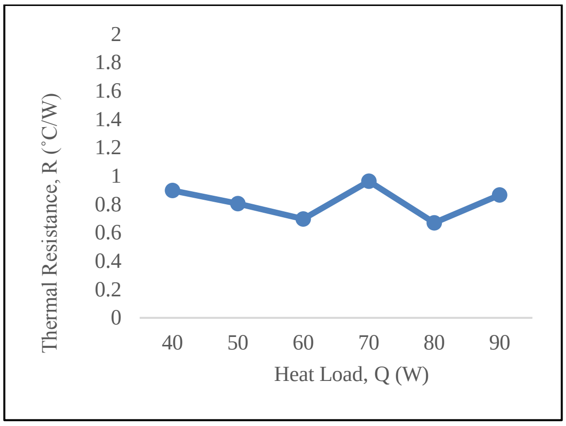

(c) 20 degree inclination angle

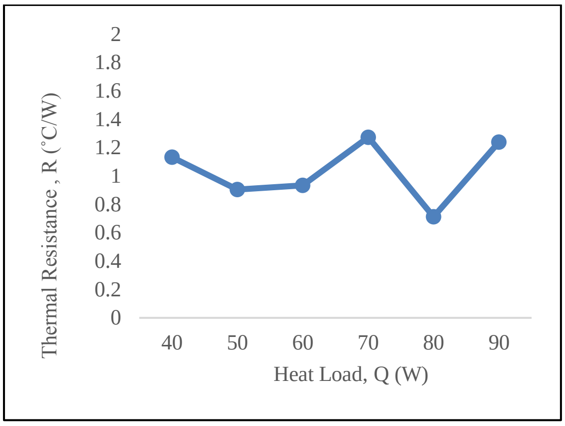

(d) 30 degree inclination angle

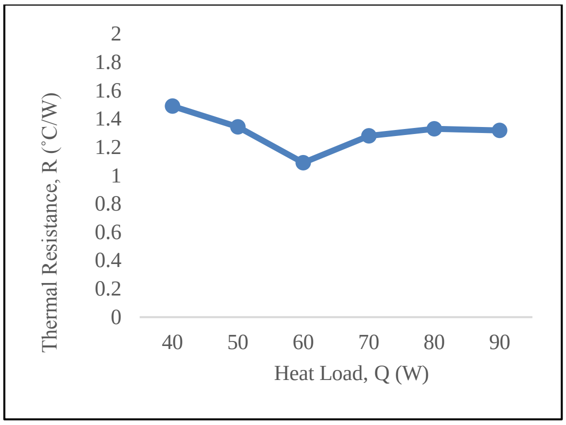

(e) 60 degree inclination angle

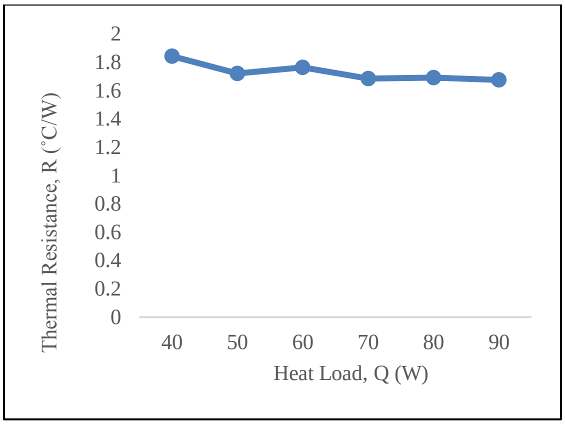

(f) 90 degree inclination angle

Fig.4.1.3.1: Thermal resistance vs heat load at various inclination angles for 60% fill ratio

From the Fig. 4.1.3.1 (a) to (f), it is found that, at vertical position (0 Degree inclination angle), the thermal resistance is lowest at 70W. Due to bulk amount of fluid in the evaporator, it needs more heat to produce fluid motion. In between vertical and horizontal position, after 70W input heat load the system does not come to a steady state. So, among the range of steady state heat input conditions (40W-70W), 60W shows lowest thermal resistances in between vertical and horizontal inclinations. At horizontal position (90 Degree inclination angle), the highest value of thermal resistance is found out at 50W due to lack of working fluid in evaporator. So, 60W is advised to be the suitable operating input heat load for the device basing on lower thermal resistance values.

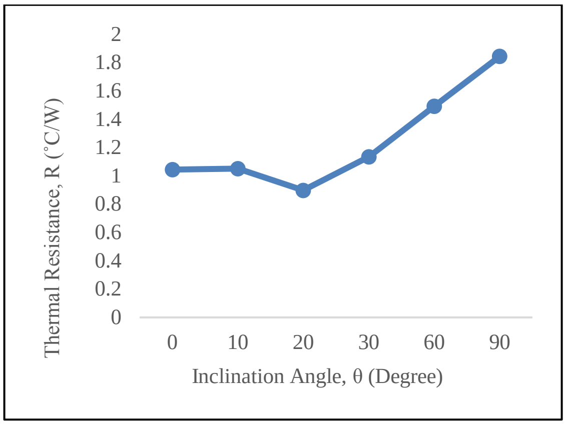

(a) 40W

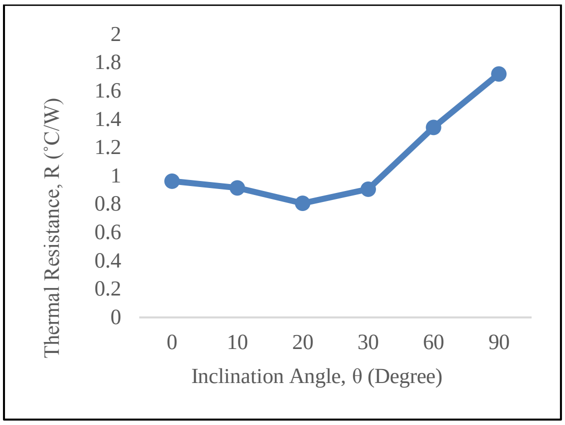

(b) 50W

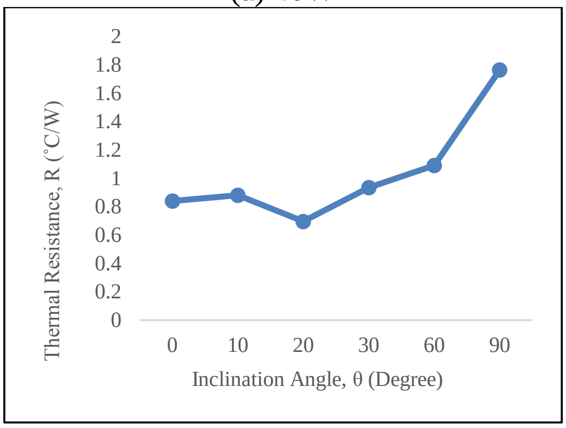

(c) 60W

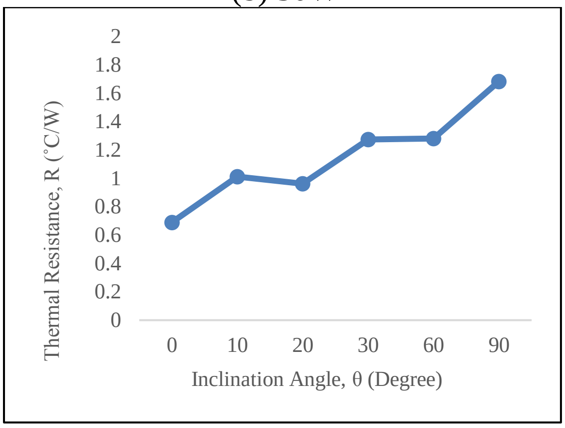

(d) 70W

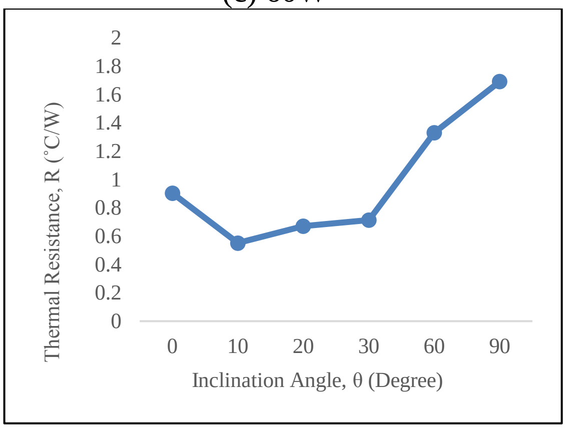

(e) 80W

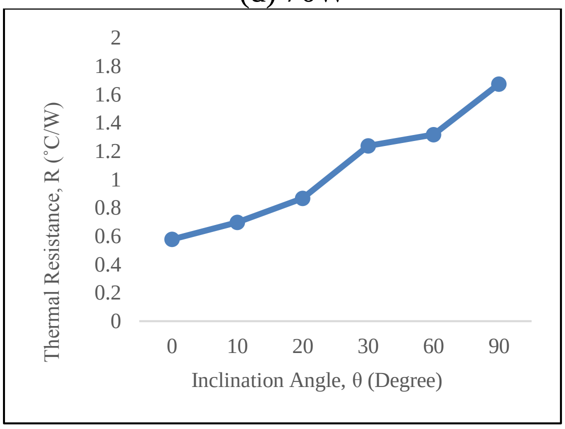

(f) 90W

Fig.4.1.3.2: Thermal resistance vs inclination angle at various heat load for 60% fill ratio.

Studying Fig. 4.1.3.2 (a) to (f) it is evident that 20˚ inclination angle produces lowest thermal resistance before 70 W input heat load. After 70W, the system does not come to a steady state. Though, at 70 W, vertical position (0 Degree inclination angle) can show lowest thermal resistance, 60 W has produced much decreased thermal resistance comparing to other inclinations. At a very high heat load of 90 W, again vertical position (0 Degree inclination angle) produces lowest thermal resistance due to bulk amount of fluid presence in the evaporator. In contrary to this due to lack of working fluid, horizontal position (90 Degree inclination angle) shows highest thermal resistances for all the input heat loads. So, it is suggested to operate the system at 20 Degree inclination angles that can produce much lower thermal resistances irrespective of heat input loads.

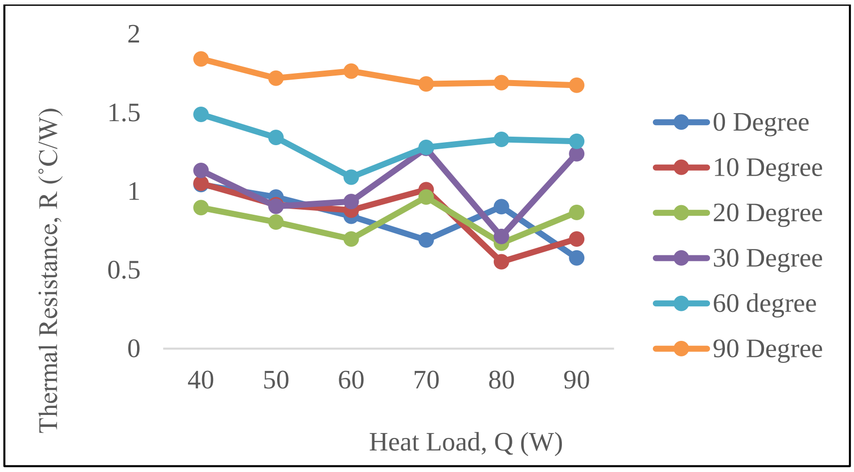

Fig.4.1.3.3: Thermal resistance vs various heat load at various inclination angles for 60% fill ratio

Thermal resistance and Overall Heat Transfer co-efficient are in a reciprocal relation. According to this condition, Fig. 4.1.3.3 follows the same trend of Fig. 4.1.2.4. as inclination angle 20˚ produces lowest thermal resistances up to 70W heat input comparing to all other inclinations. 10 Degree and 30 Degree inclinations are almost showing very close relation before critical loading. On the other hand, 60 W shows much lower thermal resistances irrespective to all inclinations. At the end, it can be suggested that, 60W and 20 Degree inclination will produce best result for this CLPHP.

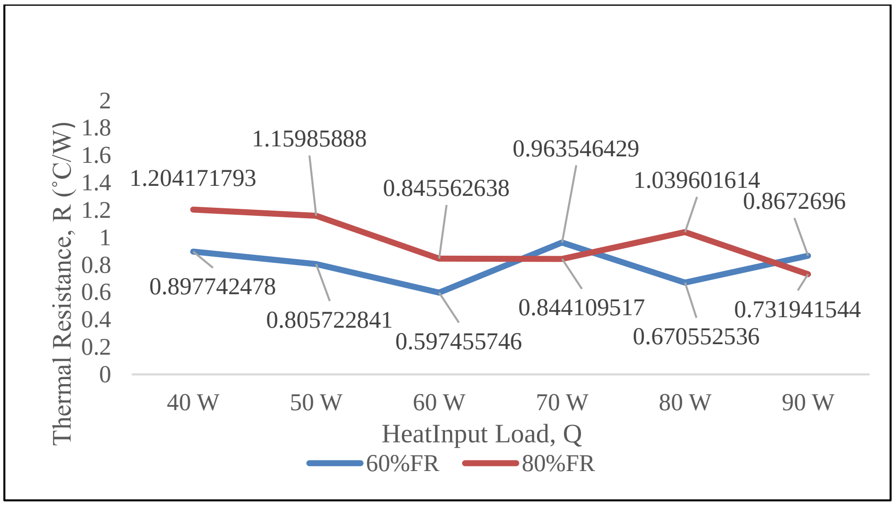

Fig.4.1.3.4: Comparison of thermal resistance vs various heat input load at 60% and 80% fill ratio at 20-degree inclination angle.

Fig. 4.1.3.4 shows the comparison of thermal resistance between 60% and 80% filling ratios at different heat loads at 20 Degree inclination angle. It is visible that, 60% filling ratio produces lowest thermal resistances. Also, it should be noted that temperature values fluctuate more in 80% filling ratio and the temperature in condenser is too high. As shown in Fig. 4.1.3.4, this phenomenon happens at 80% filling ratio due to the lack of vapor bubbles inside the alternating turnings.

4.2 Verification

Verification is the process of satisfying a set of data with existing other theoretical processes. There have been a wide range of mathematical correlations available in the field of CLPHP. The correlations have been tried to verify for the experimental data obtained in this research. Later on, comparative study will be carried out for finding best suitable correlations.

4.2.1 Theoretical mathematical modeling analysis

Chen correlation

In the year of 1962, John C. Chen [66] proposed a correlation for predicting heat transfer coefficient for boiling to saturation heat transfer condition. This equation was developed having the intension to analyze two phase heat transfer. The final equation comprises of two parts. One part is calculating the phase change heat transfer coefficient where the other is finding the boiling heat transfer coefficient.

Total 594 experimental data points had been analyzed for ordinary fluid as water, methanol, benzene, heptane, pentane etc. Studying the regime of annular or annular mist flow, the heat transfer process comprised of micro and macro convective mechanism. Micro convective contribution to the heat transfer was derived from Froster and Zuber for pool boiling correlation whereas Dittus-Boelter type correlation was formulated to account for the macro convective influence. A graph for showing the comparison of heat transfer coefficient between this new correlation with the experimental values are showed in the Fig. 4.2.1.1.

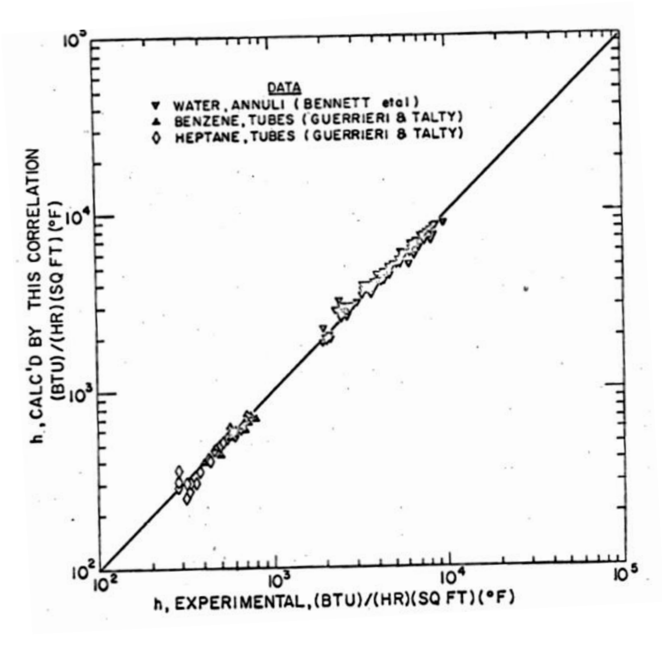

Fig.4.2.1.1: Heat transfer co-efficient from Chen correlation vs experimental values [66]

<table>
<tr><th>Reference</th><th>Correlation</th><th>Applicability Range</th></tr>
<tr><td rowspan="6">Chen Correlation [66]</td><td>Two Phase Heat Transfer Co-efficient,
$$h_{tp} = Sh_{F-Z} + Fh_L$$</td><td rowspan="6">Water, methanol, cyclohexane, pentane, heptane, benzene (594 data points)
Vertical upward and downward flow in tubes and annuli
Pressure range of 1–34.8 bar
Liquid inlet velocity range of 0.06–4.5 m/s
Vapor quality range, x= 0.01–0.71
Heat flux range of 6.2–2400 kW/m^2</td></tr>
<tr><td>Liquid Heat Transfer Coefficient,
$h_L = 0.023Re_L^{0.8}Pr_L^{0.4}\frac{K_L}{D}$, $Re_L = \frac{(1-x)GD}{\mu_L}$</td></tr>
<tr><td>Phase Change Heat Transfer Coefficient,
$$h_{F-Z} = 0.00122\frac{K_L^{0.79}C_{PL}^{0.45}\rho_L^{0.49}}{\sigma^{0.5}\mu_L^{0.29}h_{fg}^{0.2}\rho_v^{0.24}}(\Delta T)^{0.24}(\Delta P)^{0.75}$$</td></tr>
<tr><td>Convective Boiling Factor,
$$F = \begin{cases} 1 & \frac{1}{X_{tt}} \leq 0.1 \\ 2.35(0.213 + \frac{1}{X_{tt}})^{0.736} & \frac{1}{X_{tt}} > 0.1 \end{cases}$$</td></tr>
<tr><td>Martinelli Parameter, $X_{tt} = (\frac{1-x}{x})^{0.9}(\frac{\rho_v}{\rho_L})^{0.5}(\frac{\mu_L}{\mu_v})^{0.1}$</td></tr>
<tr><td>Suppression Factor,
$S = \frac{1}{1+0.00000253Re_{tp}^{1.17}}$, $Re_{tp} = Re_L F^{1.25}$</td></tr>
</table>

Table 4.2.1.1: Details of Chen correlation

This correlation can predict the data from total nine experimental arrangement with a Mean Absolute Error (MAE) of 11% only for water and all other organic fluids. The correlation is shown in Table 4.2.1.1b in details. The final equation is formulated by considering phase change heat transfer coefficient, h_{F-Z} and convective heat transfer coefficient, h_L.

Mahmoud and Karayiannis correlation

In the year 2012, Mahmoud and Karayiannis [67] published their proposed equation due to the failure of predicting heat transfer coefficient using previously available equations. They ran the experiment for R134a inside vertical stainless-steel tubes with varying diameters.

The authors focus was to identify Nusselt number from various dimensionless groups. Nusselt number represents the convection to conduction heat transfer at a boundary of liquid Theoretically they studied over six dimensionless groups such as liquid Reynolds number (Re), Boiling number (B_O), all liquid Weber number (We), Confinement number (C_O), Martinelli parameter (X_{tt}) and Convective number (N_{co}). Total 5152 experimental data points had been analyzed separately for checking the dependence of each dimensionless group. The final equation was formed to find calculate Nusselt number where the dependence constant was found by using the Multiparameter Non-Linear Least Square fitting (Multi-X MLSF). The graph for comparing the theoretically predicted heat transfer coeffect with that of experimental is shown in the Fig.4.2.1.2 below.

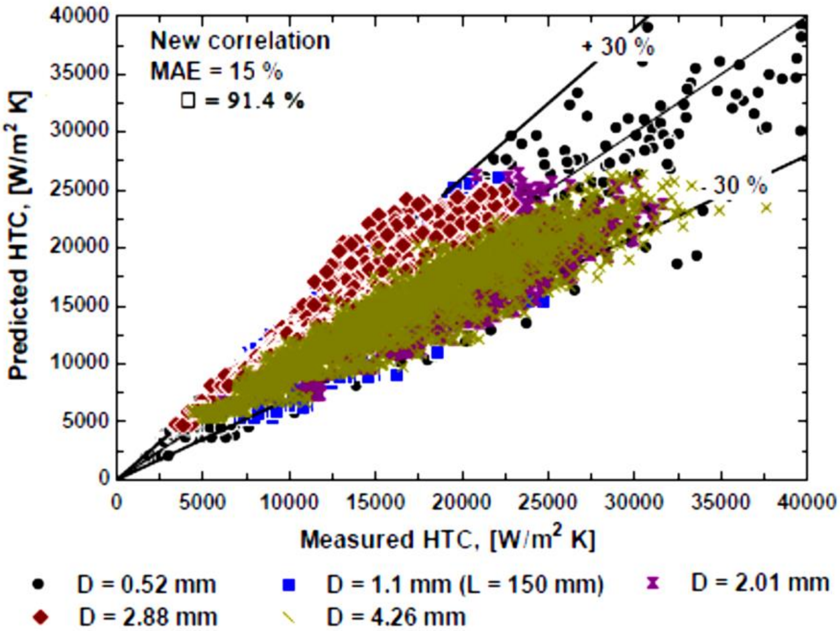

Fig.4.2.1.2: Global comparison with the new correlation [67]

This correlation could predict 91.4% data within ±30% error bandit a Mean Absolute Error (MAE) of 15%. The details of this correlation are provided in the Table 4.2.1.2 below. The first part of the equation is for higher diameter tubes whereas the bottom one is for very thin diameter cases.

Reference	**Correlation**	**Applicability Range**
Mahmoud and Karayiannis Correlation [67]	Two-phase Heat Transfer Coefficient, $\alpha_{tp} \begin{cases} 3320 \frac{B_0^{0.63} We^{0.2} Re_f^{0.11}}{C_0^{0.6}} \frac{K_L}{D} & \text{For D = 4.26, 2.88, 2.01, 1.1 before dryout and 0.52mm} \\ 5324 [\frac{B_0^{0.3} We^{0.25}}{N_{Co}^{0.25}}]^{1.79} \frac{K_L}{D} & \text{For 0.52mm and x>0.3} \end{cases}$ Convective Number, $N_{Co} = (\frac{1-x}{x})^{0.8} (\frac{\rho_g}{\rho_L})^{0.5}$	Total data=7532 Inner Diameter, D = 4.26 – 0.52 mm, Mass Flux, G = 100 – 500 kg/m^2 s Working Pressure, P = 6 – 14 bar

Table 4.2.1.2: Details of Mahmoud and Karayiannis correlation

Zhang correlation

In the year 2004, Zhang et al. [68] ran their experiment for saturated boiling in mini channels. Channel diameter were varied within the arrange of 0.78mm-6mm. The channels were also of varied shapes ranging from circular to rectangular. Water and refrigerants were used as working fluid under different pressures. They gathered 13 collected data sheets having 1203 data points in the data bank.

In this study mainly the applicability of Chen type correlation had been analyzed. Few corrections as modification of Reynold number factor, F, generalization of Chen correlation, modification of single-phase heat transfer correlations etc. The graph for comparing the theoretically predicted heat transfer coeffect with that of experimental is shown in the Fig.4.2.1.3 having Mean Absolute Error as 18.3%. the correlations are listed in Table 4.2.1.3.

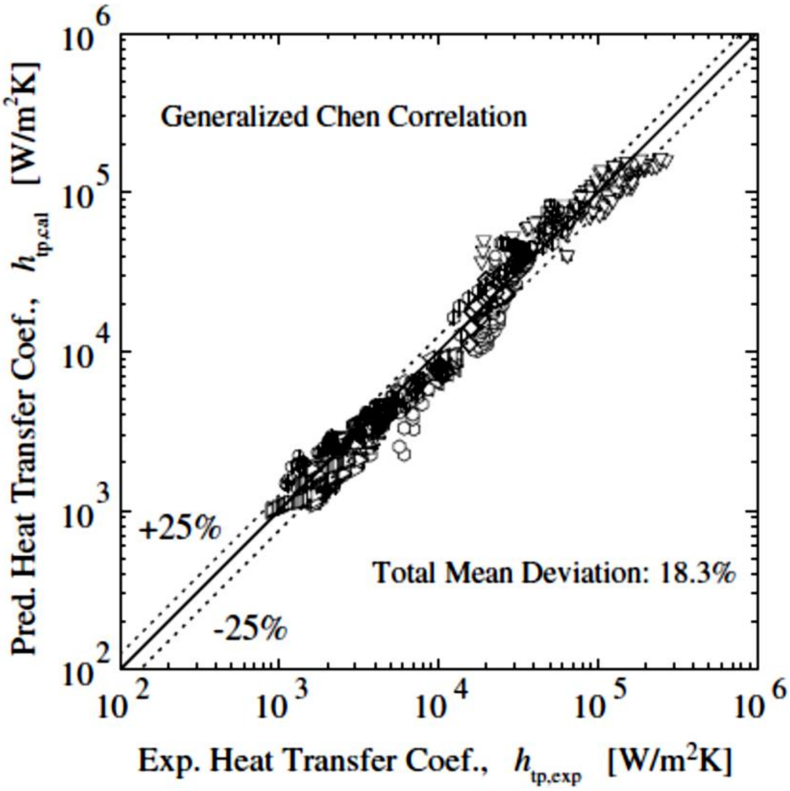

Fig.4.2.1.3: Curve fitting of Zhang modified heat transfer co-efficient (HTC) Vs experimental heat transfer co-efficient (HTC) [68]

Reference	Correlation	Applicability Range
Zhang et al. Correlation [68]	Two Phase Heat Transfer Coefficient, $\mathrm{h}_{tp} = S\mathrm{h}_{nb} + F\mathrm{h}_L$	Inner Diameter, D = 0.78–6.0 mm Mass Flux, G = 23.4–2939 kg/m^2 s Heat Flux, q = 2.95–2511 kW/m^2 Working Pressure, P = 1.01–8.66 bar Working Fluid: Water, refrigerants
	Nucleate Boiling Heat Transfer Coefficient, $\mathrm{h}_{\mathrm{nb}} = 0.00122 \frac{K_L^{0.79} C_{PL}^{0.45} \rho_L^{0.49}}{\sigma^{0.5} \mu_L^{0.29} \mathrm{h}_{fg}^{0.2} \rho_v^{0.24}} (\Delta T)^{0.24} (\Delta P)^{0.75}$	
	Suppression Factor, $S = \frac{1}{1+0.00000253 Re_{tp}^{1.17}}$, $Re_{tp} = Re_L F^{1.25}$	
	Convective Boiling Factor, F= MAX (F', 1), F'=0.64$\emptyset_L$	
	Two Phase Friction Multiplier, $\emptyset_L^2 = 1 + \frac{C}{X} + \frac{1}{X^2}$ For Re_L<1000 and Re_g<1000 X=X_{vv} and C=5 For $Re_L > 2000$ and Re_g<1000 X=X_{tv} and C=10 For Re_L<1000 and $Re_g > 2000$ X=X_{vt} and C=12 For Re_L21000 and $Re_g > 2000$ X=X_{tt} and C=20 For other regions of Re_k(k = L or g) interpolate the above values of C	
	Martinelli Parameter, $X = [\frac{(\frac{dp}{dz})_L}{(\frac{dp}{dz})_g}]^{0.5} = \left(\frac{f_L}{f_g}\right)^{0.5} \frac{(1-x)}{x} \left(\frac{\rho_g}{\varphi_L}\right)^{0.5}$	
	Convective Boiling Factor, $f_{L\,or\,g} = \begin{cases} \frac{16}{Re_{L\,or\,g}} & for\ tubes,\ Re_{L\,or\,g} < 1000 \\ 0.46 Re_{L\,or\,g}^{-0.2} & Re_{L\,or\,g} < 1000 \end{cases}$	
	Liquid Phase Heat Transfer Coefficient, $\mathrm{h}_L = (\frac{K_L}{D}) Nu$ $Nu = \begin{cases} \max(4.36 Nu_{Collier}), & for\ Re_L \le 2000 \\ 0.023 Re_L^{0.8} Pr_L^{0.4}, & for Re_L \ge 2300 \end{cases}$	
	Nusselt Number by Collier, $Nu_{Collier} = 0.17 Re_L^{0.33} Pr_L^{0.43} (\frac{Pr_L}{Pr_w})^{0.25} (\frac{g\beta\rho_L^2 D_h^3 (T_w - T_L)}{\mu_L^2})^{0.1}$	

Table 4.2.1.3: Details of Zhang correlation

Shah correlation

In the year 1976, Shah [69] presented a study on saturated boiling in tubes and annuli. The author had gathered total 780 data points from 19 individual experimental studies to calculate overall transfer coefficient. The Mean Absolute Error was found 14%.

The author also verified the correlation presented, by using 3000 data points for 12 fluids. The curve fitted data condition is shown in the Fig. 4.2.1.4 and the detailed correlation is presented in the Table 4.2.1.4 below.

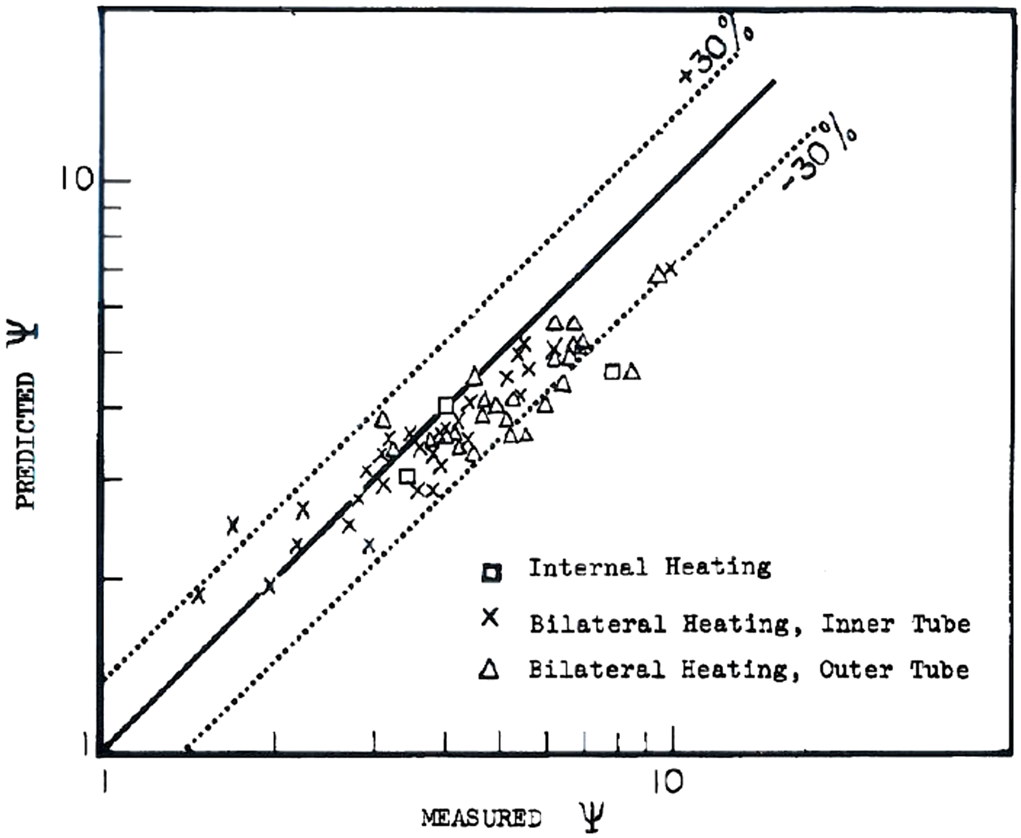

Fig.4.2.1.4: Curve fitting of Shah predicted parameter Vs experimental parameter [69]

Reference	Correlation	Applicability Range
Shah Correlation [69]	Two Phase Heat Transfer Coefficient, $h_{tp} = MAX(h_{cb} + h_{nb})$	Valid over reduced pressure range of 0.004 bar–0.8 bar Based on 780 data points
	Convective Number, $N_{Co} = (\frac{1-x}{x})^{0.8}(\frac{\rho_g}{\rho_L})^{0.5}$ Boiling Number, $B_o = \frac{q}{Gh_{fg}}$	
	Liquid Phase Heat Transfer Coefficient, $h_L = 0.023 Re_L^{0.8} Pr_L^{0.4} \frac{K_L}{D}$, $\frac{h_{cb}}{h_L} = \frac{1.8}{N_{Co}^{0.8}}$ For $N_{Co} > 1 : \frac{h_{nb}}{h_L} = \begin{cases} FB_o^{0.5} & B_o > 0.0003 \\ 1 + 46B_o^{0.5} & B_o < 0.0003 \end{cases}$ For 0.1<N_{Co}<1:$\frac{h_{nb}}{h_L}$=$FB_o^{0.5}$exp (2.74N_{Co}-0.1) Convective Boiling Factor, F= $\begin{cases} 14.7 & B_o > 0.0011 \\ 15.43 & B_o < 0.0011 \end{cases}$ For N_{Co}<0.1: $\frac{h_{nb}}{h_L}$=$FB_o^{0.5}$exp (2.74N_{Co}-0.15)	

Table 4.2.1.4: Details of Shah correlation

<u>Saitoh correlation</u>

In 2007, Saitoh et al. [70] investigated the heat transfer coefficient based on Chen correlation. The experiment had been conducted on R134a for horizontal tubes. The experiment was specially intended for identifying boiling heat transfer coefficient considering dryout phenomenon. The experimental result comparison graph is provided in the Fig. 4.2.1.5.

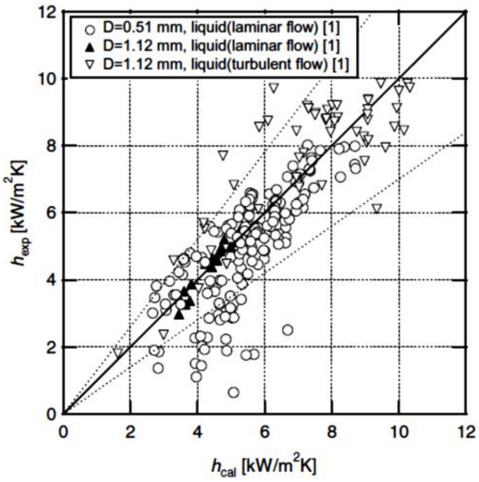

Fig.4.2.1.5: Experimental heat transfer coefficient vs calculated heat transfer coefficient for varying diameter tubes [70]

The details of this correlation is arranged in the following Table 4.2.1.5 below.

Reference	Correlation	Applicability Range
Saitoh et al. Correlation [70]	Two Phase Heat Transfer Coefficient, $\mathrm{h}_{tp} = S\mathrm{h}_{F-Z} + F\mathrm{h}_L$	Inner Diameter, D = 0.5–11 mm Mass Flux, G = 150–450 kg/m^2 s Heat Flux, q = 5–39 kW/m^2 Working Pressure, P = 3.5–5 bar Working Fluid = R134a
	Nucleate Boiling Heat Transfer Coefficient, $\mathrm{h_{nb}} = 207\frac{K_L}{D_b}(\frac{qD_b}{K_L T_L})^{0.745}(\frac{\rho_g}{\rho_L})^{0.581}Pr_L^{0.533}$	
	Bubble Diameter, $D_b = 0.512(\frac{\sigma}{g(\rho_L-\rho_g})^{0.5}$	
	Convective Boiling Factor, $F = 1 + \frac{\left(\frac{1}{x}\right)^{1.05}}{1+We_g^{-0.4}}$	
	Suppression Factor, $S = \frac{1}{(1+0.4(F^{1.25}\times Re_L\times 10^{-4})^{1.4})}$	
	Liquid Heat Transfer Coefficient, $\mathrm{h}_L = \begin{cases} 0.023Re_L^{0.8}Pr_L^{1/3}\frac{K_L}{D} & Re_L \geq 10000 \\ \frac{4.36K_L}{D} & Re_L < 10000 \end{cases}$	
	Martinelli Parameter, $\mathrm{X} = (\frac{1-x}{x})^{0.9}(\frac{\rho_v}{\rho_L})^{0.5}(\frac{\mu_L}{\mu_v})^{0.1}$ for $Re_L > 1000\ and Re_g > 1000$ $\mathrm{X} = (\frac{f_L}{f_g})^{0.5}(Re_g)^{-0.4}(\frac{g_L}{g_v})^{0.5}(\frac{\rho_L}{\rho_v})^{0.5}(\frac{\mu_L}{\mu_v})^{0.5}$	

	for $Re_L > 1000\ and Re_g > 1000$	

Table 4.2.1.5: Details of Saitoh correlation

Lee and Mudawar correlation

Jaeseon Lee and Issam Mudawar [71] proposed a correlation for high heat flux refrigeration devices considering low, medium and high qualities. The study was performed using R 134a and Water. They found that, the low-quality nucleate boiling with bubbly flow can occur only at low heat fluxes. But high heat fluxes need medium to large quality depending on the flow rate. The flow characteristics become annular for high heat fluxes. They analyzed in total 380 data points for both the working fluids and the total Mean Absolute Error became 12.26%. The comparison graph of theoretical HTC against Experimental HTC is showed in Fig. 4.2.1.6. The details of Lee and Mudawar correlation is summarized in Table 4.2.1.6.

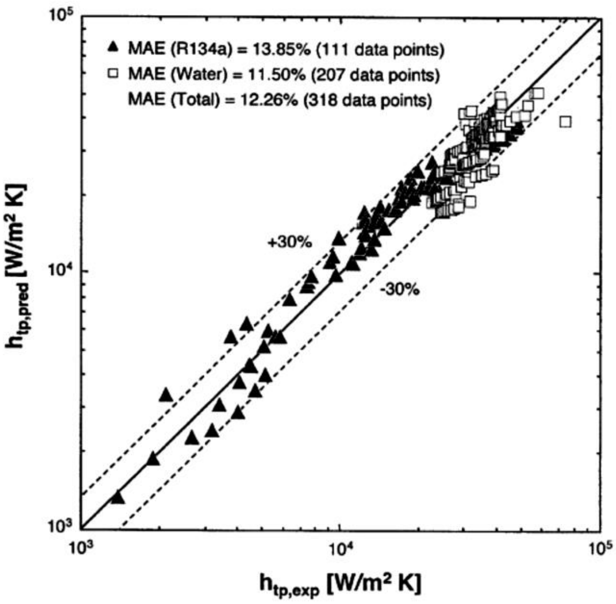

Fig.4.2.1.6: Comparison of heat transfer coefficient data for R143a and water with predictions based on new correlations [71]

Reference	Correlation	Applicability Range
Lee and Mudawar Correlation [71]	For 0< x ≤0.05 $h_{tp} = 3.856X^{0.267}h_L$ For 0.05< x ≤0.55 $h_{tp} = 436.48B_o^{0.522}We_L^{0.351}X^{0.665}h_L$ For 0.55 <x ≤ 1 $h_{tp} = MAX(108.6X^{1.665}h_g, h_g)$	Inner Diameter, D = 0.35 mm Working Fluid = Water, R134a

Table 4.2.1.6: Details of Lee and Mudawar correlation

4.2.2 Theoretical result comparison with experimental results (error analysis)

Total 14 different correlations were analyzed. Six correlations could verify the experimental results with a satisfactory level. They are presented in the following sections along with error analysis against the experimental values.

Chen Correlation, Mahmoud and Karayiannis Correlation, Zhang Correlation, Shah Correlation, Saitoh Correlation and Lee and Mudawar Correlations have been examined for the experimental data using D-type Tesla valve incorporated Pulsating Heat pipe. The theoretical analysis was carried out by setting the following range of parameters.

Reynold Number = 8.5 ~ 200

Vapor Quality = 0.1 ~ 0.5

Liquid Channel Diameter = 0.002m

Difference between Fluid and Wall Temperature = 0.5 ℃

Fluid Velocity = 0.04 m/s ~ 0.8 m/s

Reynold Number range has been selected from the research of Vries et al. [31]. Vapor quality had been chosen from Chen Correlation [66] for 0.002 m inner diameter multi-turn CLPHP.

The fluid velocity had been taken considering simulation by Vries et al [31].

Dimensionless Number	Equation	Parameters
Reynolds Number	$Re = \frac{\rho v D}{\mu}$	ρ=Fluid Density, Kg/m^3 υ= Fluid Velocity, m/s D= Fluid Surface Diameter, m μ=Dynamic Viscosity, Ns/m^2
Boiling Number	$B_o = \frac{q}{Gh_{fg}}$	q= Heat Flux, W/m^2 G=Two Phase Mass Flux in a Channel, Kg/m^2s h_{fg}=Heat of Vaporization of the fluid, J/Kg
Nusselt Number	$Nu = \frac{hD}{K}$	h=Heat Transfer Co-efficient, W/m^2K D= Inner channel Diameter, m K = Thermal Conductivity, W/mK
Weber Number	$We = \frac{v^2 L\rho}{\sigma}$	υ= Fluid Velocity, m/s L=Characteristic Length, m ρ=Fluid Density, Kg/m^3 σ=Surface Tension
Confinement Number	$C_o = \frac{[\frac{\sigma}{g(\rho_l - \rho_g)}]^{0.5}}{D}$	σ=Surface Tension g=Gravitation Acceleration, m/s^2 ρ_l=Liquid Density, Kg/m^3 ρ_g=Gas Density, Kg/m^3 D= Fluid Surface Diameter, m

Table 4.2.2.1: Description of dimensionless groups

Five types of dimensionless numbers are used for this experiment. They are presented in the Table 4.2.2.1 The theoretical two-phase analysis from six correlations are compared with the experimental values by calculating absolute error (AE). The Mean Absolute Errors (MAE) for multiple values have been calculated from following equation,

$$MAE = \frac{1}{n}\sum_{i=1}^{n}\frac{|h_{pred,i} - h_{exp,i}|}{h_{exp,i}} \times 100$$

Among these six correlations Zhang correlation produces minimum Mean Absolute Error having 72% data within error band ±30%. The graphical representations are provided in Fig. 4.2.2.2 (a) to (f). The red and purple bands are indicating positive and negative 30% error bad respectively. White dots are Absolute Errors.

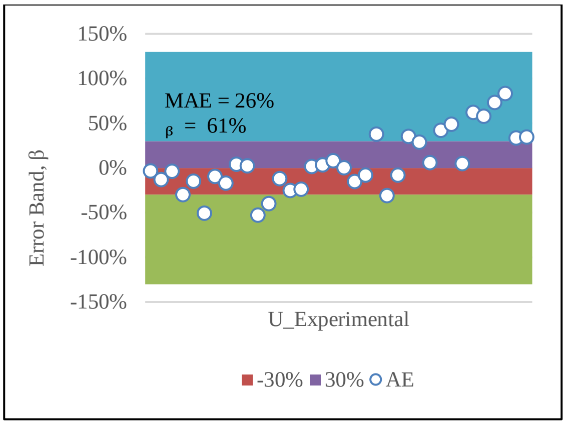

(a) Chen correlation vs experimental data

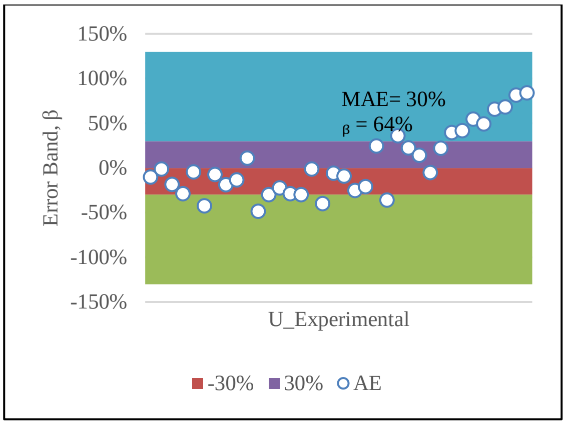

(b) Mahmoud and Karayiannis correlation vs experimental data

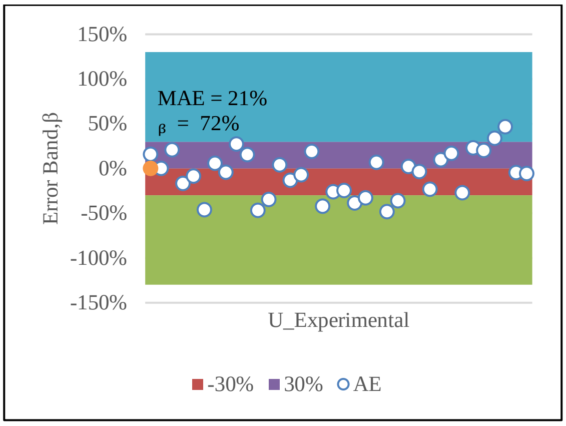

(c) Zhang correlation vs experimental data

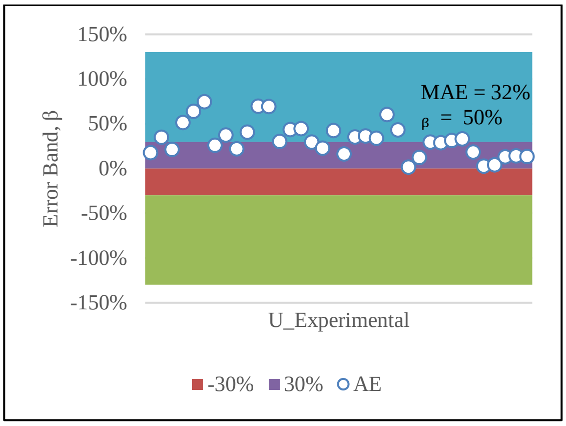

(d) Shah correlation vs experimental data

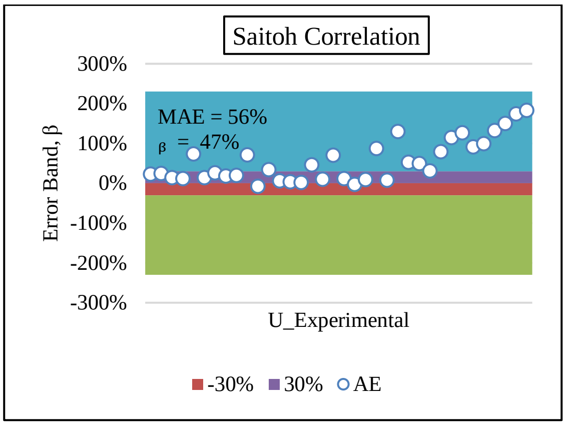

(e) Saitoh correlation vs experimental data

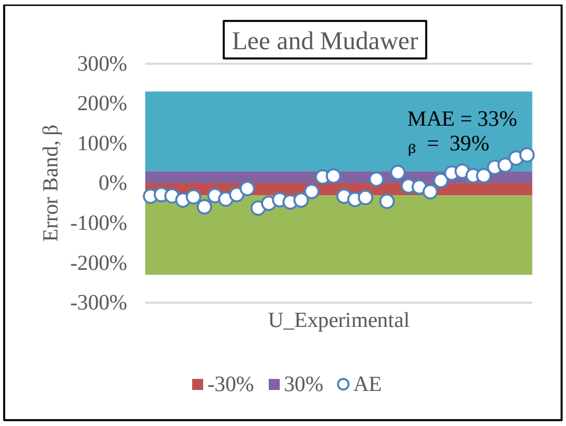

(f) Lee and Mudawer correlation vs experimental data

Fig.4.2.2.1: Result comparisons from six correlations vs experimental data

The comparisons for Overall heat Transfer Coefficient are summarized in the following Table 4.2.2.2.

Correlations	Mean Absolute Error (MAE)	±30% Error Band (β)
Chen	26%	61%
Mahmoud and Karayiannis	30%	64%
Zhang et al.	21%	72%
Shah et al.	32%	50%
Saitoh et al.	56%	47%
Lee and Mudawar	33%	39%

Table 4.2.2.2: Error comparison for experimental values using six correlations

4.3. Validation

Validation is the process to test accuracy of a system comparing with true values. Experimental thermal resistance data from D-shape Tesla Valve incorporated CLPHP have been validated by comparing with a CLPHP without having any valve incorporation. the validation process will be conducted to find out 14%-25% decrease of thermal resistances. The results will be analyzed in the following section 4.3.1. The structure similar as previously presented one but without the presence of any valves or passive devices is shown in the Fig.4.3.1 below.

Fig.4.3.1: CLPHP model without any valve incorporation.

4.3.1 Data comparison between D-type Tesla valve incorporated CLPHP and traditional CLPHP model

A model of CLPHP without having any valves to enhance diodicity, had been constructed to test the validity of D-shape Tesla Valve incorporated CLPHP. The structure had the same height and equal number of U bends as of D-valve CLPHP. Also, the tube material and internal and external diameter were equal with D-valve CLPHP. The adiabatic section height and width were maintained similar. The evaporator heating coil turn numbers were also same as D-valve CLPHP. The traditional CLPHP experiment had been run at the same ambient that of D-valve CLPHP. The internal fluid volume of this traditional CLPHP is 6.33×10^{-6} m^3. The validation test had been carried out for 60% fill ratio (3.798×10^{-6} m^3). The experiment was run at 60W input load varying inclination angles as 0˚, 10˚, 20˚, 30˚, 60˚, 90˚. The comparison graph of traditional CLPHP and D-shape CLPHP is given below.

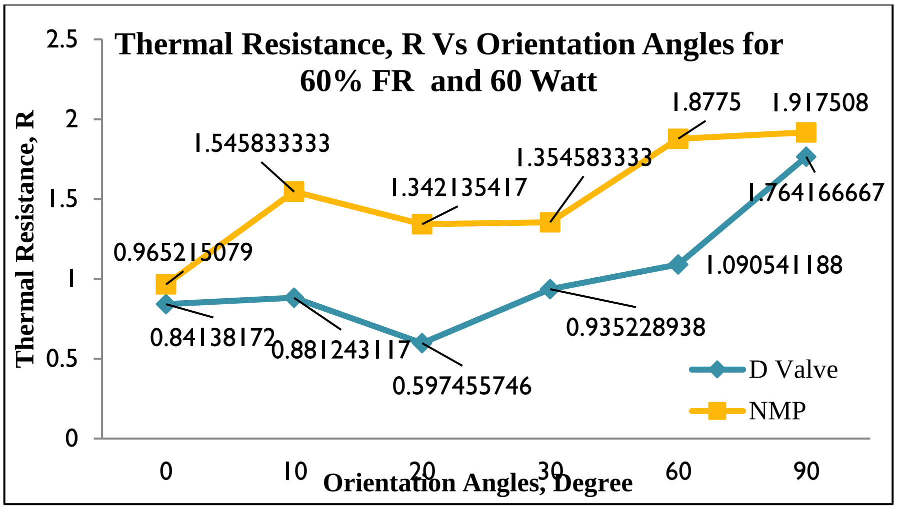

Fig.4.3.1.1: Comparison graph of thermal resistances between D-shape Tesla type CLPHP and traditional CLPHP at 60W working load

Inclinations	Thermal Resistance, **R**, ˚C/W		% Decrease of **R**
	D-Valve Incorporated CLPHP	No Valve incorporated CLPHP	
0	0.841	0.965	15%
10	0.881	1.546	75%
20	0.597	1.342	125%
30	0.935	1.355	45%
60	1.091	1.878	72%
90	1.764	1.918	9%

Table 4.3.1.1: Result comparison

As reported by Yang [33] the traditional CLPHP of 2 mm inner diameter operates best at vertical orientation, the Table 4.3.1.1 shows that, decrement of thermal resistance by using D-shape valve to CLPHP has become 15%. At the end, it is recommended that, Tesla type

D-valve incorporation to CLPHP results with a lower barrier to heat transfer than the traditional CLPHP.

4.4 Development of Empirical Correlation for D-Type Tesla Valve

Inside a closed loop pulsating heat pipe, heat transfer mechanism is two-phase instead of single phase. Sensible and latent heat transfer are the driving force for fluid motion from evaporator to condenser. But mathematically analyzing two-phase flow is not only complicated but there are too many uncertainties also. Till date, very limited suitable empirical correlations could be found. Moreover, for D-type Tesla Valve incorporated CLPHP, there is no such mathematical analysis available.

The following sections 4.4.1 and 4.4.2 will discuss curve fitting regression analysis by using various dimensionless parameters related to two phase heat transfer. Curve fitting regression analysis from dimensionless groups and dimensionless physical parameters have been analyzed inspired by previous researches. For both of the cases, the analysis has been carried out using Linear Regression numerical process. Non-linear (exponential equation) regression analysis had been run for the experimental outputs but it did not find any suitable curve to fit.

4.4.1 Empirical correlation from dimensionless groups

Dimensionless groups that express two-phase flow are analyzed to predict the behavior of data from this experiment. Mahmoud and Karayiannis [72] used six different dimensionless groups for their study. Inspired from their research, total four dimensionless groups that can predict the two-phase heat transfer inside this D-shape Tesla Valve have been taken into consideration. Boiling number is used for convective boiling, where the bubble stirring effect is under analyzation. This number will help to predict the bubble movement in two phase condition. Weber number was considered to calculate inertial force condition due to surface tension force of bubble inside the CLPHP. Confinement number expresses the buoyancy force effect over surface tension inside a capillary tube to identify two-phase pressure drop in heat transfer correlation. As Reynolds number indicates the ratio of inertial force and viscous force, it has been considered to predict the flow pattern whether laminar or turbulent.

The linear regression has been carried out by using Excel Data Analysis toolbar. The residual output was selected so as to compare the accuracy. The output results are enlisted in Appendix D.

$$Nu_{Experimental=\frac{U_{Experimental}D}{K_l}=f(B_0,We,\,C_0,Re)} \quad [72]$$

$$Nu = C+aB_0 + bWe + dC_0 + eRe$$

$$U_{Predicted} = (C+aB_0 + bWe + dC_0 + eRe)\frac{K_l}{D}$$

This is the function for Overall Heat Transfer Coefficient (U) with respect to the dimensionless groups.

The final equations developed from dimensionless groups become as follows,

$$Nu = 72.9367 - 9022374.034Bo - 0.0003672We - 34.7Co + 0.0064Re$$

$$U\_Predicted = (72.9367 - 9022374.034Bo - 0.0003672We - 34.7Co + 0.0064Re)\frac{K_l}{D}$$

From the residual output, the predicted Nusselt number best fits with the linear curve as a reference from dimensionless groups relationship. The curve fitting is showed in the Fig. 4.4.1.1 below. The residual outputs are listed in Table D-2 in Appendix D.

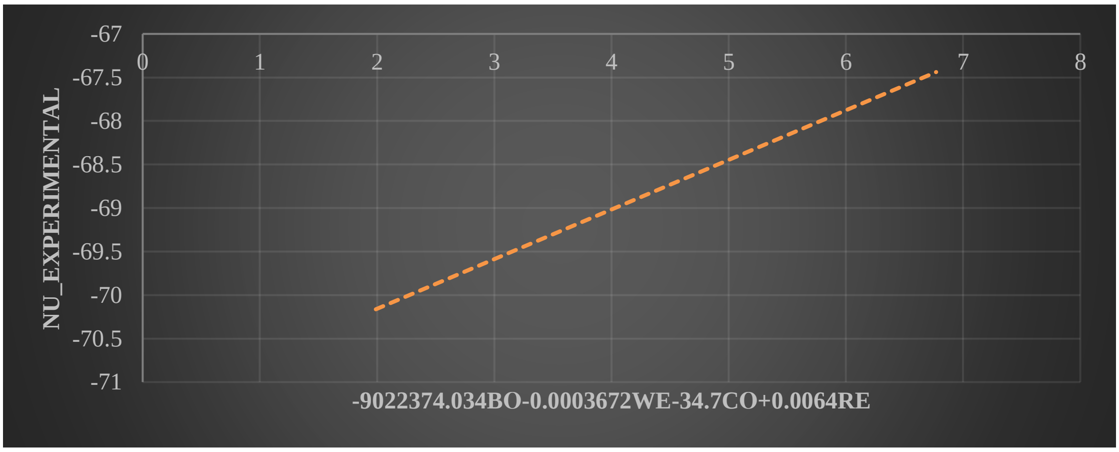

Fig.4.4.1.1: Fig: Experimental two phase Nusselt number vs dimensionless groups

From this analysis, the experimental and theoretical Nusselt number plot for 36 data points has been showed in the Fig. 4.4.1.2 below.

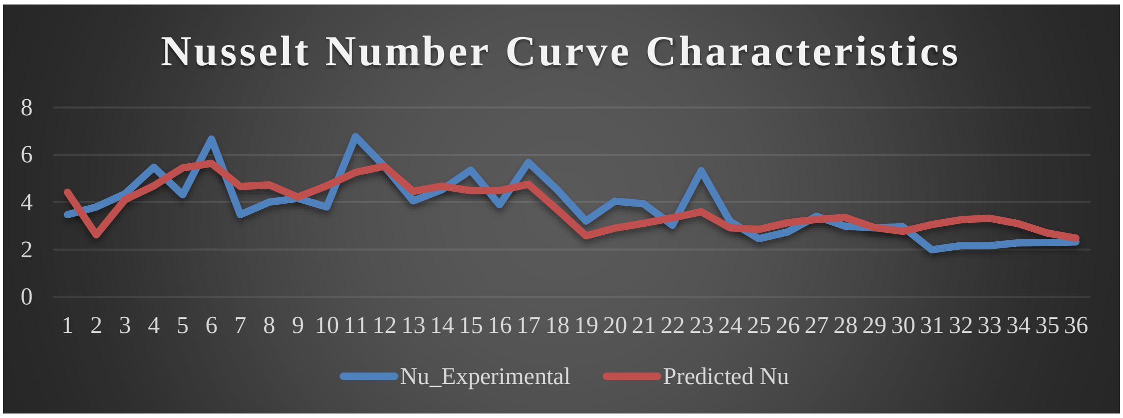

Fig.4.4.1.2: Comparison graph of experimental Nusselt number and predicted Nusselt number

Fig. 4.4.1.3 shows that the Mean Absolute Error is only 5% and 81% of predicted Overall heat transfer coefficient values fall within ±30%.

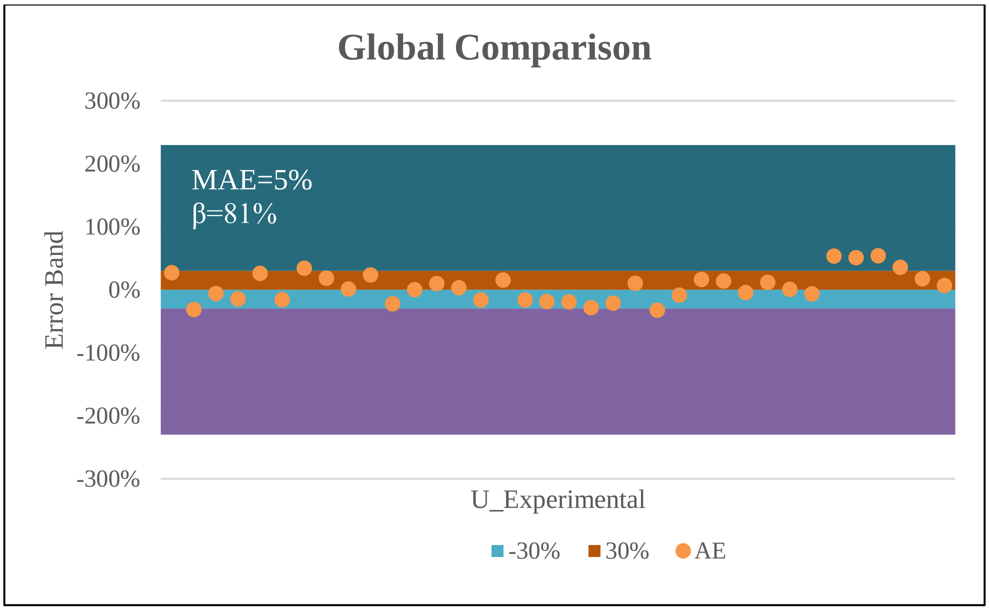

Fig.4.4.1.3: Fig: Global comparison with the new equation

4.4.2 Empirical correlation from dimensionless physical parameters

Physical influences from experimental analysis have been playing a role to predict the overall heat transfer coefficients. Dimensionless numbers from heat load, convection heat transfer from condenser to ambient and the effect of orientation angles have provided best result for building an empirical correlation. Haque [24] used these parameters to identify the direct influence over the output. There are four dimensionless parameters used in this research. At first, input heat load to maximum input heat load $\left(\frac{q}{q_{max}}\right)$ has been considered to identify the effect of heat input to the CLPHP. Inside the heat pipes, the heat is transferred by the evaporation and condensation of working fluid from evaporator and condenser section respectively. So, the heat transfer can be defined as the phase change heat transfer. Another mode of heat transfer can be occurred by the convection which is directly depends to the temperature differential of the evaporator and condenser section. From the experimental date, it is evident that, with the increase of temperature differential of evaporator to condenser section, the overall heat transfer coefficient also increases. So, to examine the effect of evaporator temperature to the ambient this ratio $\left(\frac{T_{Eva}-T_a}{T_{Eva}}\right)$ has been considered. In the heat transfer performance of looped parallel heat pipe, the condenser inclination has an effect. For considering the effect of condenser inclination at the transport section, a dimensionless group can be assumed as $\left(1+\frac{\theta}{\theta_{max}}\right)$. Here, θ is the various condenser inclination and θ_{max} is the maximum inclination angle which is at the horizontal position ($\theta_{max} = 90^{o}$). The ratios are compared with ratio of obtained Overall Heat Transfer Coefficient to the maximum obtained Overall Heat Transfer Coefficient $(\frac{U}{U_{max}})_{Experimental}$.

In this case, the linear regression has become the best fit criteria as section 4.4.1.

Adopting similar procedure described at section 4.4.1, the linear regression has been carried out by using Excel Data Analysis toolbar. The residual output had been selected so as to compare the accuracy. The residual outputs are listed in Table D-3 in Appendix D.

$$(\frac{U}{U_{max}})_{Experimental=f[\left(\frac{q}{q_{max}}\right),\left(\frac{T_{Eva}-T_a}{T_{Eva}}\right),\left(1+\frac{\theta}{\theta_{max}}\right)]} \quad [24]$$

$$(\frac{U}{U_{max}})_{Experimental=C+a\left(\frac{q}{q_{max}}\right)+b\left(\frac{T_{Eva}-T_a}{T_{Eva}}\right)+d\left(1+\frac{\theta}{\theta_{max}}\right)}$$

The final equation after linear regression analysis becomes,

$$(\frac{U}{U_{max}})_{experimental}$$

$$= 3.144 + 1.277(\frac{q}{q_{max}}) - 4.4148(\frac{T_{Eva}-T_a}{T_{Eva}}) - 0.1457\left(1+\frac{\theta}{\theta_{max}}\right)$$

The Fig. 4.4.2.1 shows the fitting of experimental result of dimensionless heat transfer coefficient proportional to the relationship of the physically influencing parameters. This graph shows an excellent result for prediction of heat transfer coefficient from physical parameters.

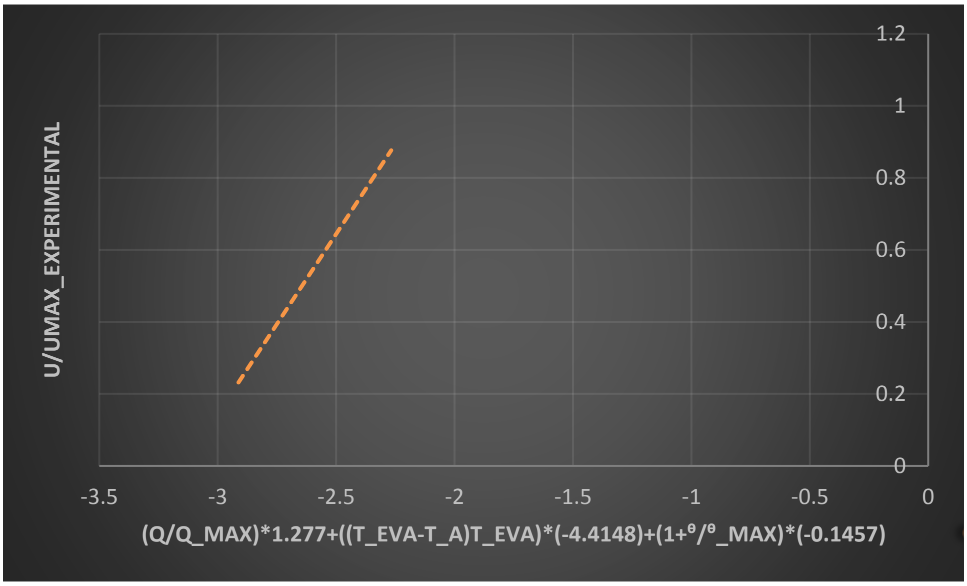

Fig.4.4.2.1: U/Umax_experiment vs dimensionless physical parameter

4.5 Closure

The experimental result analysis had been analyzed from four different angles. they are Experimental data analysis, verification, validation and building mathematical modeling. Experimental data had been investigated by four different phenomena. Temperature rise, thermal resistance and overall heat transfer coefficient values were calculated to identify the nature of the heat transfer. The results were demonstrated by graphs under various situations. The study over temperature rise through evaporator, adiabatic section and condenser shows that 20˚ inclination angle and 60W input heat load are the best operating condition for this structure. thermal resistance and overall heat transfer co-efficient also show best suitable operating condition as 20˚ inclination angle and 60W input load.

Experimental data used traditional boiling heat transfer equations for measuring heat transfer parameters through capillary tubing. But the scenario is more complicated. In practical, the heat transfer is two phases instead of single phase. Many researchers published their work on two phase behavior for CLPHP. Six correlations among them had been chosen to calculate overall heat transfer coefficient for comparing with the experimental results. The verification process finds the best result for Zhang correlation.

The results were also validated by building a structure of CLPHP having no moving part. The reading had been taken at the same ambient of D-shape Tesla type CLPHP for 60W input load and all inclinations angles. the results show very good comparison between the two devices.

Mathematical modeling from the data acquired were built from dimensionless numbers and physical parameters. The results show that best curve fitting can be attained from linear regression analysis. The next chapter summaries the overall research activities compactly.

CHAPTER 5: CONCLUSION

5.1 Summery

1. Tesla Type D-Valve incorporated with closed loop pulsating heat pipes should produce decreased thermal resistances at a range of 14%-25%. It has been proven minimum decrement of thermal resistances as **15%** than traditional CLPHP in validation section.
2. This special CLPHP can take a **higher amount of heat input** and produce **larger pressure gradients.** The average gauge pressure within CLPHP was **14 Psig**.
3. The CLCPH filled with **60%** Filling Ratio shows better performances than 80% Filling Ratio.
4. For 60% Filling Ratio the best operating heat input is **60W** and **20 Degree inclination angle**.
5. From theoretical verification it is established that the correlation by **Zhang** has the best output of mean absolute error of **21%** and **72%** data fall within ±30% error band limit.
6. The size of the Tesla type D-valve incorporated CLPHP is much lower than that of the traditional heat pipes under researches. Thus, it will consume **less space**.
7. No two-phase empirical correlation was established for this special D-shape valve. From this research, two different **empirical correlations** were found from **physical properties** and **dimensionless numbers**.
8. A **data bank** has been formed from this research for this specially designed CLPHP which was not previously available.

5.2 Recommendations for Future Works

1. Number of turns can be increased to reduce more thermal resistances.
2. The experimental setup can be made of rectangular thin plate over which the full CLPHP design would be engraved. This will reduce the unwanted flow restrictions.
3. The setup can be tested for military use specially cooling of land vehicles and air defense artillery.
4. Ammonia or Alcohol based nano-fluids can be applied to check better performances.
5. Radiographic images can be taken to visualize the flow pattern inside this special valve.
6. Critical Heat Load calculations still don't have strong mathematical prediction models. Thus, analysis in this sector can be carried out.
7. The setup was placed in open environment. The study can be examined creating a vacuum chamber also.

References

[1] Rupp, Karl, *42 Years of Microprocessor Trend Data*, Wordpress.org, 15 February 2018. [Online]. Available: https://www.karlrupp.net/2018/02/42-years-of-microprocessor-trend-data/.

[2] Airhart, Marc, *UT News*, University of Texas, 15 April 2015. [Online]. Available: https://news.utexas.edu/2015/04/15/hot-chips-managing-moores-law/.

[3] S. Khandekar, "Thermo-Hydrodynamics of Closed Loop Pulsating Heat Pipes," *Phd. Thesis*, Institut für Kernenergetik und Energiesysteme der Universität Stuttgart, Stuttgart, 2004.

[4] G. Karimi, J.R. Culham, "Review and assessment of pulsating heat pipe mechanism for high heat flux electronic cooling," in *IEEE Xplore*, Las Vegas, NV, USA, 9 August, 2004.

[5] S.Khairnasov, A.Naumova, "Heat pipes application in electronics thermal control systems," *Frontiers in Heat Pipes,* vol. 6, no. 6, 2015.

[6] M. S.Ahamed, Y.Saito, K.Mashiko and M.Mochizuki, "Characterization of a high performance ultra-thin heat pipe cooling module for mobile hand held electronic devices," *International Journal of Heat and Mass Transfer,* vol. 53, no. 11, pp. 3241-3247, 2017.

[7] T. D. Swanson and G. C. Birur, "NASA thermal control technologies for robotic spacecraft," *Applied Thermal Engineering,* vol. 23, no. 9, pp. 1055-1065, 2003.

[8] W. Srimuang and P. Amatachaya, "A review of the applications of heat pipe heat exchangers for heat recovery," *Renewable and Sustainable Energy Reviews,* vol. 16, no. 9, pp. 4303-4315, 2012.

[9] M. A. Nazari, M. H. Ahmadi, R. Ghasempour, M. B. Shafii, O. Mahian, S. Kalogirou and S. Wongwises, "A review on pulsating heat pipes: From solar to cryogenic applications," *Applied Energy,* vol. 222, pp. 475-484, 2018.

[10] H. K. Balotaki and M. H. Saidi, "Design and performance of a novel hybrid photovoltaic–thermal collector with pulsating heat pipe (PVTPHP)," *Iranian Journal of Science and Technology Transactions of Mechcanical Engineering*, vol. 43, no. S1, pp. 371-381, 2018.

[11] J. Zuo, C. Park, P. Rogers and J. Perez, "*Two-phase flow cooling for vehicle thermal management*," SAE Technical Paper, Detroit, Michigan, 2005.

[12] J. Zuo, W. Anderson and R. Bonner, "*Advanced thermal management technologies for high power density automotive equipment*," Advanced Cooling Technologies, Inc., New Holland Avenue, Lancaster, 2019.

[13] Z. J. Zuo, M. T. North and K. L. Wert, "High heat flux heat pipe mechanism for cooling of electronics," *IEEE Transactions On Components And Packaging Technologies,* vol. 24, no. 2, pp. 220-225, June, 2001.

[14] G. Burban, V. Ayel, A. Alexandre, P. Lagonotte, Y. Bertin and C. Romestant, "Experimental investigation of a pulsating heat pipe for hybrid vehicle applications," *Applied Thermal Engineering,* vol. 50, no. 1, pp. 94-103, 2013.

[15] R.-G. Chi, W.-S. Chung and S.-H. Rhi, "Thermal characteristics of an oscillating heat pipe cooling system for electric vehicle Li-Ion batteries," *Energies,* vol. 11, no. 3, p. 2018, 15 March 2018.

[16] N. Qian, Y. Fu , Y. Zhang , J. Chen and J. Xu, "Experimental investigation of thermal performance of the oscillating heat pipe for the grinding wheel," *International Journal of Heat and Mass Transfer,* vol. 136, pp. 911-923, 2019.

[17] B. G. PATIL and P. R. PACHGHARE, "Experimental analysis of pulsating heat pipe for air conditioning system," *International Journal of Mechanical And Production Engineering,* vol. 4, no. 6, 2016.

[18] M. J. Connors and J. A. Zunner, "*The use of vapor chambers and heat pipes for cooling military embedded,"* Thermacore Inc., August 5, 2009.

[19] X. Tang, J. Zuo and M. Goryca, "Development of heat pipe loop technology for military vehicle electronics cooling," in *2010 Ndia Ground Vehicle Systems Engineering And Technology Symposium*, Dearborn, Michigan, August 17-19, 2010.

[20] R. S. Gaugler., "*Heat Transfer Device*". Dayton, Ohio Patent 2,350,348, 6 June 1944.

[21] B. Zohuri, "Basic principles of heat pipes and history," in *Heat Pipe Design and Technology: Modern Applications for Practical Thermal Management*, Springer International Publishing, 2016, pp. 1-41.

[22] A. Faghri, "Review and advances in heat pipe science and technology," *Journal of Heat Transfer,* vol. 134, no. 12, p. 18 pages, 2012.

[23] F. Polášek and M. Zelko, "Thermal control of electronic components by heat pipes and thermosyphons," in *A historical overview, Proc. 10 Int. Heat Pipe Conf.*, Stuttgart, Germany, 21-25 September 1997..

[24] M. S. Haque, "Thermal Characteristics Of An Alumunum Closed-Loop Pulsating Heat Pipe Charged With Ammonia," *M. Sc. Engg. Thesis,* Bangladesh University of Engineering and Technology, Dhaka, December, 2011.

[25] T. Daimaru, S. Yoshida and H. Nagai, "Study on thermal cycle in oscillating heat pipes by numerical analysis," *Applied Thermal Engineering,* vol. 113, p. 1219-1227 pages, 2016.

[26] N. Tesla, "*Valvular Conduit*". New York Patent US 1329559 A, 3 February 1920.

[27] S.M. Thompson, H.B. Ma and C. Wilson, "Investigation of a flat-plate oscillating heat pipe with Tesla-type check valves," *Experimental Thermal and Fluid Science,* vol. 35, no. 7, pp. 1265-1273, 2011.

[28] A. Gamboa, C. Morris and F. Forster, "Improvements in fixed-valve micropump performance through shape optimization of valves," *Journal of Fluids Engineering,* vol. 127, no. 2, pp. 339-346, 2005.

[29] L. J. Reed, "*Fluidic Rectifier*.". Oviedo, Fla Patent U.S. Patent No. 5,265,636, 13 January 1993.

[30] R. Bardell, "The Diodicity Mechanism of Tesla-type No-moving-parts Valves," *Phd. Thesis*, University of Washington, Washington, 2000.

[31] S.F. deVries, D. Florea, F.G.A. Homburg, A. J. H. Frijns, "Design and operation of a tesla-type valve for pulsating heat pipes," *International Journal of Heat and Mass Transfer,* vol. 105, pp. 1-11, 2017.

[32] H. Akachi, "*Structure Of Micro-Heat Pipe*". Sagamihara, Japan Patent 5,219,020, 15 August 1991.

[33] H. Yang, S. Khandekar and M. Groll, "Operational limit of closed loop pulsating heat pipes," *Applied Thermal Engineering,* vol. 28, no. 1, pp. 49-59, 2008.

[34] M. S. Haque, A. Majumdar, M. F. Kader and M. M. Razzaq, "Thermal characteristics of an ammonia-charged closed-loop pulsating heat pipe," *Journal of Mechanical Science and Technology,* vol. 33, no. 4, pp. 1907-1914, 2019.

[35] H. Barua, M. Ali, M. Nuruzzaman, M. Quamrul Islam and C. M. Feroz, "Effect of filling ratio on heat transfer characteristics and performance of a Closed Loop Pulsating Heat Pipe," *Procedia Engineering,* vol. 56, p. 88 – 95, 2013.

[36] S. Akter Jahan, M. Ali and M. Q. Islam, "Effect of inclination angles on heat transfer characteristics," *Procedia Engineering,* vol. 56, pp. 81-87, 2013.

[37] R. Naik, V. Varadarajan, G. Pundarika and K. R. Narasimha, "Experimental investigation and performance evaluation of a closed loop pulsating heat pipe," *Journal of Applied Fluid Mechanics,* vol. 6, no. 2, pp. 267-275, 2013.

[38] X. Zhihu and Q. Wei, "Experimental study on effect of inclination angles," *Chinese Journal of Aeronautics,* vol. 27, no. 5, pp. 112-1127, 2014.

[39] K.-H. Chien, Y.-T. Lin , Y.-R. Chen , K.-S. Yang and C.-C. Wang, "A novel design of pulsating heat pipe with fewer turns applicable to all orientations," *International Journal of Heat and Mass Transfer,* vol. 55, no. 21-22, pp. 5722-5728, 2012.

[40] G. H. Kwon, S. J. Kim , "Analysis of pulsating heat pipe with a dual-diameter tube," in *10th International Conference on Heat Transfer, Fluid Mechanics and Thermodynamics,* Orlando, Florida, 14-26 July, 2014.

[41] C.-Y. Tseng, K.-S. Yang, K-H. Chien, M.-S. Jeng and C.-C. Wang, "Investigation of the performance of pulsating heat pipe subject to uniform/alternating tube diameters," *Experimental Thermal and Fluid Science,* vol. 54, pp. 85-92, 2014.

[42] R. S. Borkar and P. R. Pachghare, "Thermo-hydrodynamic behavior of methanol charged closed loop pulsating heat pipe," *Frontiers in Heat Pipes (FHP),* vol. 5, no. 1, 2014.

[43] B. Tong, T. Wong, and K. Ooi, "Closed loop pulsating heat pipe," *Applied Thermal Engineering,* vol. 21, no. 18, pp. 1845-1862, 2001.

[44] M. Mameli, M. Marengo and S. Khandekar, "Local heat transfer measurement and thermo-fluid characterization of a Pulsating Heat Pipe," *International Journal of Thermal Sciences,* vol. 75, pp. 140-152, 2014.

[45] L. Fourgeaud, V. Nikolayev, E. Ercolani, J. Duplat, and Philippe, "In situ investigation of liquid films in pulsating heat pipe," *AppliedThermalEngineering,* vol. 127, pp. 1023-1028, 2017.

[46] N. Bhuwakietkumjohn and S. Rittidech, "Internal flow patterns on heat transfer characteristics of a closed loop oscillating heat-pipe with check valves using ethanol and a silver nano-ethanol mixture," *Experimental Thermal and Fluid Science,* vol. 34, no. 8, pp. 1000-1007, 2010.

[47] S. Wannapakhe, S. Rittidech, B. Bubphachot and O. Watanabe, "Heat transfer rate of a closed-loop oscillating heat pipe with check valves using silver nanofluid as working fluid," *Journal of Mechanical Science and Technology,* vol. 23, pp. 1576-1582, 2009.

[48] J. Qua, X. Li , Q. Wang, F. Liu and H. Guo, "Heat transfer characteristics of micro-grooved oscillating heat pipes," *Experimental Thermal and Fluid Science,* vol. 85, pp. 75-84, 2017.

[49] K.-S. Yang, Z.-C. Cheng , M.-S. Jeng , K.-H. Chien and J.-C. Shyu, "An experimental investigation of micro pulsating heat pipes," *Micromachines,* vol. 5, pp. 385-395, 2014.

[50] U. C. Bitencourt, "*CFD simulation of a pulsating heat pipe using ANSYS FLUENT*," Escavador, 2016.

[51] I. Nekrashevych and V. S. Nikolayev, "Pulsating heat pipe simulations: Impact of PHP orientation," *Microgravity Science and Technology,* vol. 31, no. 3, pp. 241-248, June, 2019.

[52] S. M. Pouryoussefi and Y. Zhang, "Analysis of chaotic flow in a 2D multi-turn closed-loop pulsating heat pipe," *Applied Thermal Engineering,* vol. 126, no. 5, pp. 1069-1076, November, 2017.

[53] J.V. suresh and P.Bhramara, "CFD analysis of multi turn pulsating heat pipe," *Materials Today: Proceedings,* vol. 4, pp. 2701-2710, 2017.

[54] H. B. Ma, C. Wilson, Q. Yu, K. Park, U. S. Choi, and M. Tirumala, "An experimental investigation of heat transport capability in a nanofluid oscillating heat pipe.," *Journal of Heat Transfer,* vol. 128, no. 11, p. 1213–1216, 2006.

[55] J. Qu, H. Wu and P. Cheng, "Thermal performance of an oscillating heat pipe with Al2O3-water nanofluids.," *International Communications in Heat and Mass Transfer,* vol. 37, no. 2, p. 11–115, 2010.

[56] J. Qu and H. Wu, "Thermal performance comparison of oscillating heat pipes with SiO2/water and Al2O3/water," *International Journal of Thermal Science,* vol. 50, no. 10, pp. 1954-1962, 2011.

[57] F. K. Forster, R. L. Bardell, M. A. Afromowitz, N. R. Sharma and A. Blanchard, "Design, fabrication and testing of fixed-valve micro-pumps," in *Proceedings of the ASME Fluids Engineering Division*, New York, 1995.

[58] N.-T. Nguyen and T.-Q. Truong, "Simulation and optimization of tesla valves," *TechConnect Briefs,* vol. 1, pp. 178-181, 2003.

[59] C. J. Morris and F. K. Forster, "Low-order modeling of resonance for fixed-valve," *Journal Of Microelectromechanical Systems*, vol. 12, no. 3, pp. 325-334, JUNE 2003.

[60] J.-Y. Qian, M.-R. Chen, X.-L. Liu and Z.-J. Jin, "A numerical investigation of the flow of nanofluids through a micro Tesla valve," *Journal of Zhejiang University-SCIENCE A*, vol. 20, no. 1, pp. 50-60, January 2019.

[61] R. A. Chandavar, "Stability analysis of Tesla valve based natural circulation loop for decay heat removal in nuclear power plants," in *2019 Advances in Science and Engineering Technology International Conferences (ASET)*, Dubai, United Arab Emirates, United Arab Emirates, 26 March-10 April 2019.

[62] B. L. Drolen and C. D. Smoot, "Performance limits of oscillating heat pipes: Theory and validation," *Journal of Thermophysics And Heat Transfer,* vol. 31, no. 4, pp. 920-936, 2017.

[63] P. Meena, S. Rittidech and P. Tammasaeng, "Effect of evaporator section lengths and working fluids on operational limit of closed loop oscillating heat pipes with check valves (CLOHP/CV)," *American Journal of Applied Sciences,* vol. 6, no. 1, pp. 133-136, 2009.

[64] M. A. Nazari, M. H. Ahmadi, R. Ghasempour and M. B. Shafii, "How to improve the thermal performance of pulsating heat pipes: A review on working fluid," *Renewable and Sustainable Energy Reviews*, vol. 91, pp. 630-638, 2018.

[65] J. P. Holman., *Heat Transfer,* 10th Edition, McGraw-Hill, 2010.

[66] J. C. Chen, "A correlation for boiling heat transfer to saturated fluids in convective flow," *Industrial & Engineering Chemistry Process Design and Development,* vol. 5, p. 322–329, 1966.

[67] T.G. Karayiannis and M.M. Mahmoud, "Flow boiling in microchannels: fundamentals and applications," *Applied Thermal Engineering,* vol. 115, pp. 1372-1397, 2017.

[68] W. Zhang, T. Hibiki and K. Mishima, "Correlation for flow boiling heat transfer in mini-channels," *International Journal of Heat and Mass Transfer,* vol. 47, no. 26, pp. 5749-5763, 2004.

[69] M. Shah, "Chart correlation for saturated boiling heat transfer: Equations and further study," *ASHRAE Transactions,* vol. 88, no. Part-1, pp. 185-196, 1982.

[70] S. Saitoh, H. Daiguji and E. Hihara, "Correlation for boiling heat transfer of R-134a in horizontal tubes including effect of tube diameter," *International Journal of Heat and Mass Transfer,* vol. 50, no. 25-26, pp. 5215-5225, 2007.

[71] J. Lee and I. Mudawar, "Two-phase flow in high-heat-flux micro-channel heat sink for refrigeration cooling applications: Part II—heat transfer characteristics," *International Journal of Heat and Mass Transfer,* vol. 48, no. 5, pp. 941-955, 2005.

[72] M. M. Mahmoud and T. Karayiannis, "A statistical correlation for flow boiling heat transfer in micro tubes," in *Proceedings of the 3rd European Conference on Microfluidics - Microfluidics*, Heidelberg, December 3-5, 2012.

APPENDIX-A

Property Table and NDT Test Results

Table A-1 Property Table for Methanol

Tsat1	Tsat	Psat	Prl	Kl	Cpl	ρl	ρv	µl	µv	σ	hfg
◦C	◦C	Kpa	---	W/mK	J/KgK	Kg/m^3	Kg/m^3	NS/m^2	NS/m^2	N/m	J/Kg
65.2	64.7	102000	2.54	0.1915	2830	748.2	1.22	0.0001474	0.0000111	0.0187	1101000
97.5	97	320000	3.81	0.1822	3140	714.4	3.67	0.000221	0.0000123	0.016	1030000
117.5	117	586000	3.31	0.1789	3360	691.1	6.62	0.0001761	0.000013	0.0139	975700
137.5	137	1006000	2.98	0.1714	3630	665.2	11.4	0.0001407	0.0000139	0.0118	910400
157.5	157	1637000	2.71	0.165	3960	635.5	18.99	0.0001128	0.0000148	0.00965	831500
177.5	177	2543000	2.52	0.1595	4410	600.4	30.83	0.0000912	0.0000158	0.00728	739200
297.5	297	3794000	2.45	0.1539	5110	557.1	48.55	0.0000739	0.0000172	0.00488	638600
217.5	217	5473000	2.8	0.1482	6900	497.4	80.36	0.0000602	0.0000197	0.00248	498100
237.5	237	7750000	10.4	0.1425	34600	374.5	165.7	0.0000429	0.0000255	0.00027	225500

Fig A-1: NDT Test Result of X-Ray Image

Appendix-B

Tables for Data

Table B-1

Fill Ratio (V/Vmax)	Angle (°C)	Time (min)	Heat Load (W)	Evaporator Temperature, (°C)				Average Evaporator Temperature (°C)	Condenser TipTemperature, (°C)		Average	Adiabatic Position Temperature(°C)		Average	Average Condenser Temperature (°C)
				T5	**T6**	**T7**	**T8**		**T1**	**T2**		**T3**	**T4**		
		0		94	93.7	96.4	99.1	95.80	34.5	36.3	35.4	41.6	43	42.3	38.85
		20		100.3	101.3	101.3	109.7	103.15	49.2	49.4	49.3	68.7	64.3	66.5	57.9
		40		106.9	108.3	103.4	111.8	107.60	52.6	51.6	52.1	72.5	68.1	70.3	61.2
		60		101.9	101.7	102.9	113.9	105.10	50.9	50.5	50.7	72.5	69.8	71.15	60.925
		80		104.9	101.6	102.9	92	100.35	49.8	52.4	51.1	82.3	68.8	75.55	63.325
		100		100.6	101.1	102.7	103.8	102.05	51.5	53.3	52.4	68.5	66.5	67.5	59.95
		120		99.4	99.9	101	114.1	103.60	46.4	46.5	46.45	64.1	66.6	65.35	55.9
60%	0	140	40	98.9	98.8	114.1	87.9	99.93	47.6	46.3	46.95	62.2	62.9	62.55	54.75
		160		100.4	99.4	101.4	89.3	97.63	50.8	48.6	49.7	67.3	64.3	65.8	57.75
		180		100.8	100.5	106.1	90.2	99.40	52.3	50	51.15	68.3	68.1	68.2	59.675
		200		102.1	102.5	124.1	92	105.18	54.4	52	53.2	69	64.6	66.8	60
		220		97.5	98.7	94.9	86	94.28	46.5	45	45.75	60.2	58.3	59.25	52.5
		240		97.8	99	96.4	86.3	94.88	45.9	44.1	45	58.2	59.7	58.95	51.975
		260		0	0	0	0	0.00	0	0	0	0	0	0	0
		280		0	0	0	0	0.00	0	0	0	0	0	0	0

Table B-2

Fill Ratio (V/Vmax)	Angle (°C)	Time (min)	Heat Load (W)	Evaporator Temperature, (°C)				Average Evaporator Temperature (°C)	Condenser TipTemperature, (°C)		Average	Adiabatic Position Temperature(°C)		Average	Average Condenser Temperature (°C)
				T5	**T6**	**T7**	**T8**		**T1**	**T2**		**T3**	**T4**		
		0		96.9	99.3	99.4	102.5	99.53	33	33.4	33.2	39.3	39.4	39.35	36.275
		20		106.5	138	109.1	90.7	111.08	49.6	54.3	51.95	68.8	70.1	69.45	60.7
		40		108.2	142.2	108.9	93.4	113.18	56.3	57.4	56.85	73.7	73.9	73.8	65.325
		60		109.7	139.3	111.1	95.2	113.83	57.2	58.4	57.8	74.6	74.3	74.45	66.125
		80		110.8	142.6	112	95.9	115.33	56.8	57.2	57	73.8	73.9	73.85	65.425
		100		110.6	139.9	113.4	95.3	114.80	56.4	56.6	56.5	72.8	73.5	73.15	64.825
		120		112.2	113.9	144.5	97.9	117.13	57.7	53.8	55.75	74.7	71.8	73.25	64.5
60%	0	140	50	111	111.8	140.2	95.4	114.60	52.7	51.3	52	72.1	68.2	70.15	61.075
		160		109.8	109.8	110.1	93.5	105.80	53.4	51.8	52.6	70.9	69.1	70	61.3
		180		109.9	111	142.9	96.2	115.00	55.5	52.1	53.8	72.8	67.6	70.2	62
		200		109.8	109.7	108.5	94.5	105.63	55.9	53.1	54.5	73.1	71.1	72.1	63.3
		220		0	0	0	0	0.00	0	0	0	0	0	0	0
		240		0	0	0	0	0.00	0	0	0	0	0	0	0
		260		0	0	0	0	0.00	0	0	0	0	0	0	0
		280		0	0	0	0	0.00	0	0	0	0	0	0	0

Table B-3

Fill Ratio (V/Vmax)	Angle (°C)	Time (min)	Heat Load (W)	Evaporator Temperature, (°C)				Average Evaporator Temperature (°C)	Condenser TipTemperature, (°C)		Average	Adiabatic Position Temperature(°C)		Average	Average Condenser Temperature (°C)
				T5	**T6**	**T7**	**T8**		**T1**	**T2**		**T3**	**T4**		
		0		148.2	150.4	139.8	112	137.60	40.7	40.8	40.75	55.6	64.1	59.85	50.3
		20		117.6	119	117.2	114.7	117.13	58.4	61.6	60	75.3	73	74.15	67.075
		40		116.1	118.6	116.6	109.8	115.28	56.6	59.9	58.25	74.6	72.9	73.75	66
		60		131.4	119.9	119.4	112.4	120.78	58	63.8	60.9	76.8	74.3	75.55	68.225
		80		144.6	119.6	119.3	125.4	127.23	57.9	62.3	60.1	76	74.2	75.1	67.6
		100		149.9	120.3	141.3	104.9	129.10	58.5	62.2	60.35	76.2	75.3	75.75	68.05
		120		122.8	119.3	148.3	109.4	124.95	61.4	62.1	61.75	77.2	74.3	75.75	68.75
60%	0	140	60	119.1	121.9	150.9	109.5	125.35	61.6	60.9	61.25	77.4	75.7	76.55	68.9
		160		116.4	118.6	124.1	99.9	114.75	61.3	56.8	59.05	73	74.3	73.65	66.35
		180		109	109	131.1	93.1	110.55	46.8	47.5	47.15	67.9	63.7	65.8	56.475
		200		113.2	113.6	112.7	95.9	108.85	50.7	50.7	50.7	68.6	68.7	68.65	59.675
		220		111.9	111.9	120.5	94.8	109.78	50.1	49.9	50	68.3	69.1	68.7	59.35
		240		106.7	107.4	115.4	94.4	105.98	45.6	46.8	46.2	64.1	66.2	65.15	55.675
		260		115.2	116.4	115.1	97.5	111.05	53.8	53.7	53.75	71.2	71.3	71.25	62.5
		280		113.8	114.4	115.5	96.1	109.95	55.5	54.6	55.05	71.7	72.3	72	63.525

Table B-4

Fill Ratio (V/Vmax)	Angle (°C)	Time (min)	Heat Load (W)	Evaporator Temperature, (°C)				Average Evaporator Temperature (°C)	Condenser TipTemperature, (°C)		Average	Adiabatic Position Temperature(°C)		Average	Average Condenser Temperature (°C)
				T5	T6	T7	T8		T1	T2		T3	T4		
		0		114.4	114.5	121	110.4	115.08	35.2	34.7	34.95	47.7	49.9	48.8	41.875
		20		126.4	168.6	150.7	138.3	146.00	77.7	72.4	75.05	80.3	78.6	79.45	77.25
		40		144.8	131.2	133.4	113.8	130.80	73.4	72.5	72.95	82.2	80.9	81.55	77.25
		60		127.9	141.7	140.7	112.5	130.70	83	71.7	77.35	82	80.9	81.45	79.4
		80		156.1	130.9	133.6	109.8	132.60	66.7	75.1	70.9	82	79.5	80.75	75.825
		100		129.8	130.7	134.3	135.1	132.48	68.7	82.6	75.65	82.6	79.8	81.2	78.425
		120		128.8	128.8	133	112.4	125.75	82.8	79.4	81.1	82.2	80.6	81.4	81.25
60%	0	140	70	131.4	144.7	134.8	121.2	133.03	81.5	76.3	78.9	82.5	81.3	81.9	80.4
		160		128.6	161.4	131.6	114.1	133.93	83.7	82.6	83.15	82.7	81.8	82.25	82.7
		180		128.6	132.3	156.1	114.2	132.80	83.2	83.5	83.35	82.6	81.8	82.2	82.775
		200		129.1	132.3	134.4	113.1	127.23	84	83.8	83.9	82.9	81.6	82.25	83.075
		220		127.8	139.9	137.1	113.5	129.58	82.7	82	82.35	81.4	80.5	80.95	81.65
		240		133.1	130.3	141.6	114.7	129.93	76.1	80.4	78.25	81.3	79.7	80.5	79.375
		260		131.6	130.9	135.8	114.2	128.13	80.7	79.5	80.1	83.1	82.1	82.6	81.35
		280		127.9	147.6	133.5	114.8	130.95	84.3	80.6	82.45	83.1	82.3	82.7	82.575

Table B-5

Fill Ratio (V/Vmax)	Angle (°C)	Time (min)	Heat Load (W)	Evaporator Temperature, (°C)				Average Evaporator Temperature (°C)	Condenser TipTemperature, (°C)		Average	Adiabatic Position Temperature(°C)		Average	Average Condenser Temperature (°C)
				T5	T6	T7	T8		T1	T2		T3	T4		
		0		122.2	145.7	125.4	94.9	122.05	33.9	33.9	33.9	46.7	59.1	52.9	43.4
		20		138.1	192	191.2	147.3	167.15	75.9	76.9	76.4	82.7	80.7	81.7	79.05
		40		134.7	177.5	141.6	115.8	142.40	82.6	83.1	82.85	81.8	81	81.4	82.125
		60		134.4	185.2	161.8	115.2	149.15	83	81.8	82.4	81.6	80.2	80.9	81.65
		80		140	192.1	145.7	119.4	149.30	86.6	86.7	86.65	85.5	84.4	84.95	85.8
		100		147.8	161.6	154.7	119.8	145.98	85.3	87.5	86.4	86.1	84.9	85.5	85.95
		120		186.7	188.6	172.4	119.7	166.85	88.1	87.4	87.75	86.8	86.1	86.45	87.1
60%	0	140	80	141.7	195.9	147.3	123.5	152.10	88.8	88.4	88.6	87.9	87.4	87.65	88.125
		160		141.7	201	178.9	125.9	161.88	88.8	88.7	88.75	87.9	86.7	87.3	88.025
		180		141.9	141.4	146.1	122.7	138.03	91.3	90.1	90.7	88.9	88.3	88.6	89.65
		200		141.9	142.4	148.1	123.4	138.95	92.1	91.1	91.6	89.4	89	89.2	90.4
		220		141.9	144.4	147.1	124.6	139.50	90.8	85.1	87.95	90.9	89.8	90.35	89.15
		240		183.3	195.5	146.6	122.1	161.88	88.5	87.2	87.85	87.5	87.1	87.3	87.575
		260		0	0	0	0	0.00	0	0	0	0	0	0	0
		280		0	0	0	0	0.00	0	0	0	0	0	0	0

Table B-6

Fill Ratio (V/Vmax)	Angle (°C)	Time (min)	Heat Load (W)	Evaporator Temperature, (°C)				Average Evaporator Temperature (°C)	Condenser TipTemperature, (°C)		Average	Adiabatic Position Temperature(°C)		Average	Average Condenser Temperature (°C)
				T5	T6	T7	T8		T1	T2		T3	T4		
		0		58	59.9	59.2	56.5	58.40	32.4	32.1	32.25	39.2	38.5	38.85	35.55
		20		179.4	202.8	199.3	117.7	174.80	72.2	82.8	77.5	84.2	82.4	83.3	80.4
		40		147	203.9	198.6	123.6	168.28	88.3	88.5	88.4	87.7	86.1	86.9	87.65
		60		144.3	205	196.4	129.9	168.90	87.5	87.2	87.35	87.1	85.1	86.1	86.725
		80		143.3	205.2	192.1	123.6	166.05	87.2	87.1	87.15	86.8	85	85.9	86.525
		100		143.4	200.5	176.3	120	160.05	86.9	86.6	86.75	86.2	85.1	85.65	86.2
		120		143.1	202	181.5	123.2	162.45	86	86.1	86.05	85.3	84.2	84.75	85.4
60%	0	140	90	186	190.4	156.1	121.6	163.53	88.7	88.2	88.45	87.8	87.2	87.5	87.975
		160		143.8	143	148.6	121.7	139.28	91	90.4	90.7	88.8	88	88.4	89.55
		180		146.6	147.3	151.5	125.5	142.73	93.6	92.5	93.05	91.8	90.3	91.05	92.05
		200		147.7	147.8	153	124.6	143.28	93	89	91	90.3	89.7	90	90.5
		220		147.6	148.2	153.2	125.5	143.63	93.6	90.8	92.2	91.8	90.3	91.05	91.625
		240		0	0	0	0	0.00	0	0	0	0	0	0	0
		260		0	0	0	0	0.00	0	0	0	0	0	0	0
		280		0	0	0	0	0.00	0	0	0	0	0	0	0

Table B-7

Fill Ratio (V/Vmax)	Angle (°C)	Time (min)	Heat Load (W)	Evaporator Temperature, (°C)				Average Evaporator Temperature (°C)	Condenser TipTemperature, (°C)		Average	Adiabatic Position Temperature(°C)		Average	Average Condenser Temperature (°C)
				T5	T6	T7	T8		T1	T2		T3	T4		
60%	10	0	40	97.2	114.7	94.1	106	103.00	38	37.2	37.6	50.3	63.3	56.8	47.2
		20		104.4	129.2	126.7	113.2	118.38	51.2	47.9	49.55	67.8	74.4	71.1	60.325
		40		120.4	130	127.6	115.5	123.38	54.1	49.7	51.9	71.6	76.3	73.95	62.925
		60		101.9	129.1	126.1	114.7	117.95	53.8	50.1	51.95	71.2	74.4	72.8	62.375
		80		101.5	129.5	101.1	86.4	104.63	56.3	51.8	54.05	70.2	70.8	70.5	62.275
		100		104.6	131.2	118.7	88.8	110.83	60.8	55.1	57.95	72.5	72.2	72.35	65.15
		120		105	128.9	102.4	88.4	106.18	59	52.7	55.85	71.7	71.8	71.75	63.8
		140		102.1	117.8	122.9	87	107.45	56.5	52.1	54.3	70.9	71.4	71.15	62.725
		160		103.6	105.5	102.2	87.9	99.80	57.7	54.6	56.15	71.8	72.1	71.95	64.05
		180		103.5	102.6	128	88.5	105.65	60.6	54.5	57.55	73.2	72.5	72.85	65.2
		200		101.9	102.4	101.4	87.4	98.28	56.9	53	54.95	71.4	70.8	71.1	63.025
		220		99.3	100.3	98.5	85.2	95.83	49.5	48.4	48.95	65.9	67.3	66.6	57.775
		240		98	98.5	115.8	84.3	99.15	44	45.2	44.6	62.9	66.1	64.5	54.55
		260		100.3	101.8	100.2	85	96.83	48	47.9	47.95	68.1	67.9	68	57.975
		280		0	0	0	0	0.00	0	0	0	0	0	0	0

Table B-8

Fill Ratio (V/Vmax)	Angle (°C)	Time (min)	Heat Load (W)	Evaporator Temperature, (°C)				Average Evaporator Temperature (°C)	Condenser TipTemperature, (°C)		Average	Adiabatic Position Temperature(°C)		Average	Average Condenser Temperature (°C)
				T5	T6	T7	T8		T1	T2		T3	T4		
60%	10	0	50	98.5	101.6	96.9	95.9	98.23	30.8	30.8	30.8	34.4	35.1	34.75	32.775
		20		105.7	108.4	103.9	90.8	102.20	53.1	52.4	52.75	71.4	66.7	69.05	60.9
		40		105.5	108	119.6	92.5	106.40	54.2	52.9	53.55	72.7	65.4	69.05	61.3
		60		106.7	108	104.1	105.7	106.13	53.8	53.4	53.6	71.3	71.4	71.35	62.475
		80		109.3	110	105.9	94	104.80	56.2	54.9	55.55	72.2	71	71.6	63.575
		100		107.2	110.4	136.3	92.3	111.55	57.2	54.5	55.85	73	70.4	71.7	63.775
		120		105.4	108.2	136	95.8	111.35	55.7	52.6	54.15	72.4	67.7	70.05	62.1
		140		102.2	104	119.1	89.3	103.65	54.9	53.3	54.1	71	69.3	70.15	62.125
		160		102.8	104.1	104.9	89.4	100.30	47.8	47.4	47.6	67	67.7	67.35	57.475
		180		105.9	107.5	136.7	90.4	110.13	54.4	52.2	53.3	70.8	69.4	70.1	61.7
		200		106.6	108.9	107.3	91.6	103.60	54.4	51.8	53.1	71.6	70.7	71.15	62.125
		220		0	0	0	0	0.00	0	0	0	0	0	0	0
		240		0	0	0	0	0.00	0	0	0	0	0	0	0
		260		0	0	0	0	0.00	0	0	0	0	0	0	0
		280		0	0	0	0	0.00	0	0	0	0	0	0	0

Table B-9

Fill Ratio (V/Vmax)	Angle (°C)	Time (min)	Heat Load (W)	Evaporator Temperature, (°C)				Average Evaporator Temperature (°C)	Condenser TipTemperature, (°C)		Average	Adiabatic Position Temperature(°C)		Average	Average Condenser Temperature (°C)
				T5	T6	T7	T8		T1	T2		T3	T4		
60%	10	0	60	88.4	79.5	83.7	77.1	82.18	29.7	29.7	29.7	29.8	30.6	30.2	29.95
		20		109.9	110	152.9	96	117.20	57	51.5	54.25	73.3	74.8	74.05	64.15
		40		126.4	113	159.6	101.5	125.13	58.8	54.3	56.55	76.5	77.9	77.2	66.875
		60		114	115.4	157.4	98.5	121.33	64.6	59.3	61.95	77.8	76	76.9	69.425
		80		123.1	140.1	121.7	111	123.98	66.3	71	68.65	80.6	78.3	79.45	74.05
		100		124.4	157	154.4	109.1	136.23	66.1	65.8	65.95	80.8	78.1	79.45	72.7
		120		135.9	151.2	118.5	96.9	125.63	66.6	68.7	67.65	78.3	77.1	77.7	72.675
		140		121	115.2	130.1	98.5	116.20	65	71.8	68.4	79.5	77	78.25	73.325
		160		155.1	133.7	118.9	99.7	126.85	59.1	60.2	59.65	77.5	75.8	76.65	68.15
		180		149.2	142.2	124.7	101.8	129.48	54.3	56	55.15	75.1	73	74.05	64.6
		200		122.4	119.6	113.3	92.2	111.88	56.3	54.4	55.35	72.3	72.3	72.3	63.825
		220		113.8	112.5	153.1	96.6	119.00	57.3	54.4	55.85	75.8	75.8	75.8	65.825
		240		0	0	0	0	0.00	0	0	0	0	0	0	0
		260		0	0	0	0	0.00	0	0	0	0	0	0	0
		280		0	0	0	0	0.00	0	0	0	0	0	0	0

Table B-10

Fill Ratio (V/Vmax)	Angle (°C)	Time (min)	Heat Load (W)	Evaporator Temperature, (°C)				Average Evaporator Temperature (°C)	Condenser TipTemperature, (°C)		Average	Adiabatic Position Temperature(°C)		Average	Average Condenser Temperature (°C)
				T5	T6	T7	T8		T1	T2		T3	T4		
		0		107.1	122.7	117.8	101.8	112.35	34.5	34.5	34.5	35	37.9	36.45	35.475
		20		115.1	118.4	165.4	111.6	127.63	53.3	54.9	54.1	76.6	73.3	74.95	64.525
		40		118.4	116.7	158.5	94.7	122.08	53.8	56.1	54.95	77.6	71.2	74.4	64.675
		60		154.9	113.9	161.4	95	131.30	53.1	56.1	54.6	78.6	71.8	75.2	64.9
		80		153.5	113.9	160.3	109.1	134.20	53.1	57.6	55.35	78.2	71.5	74.85	65.1
		100		154.9	114.3	160.1	121	137.58	51.1	57.2	54.15	76.6	70.6	73.6	63.875
		120		137.7	115.7	164.3	97.7	128.85	51.9	56.4	54.15	76.8	72.9	74.85	64.5
60%	10	140	70	153.7	114	161.4	107.3	134.10	51.6	55.5	53.55	76.6	71.7	74.15	63.85
		160		163.5	121.7	165.2	140.3	147.68	55.4	62.5	58.95	77.9	75.2	76.55	67.75
		180		169.7	171	173.6	151	166.33	70.4	72.3	71.35	85.6	86.4	86	78.675
		200		0	0	0	0	0.00	0	0	0	0	0	0	0
		220		0	0	0	0	0.00	0	0	0	0	0	0	0
		240		0	0	0	0	0.00	0	0	0	0	0	0	0
		260		0	0	0	0	0.00	0	0	0	0	0	0	0
		280		0	0	0	0	0.00	0	0	0	0	0	0	0

‘Table B-11

Fill Ratio (V/Vmax)	Angle (°C)	Time (min)	Heat Load (W)	Evaporator Temperature, (°C)				Average Evaporator Temperature (°C)	Condenser TipTemperature, (°C)		Average	Adiabatic Position Temperature(°C)		Average	Average Condenser Temperature (°C)
				T5	T6	T7	T8		T1	T2		T3	T4		
		0		113.5	123.7	117.4	113	116.90	33	32.9	32.95	35	43.8	39.4	36.175
		20		127.5	161.1	175.6	121.4	146.40	66.4	67.4	66.9	81.5	79.6	80.55	73.725
		40		162	154.3	152.3	132.6	150.30	65	77	71	82.1	79.2	80.65	75.825
		60		130.6	169.1	145.7	102.5	136.98	82.6	81.7	82.15	81.6	79.2	80.4	81.275
		80		125.3	124.1	165.5	101.5	129.10	80.4	71.3	75.85	80.6	77.9	79.25	77.55
		100		129.9	128	135.2	104.6	124.43	84.4	83.6	84	80.9	79.6	80.25	82.125
		120		131.3	154.8	133.8	112	132.98	83.9	72.5	78.2	83.2	81.7	82.45	80.325
60%	10	140	80	148	153.7	153.4	107.1	140.55	81.9	79.2	80.55	85.4	83.9	84.65	82.6
		160		0	0	0	0	0.00	0	0	0	0	0	0	0
		180		0	0	0	0	0.00	0	0	0	0	0	0	0
		200		0	0	0	0	0.00	0	0	0	0	0	0	0
		220		0	0	0	0	0.00	0	0	0	0	0	0	0
		240		0	0	0	0	0.00	0	0	0	0	0	0	0
		260		0	0	0	0	0.00	0	0	0	0	0	0	0
		280		0	0	0	0	0.00	0	0	0	0	0	0	0

Table B-12

Fill Ratio (V/Vmax)	Angle (°C)	Time (min)	Heat Load (W)	Evaporator Temperature, (°C)				Average Evaporator Temperature (°C)	Condenser TipTemperature, (°C)		Average	Adiabatic Position Temperature(°C)		Average	Average Condenser Temperature (°C)
				T5	T6	T7	T8		T1	T2		T3	T4		
		0		29.6	29.6	29.6	29.5	29.58	29.5	29.5	29.5	29.5	29.7	29.6	29.55
		20		179.4	196.1	197.4	139.9	178.20	71.2	83.6	77.4	84.4	80.5	82.45	79.925
		40		152	192.7	140.1	110.2	148.75	82.7	83.4	83.05	83.9	80.8	82.35	82.7
		60		141.7	178.2	143.1	125.5	147.13	83.6	83.1	83.35	83.5	81.5	82.5	82.925
		80		177.4	188.7	143.7	109.8	154.90	84.6	83.7	84.15	85.6	83.5	84.55	84.35
		100		163.3	190.8	152.3	111.6	154.50	85.8	83.7	84.75	85	82.8	83.9	84.325
		120		143.6	142.3	145.7	113.2	136.20	89.8	88.9	89.35	88.1	85.8	86.95	88.15
60%	10	140	90	146.8	171.3	149	107.2	143.58	81.5	82.1	81.8	83.7	82.5	83.1	82.45
		160		135.3	151.7	139.3	109.9	134.05	84.1	81.7	82.9	83.8	80.5	82.15	82.525
		180		150	193.4	143.1	109.4	148.98	86.8	86.2	86.5	86	84	85	85.75
		200		133.7	131	130.4	105.9	125.25	82.1	75.4	78.75	83.1	80.4	81.75	80.25
		220		137.7	134.3	142.9	111.4	131.58	86.9	82.7	84.8	86.4	83.2	84.8	84.8
		240		144.6	188.2	178.7	111.1	155.65	84.9	80.7	82.8	84.9	82.8	83.85	83.325
		260		0	0	0	0	0.00	0	0	0	0	0	0	0
		280		0	0	0	0	0.00	0	0	0	0	0	0	0

Table B-13

Fill Ratio (V/Vmax)	Angle (°C)	Time (min)	Heat Load (W)	Evaporator Temperature, (°C)				Average Evaporator Temperature (°C)	Condenser TipTemperature, (°C)		Average	Adiabatic Position Temperature(°C)		Average	Average Condenser Temperature (°C)
				T5	T6	T7	T8		T1	T2		T3	T4		
		0		93.2	93	90.1	81.6	89.48	32	31.9	31.95	34.2	39.4	36.8	34.375
		20		94.9	96.3	95.5	82.2	92.23	46.3	44.5	45.4	63.8	68.8	66.3	55.85
		40		100.9	101.1	126.9	86.4	103.83	52.5	49.5	51	73.9	74.2	74.05	62.525
		60		101.3	99.4	103.4	86.8	97.73	53.4	51.6	52.5	73.8	71.1	72.45	62.475
		80		95.4	96.1	99.1	83.5	93.53	45.2	45.6	45.4	63.4	66.9	65.15	55.275
		100		96.7	97.1	100.6	83.8	94.55	46.8	45.6	46.2	67	68.9	67.95	57.075
		120		98.6	101.3	128.3	85.5	103.43	53.2	53.6	53.4	71.1	72.4	71.75	62.575
60%	20	140	40	98.4	99.5	99.5	86.6	96.00	54.8	53.9	54.35	73.6	71.5	72.55	63.45
		160		99	98.7	124.6	86.2	102.13	52.5	51	51.75	72	71.1	71.55	61.65
		180		97.4	96.9	103.8	85.1	95.80	52.5	50.5	51.5	72.2	70.6	71.4	61.45
		200		0	0	0	0	0.00	0	0	0	0	0	0	0
		220		0	0	0	0	0.00	0	0	0	0	0	0	0
		240		0	0	0	0	0.00	0	0	0	0	0	0	0
		260		0	0	0	0	0.00	0	0	0	0	0	0	0
		280		0	0	0	0	0.00	0	0	0	0	0	0	0

Table B-14

Fill Ratio (V/Vmax)	Angle (°C)	Time (min)	Heat Load (W)	Evaporator Temperature, (°C)				Average Evaporator Temperature (°C)	Condenser TipTemperature, (°C)		Average	Adiabatic Position Temperature(°C)		Average	Average Condenser Temperature (°C)
				T5	T6	T7	T8		T1	T2		T3	T4		
		0		85.7	84.6	86.7	75.3	83.08	29.2	29.2	29.2	29.7	31.5	30.6	29.9
		20		102.5	103.2	129.9	85	105.15	47.1	45.3	46.2	66	70.5	68.25	57.225
		40		103.7	104.7	110.2	88.1	101.68	53.2	51.6	52.4	71.5	71.4	71.45	61.925
		60		101.3	102.6	112	85.8	100.43	51	49.3	50.15	70.4	70.8	70.6	60.375
		80		131.3	104.4	130	88.2	113.48	50.8	50.3	50.55	72.4	72.4	72.4	61.475
		100		105.8	102.3	128.2	87.8	106.03	51.2	50.4	50.8	73.7	71.7	72.7	61.75
		120		113.4	103.5	129.8	87.4	108.53	52.7	51	51.85	73.6	73	73.3	62.575
60%	20	140	50	126.8	107.7	108.6	90.2	108.33	54.9	54.4	54.65	75.3	72.1	73.7	64.175
		160		0	0	0	0	0.00	0	0	0	0	0	0	0
		180		0	0	0	0	0.00	0	0	0	0	0	0	0
		200		0	0	0	0	0.00	0	0	0	0	0	0	0
		220		0	0	0	0	0.00	0	0	0	0	0	0	0
		240		0	0	0	0	0.00	0	0	0	0	0	0	0
		260		0	0	0	0	0.00	0	0	0	0	0	0	0
		280		0	0	0	0	0.00	0	0	0	0	0	0	0

Table B-15

Fill Ratio (V/Vmax)	Angle (°C)	Time (min)	Heat Load (W)	Evaporator Temperature, (°C)				Average Evaporator Temperature (°C)	Condenser TipTemperature, (°C)		Average	Adiabatic Position Temperature(°C)		Average	Average Condenser Temperature (°C)
				T5	T6	T7	T8		T1	T2		T3	T4		
		0		102.4	108.2	104.8	95.6	102.75	32.1	32.2	32.15	34.1	39.9	37	34.575
		20		110.9	117.5	156.9	92.4	119.43	58.2	59	58.6	76.2	75.7	75.95	67.275
		40		113.4	114.1	156.9	94.1	119.63	64.1	62.3	63.2	78.6	76.4	77.5	70.35
		60		114.7	158	126.2	94.6	123.38	66	65.8	65.9	79.2	76.4	77.8	71.85
		80		116.2	160.4	147.4	96	130.00	73.3	78.8	76.05	81	79.1	80.05	78.05
		100		118	164	134.9	97.6	128.63	75.3	80.4	77.85	82.5	78.8	80.65	79.25
		120		116	123.1	121.5	96.3	114.23	78.5	81.3	79.9	81.7	77.5	79.6	79.75
60%	20	140	60	116.4	142.6	121.4	97.2	119.40	77.8	81	79.4	81.6	77.9	79.75	79.575
		160		117.2	152.6	126.8	98.8	123.85	74.2	81.1	77.65	82.3	79.6	80.95	79.3
		180		116.4	148.4	139	97.5	125.33	77.3	82.1	79.7	81.9	79.4	80.65	80.175
		200		0	0	0	0	0.00	0	0	0	0	0	0	0
		220		0	0	0	0	0.00	0	0	0	0	0	0	0
		240		0	0	0	0	0.00	0	0	0	0	0	0	0
		260		0	0	0	0	0.00	0	0	0	0	0	0	0
		280		0	0	0	0	0.00	0	0	0	0	0	0	0

Table B-16

Fill Ratio (V/Vmax)	Angle (°C)	Time (min)	Heat Load (W)	Evaporator Temperature, (°C)				Average Evaporator Temperature (°C)	Condenser TipTemperature, (°C)		Average	Adiabatic Position Temperature(°C)		Average	Average Condenser Temperature (°C)
				T5	**T6**	**T7**	**T8**		**T1**	**T2**		**T3**	**T4**		
		0		99.1	101.1	118.9	102.9	105.50	34.4	34.6	34.5	38.9	47.7	43.3	38.9
		20		116.7	118	163.4	94.2	123.08	61	62.8	61.9	77.5	77.5	77.5	69.7
		40		111.9	119.3	117.6	93.7	110.63	59.3	61.9	60.6	76.5	71.4	73.95	67.275
		60		126.2	112.4	122.8	109.7	117.78	54.6	61.7	58.15	77.6	72.3	74.95	66.55
		80		144.9	115	164.2	100.2	131.08	55.1	61.2	58.15	79.1	75.2	77.15	67.65
		100		152.5	116.2	162.2	110.7	135.40	57.3	60.7	59	78.3	74	76.15	67.575
		120		159	122.6	159.4	125.2	141.55	59.8	62.9	61.35	80	76.1	78.05	69.7
60%	20	140	70	145.9	133.4	143	101.7	131.00	56.9	60.9	58.9	77.1	73.5	75.3	67.1
		160		139.3	132.3	154.1	98.8	131.13	54.6	57.9	56.25	76.2	72.6	74.4	65.325
		180		117.6	143.2	162.6	99.3	130.68	59.8	58.8	59.3	78.3	74.2	76.25	67.775
		200		120.6	148.2	170.6	105.8	136.30	59	56.8	57.9	77.7	76.7	77.2	67.55
		220		0	0	0	0	0.00	0	0	0	0	0	0	0
		240		0	0	0	0	0.00	0	0	0	0	0	0	0
		260		0	0	0	0	0.00	0	0	0	0	0	0	0
		280		0	0	0	0	0.00	0	0	0	0	0	0	0

Table B-17

Fill Ratio (V/Vmax)	Angle (°C)	Time (min)	Heat Load (W)	Evaporator Temperature, (°C)				Average Evaporator Temperature (°C)	Condenser TipTemperature, (°C)		Average	Adiabatic Position Temperature(°C)		Average	Average Condenser Temperature (°C)
				T5	**T6**	**T7**	**T8**		**T1**	**T2**		**T3**	**T4**		
		0		57.4	60	58.7	59.4	58.88	36	36.3	36.15	47.4	53.4	50.4	43.275
		20		132.7	183	185.2	110.1	152.75	72.5	68.5	70.5	83.4	80	81.7	76.1
		40		176.6	196.1	195.6	162.5	182.70	72.3	80	76.15	85.7	82.9	84.3	80.225
		60		130	180.1	139.2	139	147.08	84.8	84.5	84.65	86.3	78.9	82.6	83.625
		80		158.8	184	180.3	109.9	158.25	72.3	77.7	75	85.8	81.7	83.75	79.375
		100		156.6	181.5	131.9	103.1	143.28	59.2	71.6	65.4	78.1	74.5	76.3	70.85
		120		160.7	117.6	125.7	100	126.00	56.3	62.2	59.25	79	71.2	75.1	67.175
60%	20	140	80	134.5	187.6	178.9	157.2	164.55	80.6	77.3	78.95	86.7	84.7	85.7	82.325
		160		182.7	189.2	182.3	107.6	165.45	73.7	79.2	76.45	86.2	83	84.6	80.525
		180		131.9	177.6	143.3	106.8	139.90	86.5	83.7	85.1	86	82	84	84.55
		200		0	0	0	0	0.00	0	0	0	0	0	0	0
		220		0	0	0	0	0.00	0	0	0	0	0	0	0
		240		0	0	0	0	0.00	0	0	0	0	0	0	0
		260		0	0	0	0	0.00	0	0	0	0	0	0	0
		280		0	0	0	0	0.00	0	0	0	0	0	0	0

Table B-18

Fill Ratio (V/Vmax)	Angle (°C)	Time (min)	Heat Load (W)	Evaporator Temperature, (°C)				Average Evaporator Temperature (°C)	Condenser TipTemperature, (°C)		Average	Adiabatic Position Temperature(°C)		Average	Average Condenser Temperature (°C)
				T5	**T6**	**T7**	**T8**		**T1**	**T2**		**T3**	**T4**		
		0		74.6	67.2	70	68.4	70.05	32.7	32.9	32.8	32.7	32.9	32.8	32.8
		20		158.6	148.8	129.2	136.5	143.28	35.4	35.6	35.5	48.7	66.3	57.5	46.5
		40		126.2	132.2	132	97.4	121.95	54.6	59.3	56.95	73.6	75.1	74.35	65.65
		60		120.6	123.2	126.5	92.1	115.60	38	43.3	40.65	63.4	68.8	66.1	53.375
		80		140.6	199.7	196.7	168.5	176.38	75.3	76.6	75.95	89.1	88.9	89	82.475
		100		142.5	193.7	149.2	133.4	154.70	88.1	87.5	87.8	87.9	86.4	87.15	87.475
		120		143.3	208.7	197.5	150.8	175.08	90.9	90.7	90.8	90.7	92.2	91.45	91.125
60%	20	140	90	158.4	204.9	194.4	116.5	168.55	90.4	90.2	90.3	90.2	92.6	91.4	90.85
		160		0	0	0	0	0.00	0	0	0	0	0	0	0
		180		0	0	0	0	0.00	0	0	0	0	0	0	0
		200		0	0	0	0	0.00	0	0	0	0	0	0	0
		220		0	0	0	0	0.00	0	0	0	0	0	0	0
		240		0	0	0	0	0.00	0	0	0	0	0	0	0
		260		0	0	0	0	0.00	0	0	0	0	0	0	0
		280		0	0	0	0	0.00	0	0	0	0	0	0	0

Table B-19

Fill Ratio (V/Vmax)	Angle (°C)	Time (min)	Heat Load (W)	Evaporator Temperature, (°C)				Average Evaporator Temperature (°C)	Condenser TipTemperature, (°C)		Average	Adiabatic Position Temperature(°C)		Average	Average Condenser Temperature (°C)
				T5	**T6**	**T7**	**T8**		**T1**	**T2**		**T3**	**T4**		
		0		42.4	39.3	41.2	43.1	41.50	33.6	33.8	33.7	33.8	34	33.9	33.8
		20		93.3	103.9	111.4	99.9	102.13	40.5	41.3	40.9	53.8	61.1	57.45	49.175
		40		92.5	95.5	113	80.3	95.33	41.4	42.5	41.95	57.2	62.2	59.7	50.825
		60		94.6	97.5	114	81.4	96.88	42.2	42.4	42.3	59.8	63.2	61.5	51.9
		80		105.1	97.8	110.9	98.6	103.10	41.5	42.2	41.85	55.9	61.7	58.8	50.325
		100		91.8	95.4	109.9	80.4	94.38	41.9	42.8	42.35	56.5	61.9	59.2	50.775
		120		106.2	106.1	108.4	105.4	106.53	40.8	41.8	41.3	52.5	60.3	56.4	48.85
60%	30	140	40	95.1	110.4	113.4	105.4	106.08	40.3	41.4	40.85	57.2	62.1	59.65	50.25
		160		92.2	92.6	110.1	103.1	99.50	39.5	41	40.25	55.1	60.7	57.9	49.075
		180		93.4	91.1	108.8	80.7	93.50	39.8	41.3	40.55	53.9	59.6	56.75	48.65
		200		0	0	0	0	0.00	0	0	0	0	0	0	0
		220		0	0	0	0	0.00	0	0	0	0	0	0	0
		240		0	0	0	0	0.00	0	0	0	0	0	0	0
		260		0	0	0	0	0.00	0	0	0	0	0	0	0
		280		0	0	0	0	0.00	0	0	0	0	0	0	0

Table B-20

Fill Ratio (V/Vmax)	Angle (°C)	Time (min)	Heat Load (W)	Evaporator Temperature, (°C)				Average Evaporator Temperature (°C)	Condenser TipTemperature, (°C)		Average	Adiabatic Position Temperature(°C)		Average	Average Condenser Temperature (°C)
				T5	**T6**	**T7**	**T8**		**T1**	**T2**		**T3**	**T4**		
		0		103.6	121	114.2	100.2	109.75	33.8	33	33.4	40.4	52.5	46.45	39.925
		20		110.9	140.1	137.7	88.6	119.33	56.2	52.8	54.5	71.8	71.9	71.85	63.175
		40		109.5	105.4	138.3	89.1	110.58	52.8	52	52.4	73.1	70.9	72	62.2
		60		111.2	107.8	108.8	89.1	104.23	56.2	55.4	55.8	72	69.8	70.9	63.35
		80		112.1	108.8	108.5	90.5	104.98	56.3	55.1	55.7	74.1	70.9	72.5	64.1
		100		110.6	105.6	109.7	88.4	103.58	55	53.8	54.4	72.4	69.6	71	62.7
		120		111.1	105.5	107.9	89.2	103.43	58.4	56.5	57.45	73.8	70.3	72.05	64.75
60%	30	140	50	109.8	106	138.5	92.9	111.80	55.4	52.1	53.75	73.9	72.2	73.05	63.4
		160		111.4	107.2	138.5	90.7	111.95	56.7	52.7	54.7	74.9	75.4	75.15	64.925
		180		0	0	0	0	0.00	0	0	0	0	0	0	0
		200		0	0	0	0	0.00	0	0	0	0	0	0	0
		220		0	0	0	0	0.00	0	0	0	0	0	0	0
		240		0	0	0	0	0.00	0	0	0	0	0	0	0
		260		0	0	0	0	0.00	0	0	0	0	0	0	0
		280		0	0	0	0	0.00	0	0	0	0	0	0	0

Table B-21

Fill Ratio (V/Vmax)	Angle (°C)	Time (min)	Heat Load (W)	Evaporator Temperature, (°C)				Average Evaporator Temperature (°C)	Condenser TipTemperature, (°C)		Average	Adiabatic Position Temperature(°C)		Average	Average Condenser Temperature (°C)
				T5	**T6**	**T7**	**T8**		**T1**	**T2**		**T3**	**T4**		
		0		90.8	87.3	89.6	80.1	86.95	32.8	33.2	33	33.2	33.9	33.55	33.275
		20		132.8	140.1	136.8	96.2	126.48	62.3	64.9	63.6	79.2	76.3	77.75	70.675
		40		114.7	115	119	95.2	110.98	79.1	66.4	72.75	78.6	74.2	76.4	74.575
		60		128.3	157	119	96.6	125.23	66.8	68.9	67.85	80.1	75.7	77.9	72.875
		80		139.5	160.7	149.7	97.8	136.93	67.8	66.1	66.95	81.3	77.4	79.35	73.15
		100		115.8	123.2	119.7	95.5	113.55	78	68.4	73.2	79.9	76.4	78.15	75.675
		120		118.1	125.4	118.6	96.7	114.70	68.9	69.9	69.4	80.3	77.2	78.75	74.075
60%	30	140	60	147.9	149.1	145.6	97.5	135.03	62.8	60.4	61.6	78.4	74.6	76.5	69.05
		160		150	148.4	152	93.9	136.08	59.8	58.2	59	77.4	74.1	75.75	67.375
		180		121.7	150.4	152.3	94	129.60	62.7	57.8	60.25	77.3	78	77.65	68.95
		200		115.2	144.1	120	95.2	118.63	65.6	57.5	61.55	78.2	74.6	76.4	68.975
		220		114.4	146.4	133.2	94.4	122.10	67.8	60.1	63.95	77.9	74.8	76.35	70.15
		240		115.1	126.2	125.5	95.3	115.53	71.8	62.7	67.25	78.5	75.1	76.8	72.025
		260		0	0	0	0	0.00	0	0	0	0	0	0	0
		280		0	0	0	0	0.00	0	0	0	0	0	0	0

Table B-22

Fill Ratio (V/Vmax)	Angle (°C)	Time (min)	Heat Load (W)	Evaporator Temperature, (°C)				Average Evaporator Temperature (°C)	Condenser TipTemperature, (°C)		Average	Adiabatic Position Temperature(°C)		Average	Average Condenser Temperature (°C)
				T5	T6	T7	T8		T1	T2		T3	T4		
		0		33.6	33.2	33	33.1	33.23	33	33	33	33	33	33	33
		20		119.5	138.7	158.6	99.6	129.10	66.4	60.2	63.3	77.9	75.4	76.65	69.975
		40		133.7	164.1	149.2	124.6	142.90	67.1	73.3	70.2	80.5	74.9	77.7	73.95
		60		153.6	164.7	165.3	106.9	147.63	62.1	61.3	61.7	79.1	71.8	75.45	68.575
		80		157.6	165.7	170.7	112.3	151.58	66.1	63.9	65	80.5	75.4	77.95	71.475
		100		160.8	170.2	165.4	114.8	152.80	66.4	64.5	65.45	80.9	75.8	78.35	71.9
		120		144.7	165.7	128.9	101.6	135.23	75.6	71.6	73.6	82.5	75.8	79.15	76.375
60%	30	140	70	121.2	120.1	126.8	96.9	116.25	78.8	67.2	73	79.6	72.8	76.2	74.6
		160		122	147	131.2	99.7	124.98	81.3	70.3	75.8	80.9	75.9	78.4	77.1
		180		121.5	129.9	136	98.9	121.58	80	67	73.5	79.9	73.6	76.75	75.125
		200		146.8	151.5	125.7	104.9	132.23	65.4	64	64.7	79.7	73	76.35	70.525
		220		147.1	172.1	169.5	116.8	151.38	66	68.7	67.35	80.8	75.7	78.25	72.8
		240		142.7	162.6	165.8	105.9	144.25	63.6	60.9	62.25	79.8	73.2	76.5	69.375
		260		161.6	165.4	167.9	125	154.98	62.3	60.5	61.4	79.1	72.9	76	68.7
		280		166.7	172.2	173.5	141.8	163.55	74.8	65.9	70.35	81.7	76.4	79.05	74.7

Table B-23

Fill Ratio (V/Vmax)	Angle (°C)	Time (min)	Heat Load (W)	Evaporator Temperature, (°C)				Average Evaporator Temperature (°C)	Condenser TipTemperature, (°C)		Average	Adiabatic Position Temperature(°C)		Average	Average Condenser Temperature (°C)
				T5	T6	T7	T8		T1	T2		T3	T4		
		0		32	32	32	32.1	32.03	32	32	32	32	31.9	31.95	31.975
		20		173	138.9	138.6	103.3	138.45	68.1	80.3	74.2	81.5	75.3	78.4	76.3
		40		169.1	134.7	131.4	102.3	134.38	69	70	69.5	80.4	73.6	77	73.25
		60		165.9	139.8	129.4	100.1	133.80	68.4	67.8	68.1	80.1	73.5	76.8	72.45
		80		134	186.5	167.3	105.1	148.23	83.5	82.8	83.15	83.2	77.2	80.2	81.675
		100		131	177	132.2	102.3	135.63	81.3	80.9	81.1	81.1	73.3	77.2	79.15
		120		125.8	170.3	136.4	105	134.38	80.6	80.2	80.4	80.2	75.5	77.85	79.125
60%	30	140	80	130.5	156.2	135.1	101.1	130.73	81	78.8	79.9	80.8	73.8	77.3	78.6
		160		0	0	0	0	0.00	0	0	0	0	0	0	0
		180		0	0	0	0	0.00	0	0	0	0	0	0	0
		200		0	0	0	0	0.00	0	0	0	0	0	0	0
		220		0	0	0	0	0.00	0	0	0	0	0	0	0
		240		0	0	0	0	0.00	0	0	0	0	0	0	0
		260		0	0	0	0	0.00	0	0	0	0	0	0	0
		280		0	0	0	0	0.00	0	0	0	0	0	0	0

Table B-24

Fill Ratio (V/Vmax)	Angle (°C)	Time (min)	Heat Load (W)	Evaporator Temperature, (°C)				Average Evaporator Temperature (°C)	Condenser TipTemperature, (°C)		Average	Adiabatic Position Temperature(°C)		Average	Average Condenser Temperature (°C)
				T5	T6	T7	T8		T1	T2		T3	T4		
		0		118.9	107.5	116	106.3	112.18	34.3	34.5	34.4	34.8	36.6	35.7	35.05
		20		162.9	141.5	187.4	107	149.70	56.6	70.7	63.65	78.5	74.5	76.5	70.075
		40		141.8	183.1	187	155.3	166.80	64	72.1	68.05	78.9	73.6	76.25	72.15
		60		171.5	173.3	182.7	140.6	167.03	61.4	62.5	61.95	78.7	72.5	75.6	68.775
		80		135.5	180.2	187.1	140.9	160.93	60.6	59.3	59.95	77.8	71.8	74.8	67.375
		100		163.3	185.9	190.8	150.5	172.63	66.1	61.4	63.75	78.9	73.5	76.2	69.975
		120		163.1	193	192.2	150.9	174.80	63.4	62.1	62.75	79.5	73.2	76.35	69.55
60%	30	140	90	174.9	197.1	194.1	157.3	180.85	67.2	70.8	69	82.8	76.7	79.75	74.375
		160		185.3	204.1	197.1	128	178.63	73.3	84.5	78.9	85.1	79.1	82.1	80.5
		180		195	202.7	195.5	163.2	189.10	78.7	85.1	81.9	85.1	34.6	59.85	70.875
		200		0	0	0	0	0.00	0	0	0	0	0	0	0
		220		0	0	0	0	0.00	0	0	0	0	0	0	0
		240		0	0	0	0	0.00	0	0	0	0	0	0	0
		260		0	0	0	0	0.00	0	0	0	0	0	0	0
		280		0	0	0	0	0.00	0	0	0	0	0	0	0

Table B-25

Fill Ratio (V/Vmax)	Angle (°C)	Time (min)	Heat Load (W)	Evaporator Temperature, (°C)				Average Evaporator Temperature (°C)	Condenser TipTemperature, (°C)		Average	Adiabatic Position Temperature(°C)		Average	Average Condenser Temperature (°C)
				T5	T6	T7	T8		T1	T2		T3	T4		
60%	60	0	40	118.9	107.5	116	106.3	112.18	34.3	34.5	34.4	34.8	36.6	35.7	35.05
		20		162.9	141.5	187.4	107	149.70	56.6	70.7	63.65	78.5	74.5	76.5	70.075
		40		141.8	183.1	187	155.3	166.80	64	72.1	68.05	78.9	73.6	76.25	72.15
		60		171.5	173.3	182.7	140.6	167.03	61.4	62.5	61.95	78.7	72.5	75.6	68.775
		80		135.5	180.2	187.1	140.9	160.93	60.6	59.3	59.95	77.8	71.8	74.8	67.375
		100		163.3	185.9	190.8	150.5	172.63	66.1	61.4	63.75	78.9	73.5	76.2	69.975
		120		163.1	193	192.2	150.9	174.80	63.4	62.1	62.75	79.5	73.2	76.35	69.55
		140		174.9	197.1	194.1	157.3	180.85	67.2	70.8	69	82.8	76.7	79.75	74.375
		160		185.3	204.1	197.1	128	178.63	73.3	84.5	78.9	85.1	79.1	82.1	80.5
		180		195	202.7	195.5	163.2	189.10	78.7	85.1	81.9	85.1	34.6	59.85	70.875
		200		0	0	0	0	0.00	0	0	0	0	0	0	0
		220		0	0	0	0	0.00	0	0	0	0	0	0	0
		240		0	0	0	0	0.00	0	0	0	0	0	0	0
		260		0	0	0	0	0.00	0	0	0	0	0	0	0
		280		0	0	0	0	0.00	0	0	0	0	0	0	0

Table B-26

Fill Ratio (V/Vmax)	Angle (°C)	Time (min)	Heat Load (W)	Evaporator Temperature, (°C)				Average Evaporator Temperature (°C)	Condenser TipTemperature, (°C)		Average	Adiabatic Position Temperature(°C)		Average	Average Condenser Temperature (°C)
				T5	T6	T7	T8		T1	T2		T3	T4		
60%	60	0	50	99	103.2	97.3	91	97.63	31.8	32.1	31.95	34.4	34.4	34.4	33.175
		20		105.5	141.1	135.1	90.2	117.98	49.5	49	49.25	70.1	65.1	67.6	58.425
		40		103.5	134.8	134.3	124.4	124.25	52.8	51.7	52.25	70.5	68.1	69.3	60.775
		60		106.8	141.5	109.6	91.9	112.45	53.1	53.2	53.15	70.8	70.1	70.45	61.8
		80		104.8	138.5	108.8	128.8	120.23	52.2	52.4	52.3	71	70.1	70.55	61.425
		100		107.2	140	110.3	90.7	112.05	52.6	54.7	53.65	70.7	72.5	71.6	62.625
		120		137.2	141.8	113.2	90.8	120.75	51.6	55.5	53.55	72.4	71.4	71.9	62.725
		140		115.5	138.3	109.9	90.2	113.48	51.4	55.5	53.45	69.6	72.5	71.05	62.25
		160		135.1	141.8	110.9	92.4	120.05	51.4	54.3	52.85	72.8	71.1	71.95	62.4
		180		121.6	144.1	137.2	93.4	124.08	52.1	55.6	53.85	71.7	72.7	72.2	63.025
		200		135.1	146.5	112.9	94.8	122.33	53.6	56	54.8	71.8	73.8	72.8	63.8
		220		0	0	0	0	0.00	0	0	0	0	0	0	0
		240		0	0	0	0	0.00	0	0	0	0	0	0	0
		260		0	0	0	0	0.00	0	0	0	0	0	0	0
		280		0	0	0	0	0.00	0	0	0	0	0	0	0

Table B-27

Fill Ratio (V/Vmax)	Angle (°C)	Time (min)	Heat Load (W)	Evaporator Temperature, (°C)				Average Evaporator Temperature (°C)	Condenser TipTemperature, (°C)		Average	Adiabatic Position Temperature(°C)		Average	Average Condenser Temperature (°C)
				T5	T6	T7	T8		T1	T2		T3	T4		
60%	60	0	60	88.8	83.5	87.9	81	85.30	33.3	33.3	33.3	33.7	33.6	33.65	33.475
		20		114.7	131.3	160.9	92.6	124.88	52.7	51.2	51.95	72.9	64.4	68.65	60.3
		40		116.4	115.4	151	93.6	119.10	56.9	56.4	56.65	75.5	74	74.75	65.7
		60		122.5	119.3	155.3	99.6	124.18	54.5	52.5	53.5	74.1	69.9	72	62.75
		80		126.5	115.4	152.5	91.6	121.50	49.5	48.3	48.9	72.3	66.9	69.6	59.25
		100		139.1	136.4	150.6	90.7	129.20	50.6	49.4	50	72.3	68.6	70.45	60.225
		120		119.9	123.5	155.8	95.7	123.73	53.9	52.4	53.15	74.3	72.6	73.45	63.3
		140		121.4	126.2	155.1	94.7	124.35	55.1	51.2	53.15	73.5	67.2	70.35	61.75
		160		120.5	127.8	152.3	92.5	123.28	53.9	53.2	53.55	74.1	72.9	73.5	63.525
		180		112.4	131.7	152.4	91.3	121.95	54.5	52.9	53.7	74	72.1	73.05	63.375
		200		119.1	134	152.6	93.7	124.85	54.6	53.5	54.05	74.2	70.1	72.15	63.1
		220		115.9	147.1	158.3	96.1	129.35	57.4	54.2	55.8	74.4	72.8	73.6	64.7
		240		0	0	0	0	0.00	0	0	0	0	0	0	0
		260		0	0	0	0	0.00	0	0	0	0	0	0	0
		280		0	0	0	0	0.00	0	0	0	0	0	0	0

Table B-28

Fill Ratio (V/Vmax)	Angle (°C)	Time (min)	Heat Load (W)	Evaporator Temperature, (°C)				Average Evaporator Temperature (°C)	Condenser TipTemperature, (°C)		Average	Adiabatic Position Temperature(°C)		Average	Average Condenser Temperature (°C)
				T5	T6	T7	T8		T1	T2		T3	T4		
		0		30.8	31	30.9	30.8	30.88	30.8	30.8	30.8	30.8	30.9	30.85	30.825
		20		153.8	159.2	174.9	122	152.48	57.4	57.4	57.4	74.3	74.4	74.35	65.875
		40		168.3	154.1	159.3	101	145.68	58.6	61.7	60.15	74.9	75.7	75.3	67.725
		60		135.2	157.8	174.9	101	142.23	64.2	61.5	62.85	75.7	75.5	75.6	69.225
		80		153	154.2	169.8	129.5	151.63	56	60.3	58.15	75.7	72.9	74.3	66.225
		100		168.5	151	156	141.2	154.18	56.2	60.5	58.35	75.9	74.4	75.15	66.75
		120		160.5	171	174.2	138.1	160.95	58.6	59.8	59.2	76.4	72	74.2	66.7
60%	60	140	70	169.2	164	172.8	135.3	160.33	55.9	58.8	57.35	76.2	75.4	75.8	66.575
		160		139	169	172.1	130.9	152.75	58.7	60.5	59.6	76	75.5	75.75	67.675
		180		136.4	166	168.2	128.5	149.78	59.1	60	59.55	76.7	75.4	76.05	67.8
		200		144.2	161.7	166.4	127.1	149.85	56.1	57.9	57	74.5	74.4	74.45	65.725
		220		151.2	166	167.9	131.5	154.15	57	57.5	57.25	74.6	75.1	74.85	66.05
		240		158	165.2	168.8	114	151.50	56.6	57.6	57.1	75.9	71.7	73.8	65.45
		260		166.5	164.8	172	130.4	158.43	57	61.2	59.1	75.9	76	75.95	67.525
		280		0	0	0	0	0.00	0	0	0	0	0	0	0

Table B-29

Fill Ratio (V/Vmax)	Angle (°C)	Time (min)	Heat Load (W)	Evaporator Temperature, (°C)				Average Evaporator Temperature (°C)	Condenser TipTemperature, (°C)		Average	Adiabatic Position Temperature(°C)		Average	Average Condenser Temperature (°C)
				T5	T6	T7	T8		T1	T2		T3	T4		
		0		167.4	170.8	177	143.7	164.73	38.8	37	37.9	55.7	54	54.85	46.375
		20		170.1	174.4	172.3	102.8	154.90	55.1	59.3	57.2	74.8	75.6	75.2	66.2
		40		169.7	175.5	174.7	102.7	155.65	58.7	61.2	59.95	76.4	75.7	76.05	68
		60		123.6	172.1	179.6	132.2	151.88	66.3	59.7	63	77.1	74.1	75.6	69.3
		80		170.6	179	181.3	147.7	169.65	59.8	59.7	59.75	77.1	73.9	75.5	67.625
		100		165.9	170.8	175	138	162.43	57.2	59.7	58.45	76.8	75.3	76.05	67.25
		120		164.6	173.9	177.7	141.5	164.43	59.3	59.1	59.2	77.2	76.4	76.8	68
60%	60	140	80	158.4	168.7	174.9	129.9	157.98	58.5	59.1	58.8	76.9	76.2	76.55	67.675
		160		163.9	174	181	152.4	167.83	58.2	58.3	58.25	77.4	76.9	77.15	67.7
		180		158.7	176.9	181.8	140.6	164.50	57.7	60.1	58.9	77.4	77.2	77.3	68.1
		200		0	0	0	0	0.00	0	0	0	0	0	0	0
		220		0	0	0	0	0.00	0	0	0	0	0	0	0
		240		0	0	0	0	0.00	0	0	0	0	0	0	0
		260		0	0	0	0	0.00	0	0	0	0	0	0	0
		280		0	0	0	0	0.00	0	0	0	0	0	0	0

Table B-30

Fill Ratio (V/Vmax)	Angle (°C)	Time (min)	Heat Load (W)	Evaporator Temperature, (°C)				Average Evaporator Temperature (°C)	Condenser TipTemperature, (°C)		Average	Adiabatic Position Temperature(°C)		Average	Average Condenser Temperature (°C)
				T5	T6	T7	T8		T1	T2		T3	T4		
		0		124.4	146.6	158.2	125.2	138.60	30.8	30.7	30.75	34.7	35.3	35	32.875
		20		190.9	196.4	205.2	177.7	192.55	61.1	63.3	62.2	78.7	74.5	76.6	69.4
		40		191.9	199.5	206	169.6	191.75	67	69.1	68.05	81	80.1	80.55	74.3
		60		189.5	196.3	201.4	168.8	189.00	64	66.6	65.3	79.7	79.6	79.65	72.475
		80		196.2	199.5	208.7	170.1	193.63	64.1	64.4	64.25	79.7	78.9	79.3	71.775
		100		194.7	198.1	207	174.4	193.55	67.5	64.9	66.2	79.5	78.3	78.9	72.55
		120		193	199.9	205.5	175.2	193.40	64.8	65.5	65.15	79.9	79.4	79.65	72.4
60%	60	140	90	198.7	201.7	209.1	178.6	197.03	63.1	66.3	64.7	79.7	79.6	79.65	72.175
		160		197.6	200.1	205.9	171.3	193.73	62	66.2	64.1	79.5	79.1	79.3	71.7
		180		194.2	196.8	200.3	173.7	191.25	60.1	67.9	64	79	78.6	78.8	71.4
		200		192.3	194.4	197	169.2	188.23	57.1	67.7	62.4	78	77.1	77.55	69.975
		220		185.9	188.9	196.6	166.4	184.45	57.2	65.8	61.5	76.9	72.4	74.65	68.075
		240		188.5	194.9	201.6	170.4	188.85	58.8	62.3	60.55	77.6	77.2	77.4	68.975
		260		188.6	196.4	201.6	164.4	187.75	60.7	61.7	61.2	77.9	75.2	76.55	68.875
		280		0	0	0	0	0.00	0	0	0	0	0	0	0

Table B-31

Fill Ratio (V/Vmax)	Angle (°C)	Time (min)	Heat Load (W)	Evaporator Temperature, (°C)				Average Evaporator Temperature (°C)	Condenser TipTemperature, (°C)		Average	Adiabatic Position Temperature(°C)		Average	Average Condenser Temperature (°C)
				T5	T6	T7	T8		T1	T2		T3	T4		
		0		89.4	92.5	94.5	81.8	89.55	27.3	27.2	27.25	28.8	29.1	28.95	28.1
		20		112.4	115.4	117.4	108	113.30	34.5	34.9	34.7	46.3	45.9	46.1	40.4
		40		117.6	118.9	121.4	111.9	117.45	36.9	37.2	37.05	49.3	48.8	49.05	43.05
		60		114.4	117.7	119.9	110.8	115.70	36.5	36.8	36.65	49.2	48.6	48.9	42.775
		80		113	115.5	117.7	109.1	113.83	36.1	36.6	36.35	48.5	48.1	48.3	42.325
		100		113.8	116.6	119.2	110.1	114.93	36.5	36.6	36.55	49.1	48.4	48.75	42.65
		120		115.7	118	120.1	111	116.20	36.6	36.8	36.7	49.2	48.7	48.95	42.825
60%	90	140	40	114.5	117.8	120.1	111.3	115.93	36.8	36.8	36.8	49.2	48.6	48.9	42.85
		160		117.4	120.2	122.5	113	118.28	36.9	37.5	37.2	49.9	49.4	49.65	43.425
		180		116.3	118.9	121.6	112.8	117.40	36.5	36.9	36.7	49.6	49.1	49.35	43.025
		200		116.9	119.8	120.6	109.1	116.60	36.1	36.3	36.2	48.9	47.8	48.35	42.275
		220		0	0	0	0	0.00	0	0	0	0	0	0	0
		240		0	0	0	0	0.00	0	0	0	0	0	0	0
		260		0	0	0	0	0.00	0	0	0	0	0	0	0
		280		0	0	0	0	0.00	0	0	0	0	0	0	0

Table B-32

Fill Ratio (V/Vmax)	Angle (°C)	Time (min)	Heat Load (W)	Evaporator Temperature, (°C)				Average Evaporator Temperature (°C)	Condenser TipTemperature, (°C)		Average	Adiabatic Position Temperature(°C)		Average	Average Condenser Temperature (°C)
				T5	T6	T7	T8		T1	T2		T3	T4		
		0		113.7	117.1	119.3	107.4	114.38	28.9	28.9	28.9	35.6	35.5	35.55	32.225
		20		127.6	132.4	135	124.3	129.83	36.8	37.2	37	51.2	50.8	51	44
		40		129.3	132.9	136.6	125.1	130.98	37.9	38.5	38.2	52.7	52.2	52.45	45.325
		60		127.9	131.8	135.3	124	129.75	38.2	38.8	38.5	52.7	52.1	52.4	45.45
		80		126.2	131.1	133.6	119	127.48	35.1	35.9	35.5	50	49.3	49.65	42.575
		100		130.9	134.1	135	120.3	130.08	34.5	35.3	34.9	49.6	48.5	49.05	41.975
		120		132.1	134.5	136.5	122	131.28	36.1	36.8	36.45	51.6	50.6	51.1	43.775
60%	90	140	50	131.1	133.9	136.9	122.9	131.20	35.7	36.4	36.05	51.2	50.1	50.65	43.35
		160		131.6	134.1	136.4	122.8	131.23	36.8	37.1	36.95	52	51.1	51.55	44.25
		180		132.3	134.6	137.4	124.7	132.25	36.6	37.1	36.85	51.9	50.9	51.4	44.125
		200		131.1	133.1	136.2	122.9	130.83	36.5	37.1	36.8	51.9	51.1	51.5	44.15
		220		131.8	134.1	136.7	123.4	131.50	36.3	36.9	36.6	51.9	51	51.45	44.025
		240		0	0	0	0	0.00	0	0	0	0	0	0	0
		260		0	0	0	0	0.00	0	0	0	0	0	0	0
		280		0	0	0	0	0.00	0	0	0	0	0	0	0

Table B-33

Fill Ratio (V/Vmax)	Angle (°C)	Time (min)	Heat Load (W)	Evaporator Temperature, (°C)				Average Evaporator Temperature (°C)	Condenser TipTemperature, (°C)		Average	Adiabatic Position Temperature(°C)		Average	Average Condenser Temperature (°C)
				T5	T6	T7	T8		T1	T2		T3	T4		
		0		28.2	28.1	28.1	28.1	28.13	28	28	28	28.2	28	28.1	28.05
		20		146	148.8	151.5	140.3	146.65	36.3	37.2	36.75	53.3	52.5	52.9	44.825
		40		148.5	151.6	156	144.3	150.10	39.4	40	39.7	56.2	55.6	55.9	47.8
		60		147.8	150.7	154.4	142	148.73	39.2	39.8	39.5	56.3	55.6	55.95	47.725
		80		149.4	153.2	156.1	142.7	150.35	38	38.6	38.3	55.6	54.7	55.15	46.725
		100		147.3	150.8	154.6	142.9	148.90	39.2	39.6	39.4	56.5	55.7	56.1	47.75
		120		148.1	152.3	156.2	143.8	150.10	39.4	39.9	39.65	57	56.1	56.55	48.1
60%	90	140	60	147.6	149.8	152.7	137.6	146.93	38	39.1	38.55	56.1	55.3	55.7	47.125
		160		147.6	151.3	154.2	140.1	148.30	38.1	38.8	38.45	55.3	54.4	54.85	46.65
		180		150.5	154.3	158.5	145.8	152.28	39.1	39.8	39.45	56.9	56	56.45	47.95
		200		0	0	0	0	0.00	0	0	0	0	0	0	0
		220		0	0	0	0	0.00	0	0	0	0	0	0	0
		240		0	0	0	0	0.00	0	0	0	0	0	0	0
		260		0	0	0	0	0.00	0	0	0	0	0	0	0
		280		0	0	0	0	0.00	0	0	0	0	0	0	0

Table B-34

Fill Ratio (V/Vmax)	Angle (°C)	Time (min)	Heat Load (W)	Evaporator Temperature, (°C) T5	T6	T7	T8	Average Evaporator Temperature (°C)	Condenser TipTemperature, (°C) T1	T2	Average	Adiabatic Position Temperature(°C) T3	T4	Average	Average Condenser Temperature (°C)
60%	90	0	70	158.5	159	162.9	148	157.10	33.2	33.7	33.45	50.6	48.7	49.65	41.55
		20		157.8	162	166.7	149.7	159.05	36.3	37.1	36.7	55.3	54.3	54.8	45.75
		40		166.7	168.6	174	159	167.08	39	39.4	39.2	58.6	57.6	58.1	48.65
		60		167.2	171.3	176.5	162.9	169.48	39.6	40.1	39.85	59.3	58.4	58.85	49.35
		80		167.8	171	176.2	162.8	169.45	40.3	40.8	40.55	59.8	59	59.4	49.975
		100		169.3	170.9	175.5	162.3	169.50	41	41.4	41.2	60.6	59.7	60.15	50.675
		120		166.1	169.2	174.1	158.2	166.90	39.2	39.8	39.5	58.8	57.9	58.35	48.925
		140		168.9	171.9	177.5	163.9	170.55	40.8	41.3	41.05	60.5	59.7	60.1	50.575
		160		166.4	169.6	175.3	162.2	168.38	40.6	41.2	40.9	60.5	59.6	60.05	50.475
		180		167	170.7	175.5	161.2	168.60	40.3	40.7	40.5	59.6	58.8	59.2	49.85
		200		166.6	169.4	174.9	159.7	167.65	40	40.6	40.3	60.1	59.1	59.6	49.95
		220		170	173.5	178.4	163.9	171.45	40.4	41	40.7	60.2	59.2	59.7	50.2
		240		165.7	169.7	174.6	160.1	167.53	38.8	39.5	39.15	59.2	58.3	58.75	48.95
		260		0	0	0	0	0.00	0	0	0	0	0	0	0
		280		0	0	0	0	0.00	0	0	0	0	0	0	0

Table B-35

Fill Ratio (V/Vmax)	Angle (°C)	Time (min)	Heat Load (W)	Evaporator Temperature, (°C) T5	T6	T7	T8	Average Evaporator Temperature (°C)	Condenser TipTemperature, (°C) T1	T2	Average	Adiabatic Position Temperature(°C) T3	T4	Average	Average Condenser Temperature (°C)
60%	90	0	80	170.7	168.8	174.7	158.8	168.25	30	30.2	30.1	44.4	44.2	44.3	37.2
		20		184.8	186.2	191.8	177.2	185.00	40.2	40.8	40.5	61.6	61	61.3	50.9
		40		185.1	185.5	191.5	176.7	184.70	41.3	42.2	41.75	63.3	62.4	62.85	52.3
		60		183.8	186.1	192	176.9	184.70	41.4	41.8	41.6	63.4	62.6	63	52.3
		80		185.2	185.6	190.9	176.5	184.55	41.9	42.4	42.15	63.8	62.6	63.2	52.675
		100		182.1	184.7	191.1	177	183.73	41.8	42.3	42.05	63.5	62.4	62.95	52.5
		120		187.1	188.6	194.4	179.6	187.43	41.9	42.2	42.05	64	63	63.5	52.775
		140		182	186	192.6	178.7	184.83	42	42.8	42.4	63.7	62.9	63.3	52.85
		160		186.7	188	191.4	174.1	185.05	41.5	41.4	41.45	64.1	62.6	63.35	52.4
		180		192.2	194.2	196	177.8	190.05	42.5	41.3	41.9	64.4	62.9	63.65	52.775
		200		186.4	189.8	192.2	174.5	185.73	42.3	41.1	41.7	64.1	62.5	63.3	52.5
		220		192.5	188.7	193.2	174.7	187.28	42	41.5	41.75	64.2	62.7	63.45	52.6
		240		191.8	195.7	198.9	181.4	191.95	42.2	41.6	41.9	64.5	63.1	63.8	52.85
		260		0	0	0	0	0.00	0	0	0	0	0	0	0
		280		0	0	0	0	0.00	0	0	0	0	0	0	0

Table B-36

Fill Ratio (V/Vmax)	Angle (°C)	Time (min)	Heat Load (W)	Evaporator Temperature, (°C) T5	T6	T7	T8	Average Evaporator Temperature (°C)	Condenser TipTemperature, (°C) T1	T2	Average	Adiabatic Position Temperature(°C) T3	T4	Average	Average Condenser Temperature (°C)
60%	90	0	90	196.4	200.5	209.2	192.6	199.68	42	43	42.5	66.1	65.6	65.85	54.175
		20		198.9	203.6	211.8	194.6	202.23	42.7	43.7	43.2	67	66.4	66.7	54.95
		40		197.8	201.1	208.8	190.9	199.65	42.8	44.1	43.45	67.3	66.7	67	55.225
		60		195.5	200.1	208.2	192	198.95	42.9	43.9	43.4	67	66.3	66.65	55.025
		80		193.4	202.7	211.4	194.8	200.58	43	44.4	43.7	68	67.5	67.75	55.725
		100		199.2	203.3	212.5	196.2	202.80	43.5	44.2	43.85	67.8	67.1	67.45	55.65
		120		201.3	205.6	213.2	195.9	204.00	43.6	44.3	43.95	68.4	67.7	68.05	56
		140		199.9	204	212.4	195.5	202.95	43.7	44.6	44.15	68.3	67.6	67.95	56.05
		160		204	207.5	215.8	198.7	206.50	44.2	44.6	44.4	68.8	68.1	68.45	56.425
		180		205	209.1	217	199.9	207.75	44.4	45	44.7	69.5	68.8	69.15	56.925
		200		0	0	0	0	0.00	0	0	0	0	0	0	0
		220		0	0	0	0	0.00	0	0	0	0	0	0	0
		240		0	0	0	0	0.00	0	0	0	0	0	0	0
		260		0	0	0	0	0.00	0	0	0	0	0	0	0
		280		0	0	0	0	0.00	0	0	0	0	0	0	0

APPENDIX-C

Uncertainty Analysis

Propagation of uncertainty analysis have followed the process described by John M. Cimbala from Penn State University in the year 2013.
If there are N number of physical variables expressed as x_1, x_2, x_3, x_4, ……,x_N etc. Individual variables are having experimental uncertainties associated with them known as component uncertainties, $x_i = \overline{x_i} \pm u_{x_i}$. Generally, each of these uncertainties have 95% confidence level. Let us consider a new variable R, which is a function of these measured quantities as, R=R(x_1, x_2, x_3, x_4, ……,x_N). The ultimate mission of this analyzation should be achieving the uncertainty of R to the same confidence level as 95%. Expressing R in terms of predicted uncertainty, $R = \bar{R} \pm u_R$. Now there will be two types of uncertainty on R as,

i. Maximum Uncertainty, $U_{R,\,max} = \sum_{i=1}^{i=N} u_{x_i} \frac{\partial R}{\partial x_i}$

ii. Expected Uncertainty, $U_{R,RSS} = \sqrt{(\sum_{i=1}^{i=N} u_{x_i} \frac{\partial R}{\partial x_i})^2}$

For the case of combining repeating elements, uncertainty will be calculated as the combination of bias (system) and precision (random) uncertainties. The overall uncertainty will have 95% confidence level and express as,

$$U_x = \sqrt{(U)^2 + (U_{random})^2}$$

For this research, the uncertainty propagation of input heat load and thermocouple readings will be analyzed in the following segments using the process discussed above. For the heat input load, maximum and expected uncertainties have been calculated having 95% confidence. The thermocouple readings are the repeating constants. That's why, these readings will find the uncertainty propagation of a combination of systematic and random uncertainties along with 95% confidence level.

1. Electrical Power Uncertainty

Uncertainty propagation analysis has been carried out for 60 W heat input.
Electric Power, P = VI = 38 × 1.59 W= 60W
Here, V =38 ± u_v = 38 ± 1 V
I = 1.59 ± 0.01 A = 1.59 ± 0.01 A
Maximum Uncertainty, $U_{R,max} = \sum_{i=1}^{i=N} u_{x_i} \frac{\partial R}{\partial x_i} = \left|u_V \frac{\partial P}{\partial V}\right| + \left|u_I \frac{\partial P}{\partial I}\right| = |u_V I| + |u_I V| =$ $|\pm 1 \times 1.59| + |\pm 0.01 \times 38|$= 1.970 W
Now, Root of the Sum of the Squares Uncertainty or Expected Uncertainty,
$u_{R,RSS} = \sqrt{(\sum_{i=1}^{i=N} u_{x_i} \frac{\partial R}{\partial x_i})^2} = \sqrt{\left|u_V \frac{\partial P}{\partial V}\right|^2 + \left|u_I \frac{\partial P}{\partial I}\right|^2} = \sqrt{|u_V I|^2 + |u_I V|^2} =$ $\sqrt{|\pm 1 \times 1.59|^2 + |0.01 \times 38|^2}$ = 1.635 W
Thus, the Electric Power input = 60 ± 1.635 W

2. Thermocouple Readings Uncertainty

For 60W input load and six different orientation angles, the uncertainty analysis of three section as evaporator, adiabatic and condenser have been carried out. Error from the manufacturer is also given as a fixed value. According to the convention, the error should be expressed considering three digits after decimal. The final error calculations are shown in the following paragraphs.

a) Evaporator Section Temperature Reading Uncertainty

After reaching steady state condition,

Thermocouple Readings, ˚C				Average of T1 to T4	Average of All 2639 Readings	Standard Deviation σ	Average σ	Umeasurement	RSS_U_N
T1	T2	T3	T4						
117	155.2	119.8	98.2	122.55	120.961332983	0.000602110	0.000907438	0.001814877	1.200001372
117	155.2	119.8	98.2	122.55		0.000602110			
116.6	154.9	120.2	98.2	122.475		0.000573685			
---	---	---	---	---	---	---	---	---	---
---	---	---	---	---	---	---	---	---	---
110.8	119.7	117.9	94.5	110.725		0.003879603			
110.8	117.8	117.5	94.5	110.15		0.004097530			
110.8	117.8	117.5	94.5	110.15		0.004097530			
110.8	115.8	116.9	94.5	109.5		0.004343882			
110.8	115.8	116.9	94.5	109.5		0.004343882			
110.5	114.5	116.9	94.5	109.1		0.004495483			
110.5	114.5	116.9	94.4	109.075		0.004504959			

Measurement Uncertainty of 95% confidence, $U_{measurement} = \pm 2 *$0.000907438˚C = 0.001814877

Manufactures Uncertainty, $U_{manufacture} = \pm 1.2$ ˚C

Root of the Sum of the Squares Uncertainty (RSS), $U_N = \sqrt{\sum_{i=1}^{i=K} u_i^2} = \sqrt{U_{measurement}^2 + U_{manufacture}^2}$ = 1.200002415 ˚C ≈ 1.2 ˚C

Thus, the Evaporator Section average temperature will be 120.961 ± 1.2 ˚C

b) <u>Adiabatic Section Temperature Reading Uncertainty</u>

After reaching steady state condition,

Thermocouple Readings, ˚C		Average of T3 to T4	Average of All 2639 Readings	Standard Deviation σ	Average σ	Umeasurement	RSS_U_N
T3	T4						
82	79.2	80.6	80.48644633	0.000043037	0.000102938	0.000205875	1.200000018
82	79.2	80.6		0.000043037			
82	79.2	80.6		0.000043037			
---	---	---	---	---	---	---	---
---	---	---	---	---	---	---	---
80.7	74.8	77.75		0.001037122			
80.7	74.8	77.75		0.001037122			
80.5	74.8	77.65		0.001075022			
80.5	74.7	77.6		0.001093972			
80.5	74.7	77.6		0.001093972			
80.5	74.5	77.5		0.001131873			
80.5	74.5	77.5		0.001131873			

Measurement Uncertainty of 95% confidence, $U_{measurement} = \pm 2$ ∗0.000102938˚C = 0.000205875

Manufactures Uncertainty, $U = \pm 1.2$ ˚C

Root of the Sum of the Squares Uncertainty (RSS), $U_N = \sqrt{\sum_{i=1}^{i=K} u_i^2}$ = $\sqrt{U_{measurement}^2 + U_{manufacture}^2}$ = 1.200000018˚C ≈ 1.2 ˚C

Thus, the Adiabatic Section average temperature will be 80.486 ± 1.2 ˚C

c) <u>Condenser Section Temperature Reading Uncertainty</u>

After reaching steady state condition,

Thermocouple Readings, ˚C		Average of T1 to T2	Average of All 2639 Readings	Standard Deviation σ	Average σ	Umeasurement	RSS_U_N
T1	T2						
76.1	81.6	78.85	77.74610818	0.000418379	0.000285013	0.000570026	1.200000135
76.1	81.8	78.95		0.000456279			
76.1	81.8	78.95		0.000456279			
---	---	---	---	---	---	---	---
---	---	---	---	---	---	---	---
72.4	80.2	76.3		0.00054808			
72.4	80.2	76.3		0.00054808			
71.3	80	75.65		0.000794432			
71.3	80	75.65		0.000794432			
70.8	80.1	75.45		0.000870232			
70.8	80.1	75.45		0.000870232			
71.6	80.1	75.85		0.000718631			

Measurement Uncertainty of 95% confidence, $U_{measurement} = \pm 2 *$0.000285013˚C = 0.000570026
Manufactures Uncertainty, $U_{manufacture} = \pm 1.2$ ˚C

Root of the Sum of the Squares Uncertainty (RSS), $U_N = \sqrt{\sum_{i=1}^{i=K} u_i^2}$ = $\sqrt{U_{measurement}^2 + U_{manufacture}^2}$ = 1.200000135 ˚C ≈ 1.2 ˚C

Thus, the Condenser Section average temperature will be 77.746 ± 1.2 ˚C

Appendix-D

Linear Regression for Mathematical Modeling from Dimensionless Groups

Table D-1 Data Table from Dimensionless Groups

B_0	We	C_0	Re	Kl	U	Nu_Experimental	U_Predicted	U_Experimental	AE
9.18E-07	20756.16	1.55915	234	0.187163	325.3826	3.476995963	413.3119337	325.3825705	27%
1.19E-06	21711.29	1.530135	234	0.185699	352.578	3.797311851	242.9350085	352.5779696	-31%
1.42E-06	12288.11	1.526158	234	0.185531	403.7048	4.351874679	380.7103597	403.7047947	-6%
1.54E-06	13444.13	1.465837	234	0.179802	492.1317	5.474157302	421.1545508	492.1317415	-14%
1.17E-06	27626.63	1.390885	234	0.17435	376.2561	4.316090222	475.2542876	376.2560668	26%
1.1E-06	25491.05	1.426876	234	0.176379	588.3302	6.671214071	497.4068439	588.3301903	-15%
9.42E-07	21411.93	1.538857	234	0.186073	323.2147	3.474056749	433.9017022	323.2147414	34%
9.49E-07	21612.58	1.532977	234	0.18582	371.0027	3.993149733	439.663048	371.0027354	19%
1.44E-06	12497.32	1.515795	234	0.184962	385.444	4.167826659	389.9328771	385.4439576	1%
1.65E-06	14592.84	1.425319	234	0.176906	335.7932	3.79629165	415.2855525	335.793153	24%
1.01E-06	23156.14	1.485532	234	0.181679	614.9894	6.770062932	477.914762	614.9893722	-22%
1.1E-06	25694.21	1.427122	234	0.176756	486.9881	5.510297777	487.1815807	486.9880981	0%
9.23E-07	20866.74	1.555577	234	0.186823	378.36	4.050467058	416.5812946	378.3599896	10%
9.43E-07	21411.34	1.538563	234	0.185971	421.5716	4.533735634	434.2687771	421.5715596	3%
1.49E-06	12892.17	1.491536	234	0.182254	487.309	5.34758296	408.9228218	487.3090174	-16%
1.52E-06	13331.28	1.478476	234	0.181467	352.5205	3.885218984	406.4781692	352.5204647	15%
1.06E-06	24537.75	1.451108	117	0.178521	506.5522	5.674980494	424.1451809	506.5521587	-16%
1.83E-06	16493.98	1.363387	93.6	0.172868	391.6543	4.531253469	319.2163266	391.6542616	-18%
1.37E-06	11666.35	1.55949	58.5	0.187199	299.6646	3.201563552	241.9089149	299.6646094	-19%
1.41E-06	12138.22	1.533782	58.5	0.185854	375.1999	4.037576381	269.1276642	375.1999279	-28%
1.45E-06	12540.02	1.513973	58.5	0.184796	363.1943	3.930754038	287.2589302	363.1943164	-21%
1.72E-06	15373.39	1.407055	58.5	0.176417	266.6097	3.02250162	294.8044989	266.6096906	11%
1.57E-06	13722.98	1.455946	58.5	0.179052	476.3793	5.321127298	321.8980169	476.3793137	-32%
1.93E-06	17957.19	1.336787	58.5	0.172406	274.2232	3.18113958	251.0833465	274.2231735	-8%
1.4E-06	12065.69	1.537557	58.5	0.186017	227.9013	2.450329414	265.1647453	227.9012872	16%
1.45E-06	12600.97	1.511165	58.5	0.184526	252.8709	2.740756873	288.702176	252.8709241	14%
1.5E-06	13052.53	1.491261	58.5	0.182685	311.4691	3.409897178	298.1218908	311.4690564	-4%
1.67E-06	14852.15	1.425642	58.5	0.17776	265.1757	2.983529858	297.3352948	265.1756742	12%
1.84E-06	16912.64	1.371605	58.5	0.175217	255.1975	2.912926578	257.0984756	255.1974553	1%
1.88E-06	17505.79	1.358366	58.5	0.174609	257.7756	2.952603811	241.4682155	257.7756464	-6%
1.43E-06	12407.12	1.520271	58.5	0.185288	184.2849	1.989174731	282.9284447	184.2849254	54%
1.5E-06	13041.14	1.491819	58.5	0.182741	197.4592	2.161081863	297.7789759	197.459204	51%
1.64E-06	14573.12	1.436355	58.5	0.178632	192.5384	2.155703347	296.3823652	192.5384042	54%
1.75E-06	15845.6	1.400464	58.5	0.176812	201.7216	2.281765468	273.7058074	201.7216205	36%
1.87E-06	17438.02	1.363563	58.5	0.175244	200.7901	2.291550725	236.1450446	200.7901279	18%
1.92E-06	18003.91	1.352468	58.5	0.174782	202.7841	2.320419574	216.5818025	202.7840808	7%

Table D-2 Predicted Nu Number and Its Residuals from Developed Equation

Observation	*Predicted Nu*	*Residuals*
1	4.416597737	-0.939601774
2	2.616442507	1.180869344
3	4.103998258	0.247876421
4	4.684652635	0.789504667
5	5.451713779	-1.135623556
6	5.640212913	1.031001158
7	4.66376976	-1.189713011
8	4.732149429	-0.738999696
9	4.216365592	-0.048538932
10	4.694988749	-0.898697099
11	5.261087689	1.508975243
12	5.512487043	-0.002189266
13	4.459638589	-0.409171532
14	4.670286182	-0.136550548
15	4.487396366	0.860186594
16	4.479900765	-0.594681781
17	4.75176265	0.923217844
18	3.693181025	0.838072444
19	2.584511953	0.6170516
20	2.896118628	1.141457753
21	3.108925852	0.821828186
22	3.342140616	-0.319638997
23	3.595580823	1.725546475
24	2.912704864	0.268434716
25	2.85097545	-0.400646037
26	3.129116073	-0.388359201
27	3.26377524	0.146121939
28	3.345362401	-0.361832543
29	2.93462559	-0.021699013
30	2.765815869	0.186787942
31	3.053934616	-1.064759885
32	3.259026324	-1.097944462
33	3.318363727	-1.16266038
34	3.096011514	-0.814246046
35	2.69504459	-0.403493866
36	2.478304273	-0.157884699

Table D-3 Data Table for Dimensionless Physical Parameters

U, W/m2°C	**U/U_max**	**q/q_max**	**(T_Eva-T_a)/T_Eva**	**$1+\theta/\theta$_max**	*Predicted U/U_max*	*Residuals*	*AE*
325.382571	0.529086	0.444444	0.651992	1	0.687568064	-0.15848	-30%
352.57797	0.573307	0.555556	0.702582	1	0.606153474	-0.03285	-6%
403.704795	0.656442	0.666667	0.707919	1	0.724515289	-0.06807	-10%
492.131741	0.800228	0.777778	0.749154	1	0.68440099	0.115827	14%
376.256067	0.611809	0.888889	0.794501	1	0.626130139	-0.01432	-2%
588.33019	0.956651	1	0.770914	1	0.872184254	0.084467	9%
323.214741	0.525561	0.444444	0.689889	1.111111111	0.504074651	0.021487	4%
371.002735	0.603267	0.555556	0.698602	1.111111111	0.607535297	-0.00427	-1%
385.443958	0.626749	0.666667	0.720265	1.111111111	0.653823577	-0.02707	-4%
335.793153	0.546015	0.777778	0.781808	1.111111111	0.524051378	0.021963	4%
614.989372	1	0.888889	0.734081	1.111111111	0.876678556	0.123321	12%
486.988098	0.791864	1	0.776925	1.111111111	0.829459651	-0.0376	-5%
378.35999	0.61523	0.444444	0.660942	1.222222222	0.61567875	-0.00045	0%
421.57156	0.685494	0.555556	0.688557	1.222222222	0.635690937	0.049803	7%
487.309017	0.792386	0.666667	0.728031	1.222222222	0.603351233	0.189035	24%
352.520465	0.573214	0.777778	0.755265	1.222222222	0.625041066	-0.05183	-9%
506.552159	0.823676	0.888889	0.760522	1.222222222	0.743760659	0.079916	10%
391.654262	0.636847	1	0.804543	1.222222222	0.69134282	-0.0545	-9%
299.664609	0.487268	0.444444	0.651076	1.333333333	0.643048274	-0.15578	-32%
375.199928	0.610092	0.555556	0.697448	1.333333333	0.58024916	0.029843	5%
363.194316	0.59057	0.666667	0.723046	1.333333333	0.609168291	-0.0186	-3%
266.609691	0.433519	0.777778	0.796195	1.333333333	0.428159526	0.00536	1%
476.379314	0.774614	0.888889	0.760283	1.333333333	0.728624685	0.045989	6%
274.223174	0.445899	1	0.830587	1.333333333	0.560176296	-0.11428	-26%
227.901287	0.370578	0.444444	0.691873	1.666666667	0.41437051	-0.04379	-12%
252.870924	0.411179	0.555556	0.726352	1.666666667	0.404080362	0.007099	2%
311.469056	0.506462	0.666667	0.74672	1.666666667	0.456086868	0.050376	10%
265.175674	0.431187	0.777778	0.790335	1.666666667	0.405460667	0.025727	6%
255.197455	0.414962	0.888889	0.811459	1.666666667	0.454129889	-0.03917	-9%
257.775646	0.419155	1	0.824226	1.666666667	0.539693377	-0.12054	-29%
184.284925	0.299655	0.444444	0.715359	2	0.262118536	0.037537	13%
197.459204	0.321077	0.555556	0.746377	2	0.267107742	0.05397	17%
192.538404	0.313076	0.666667	0.786566	2	0.231606463	0.08147	26%
201.721621	0.328008	0.777778	0.802937	2	0.301259758	0.026749	8%
200.790128	0.326494	0.888889	0.824446	2	0.348228012	-0.02173	-7%
202.784081	0.329736	1	0.841163	2	0.416350132	-0.08661	-26%

APPENDIX-E

Sample Calculations

Chen Correlation:

For 60W Filling ratio and 20 Degree inclination:
Given,

Locations	**Tsat**	**Prl**	**Kl**	**Cpl**	**ρl**	**ρv**	**µl**	**µv**	**σ**	**hfg**	**Psat_Fluid**	**Psat_Wall**	**ΔP**	**ΔT**	**D**	**X**
Evaporator	121.337	3.238	0.177	3418.551	685.483	7.657	0.000168	0.00001	0.013445	961539.1	677080.5	687580.44	10500	0.5	0.002	0.5
Condenser	79.515	3.123	0.187	2972.189	732.696	2.344	0.000181	0.00001	0.017461	1068433.9	201991.6	205366.16	3374.61	0.5	0.002	0.1

For Evaporator Section,

	Rel	**hl**	**Xtt**	**F**	**ReTP**	**S**	**Hf-z**	**HTP**
For Main Forward	200	226.099698	0.136338245	10.4025399	3736.407487	0.963137869	628.477696	2957.3218
For Side Forward	34	54.78467876	0.136338245	10.4025399	635.1892728	0.995208941	628.477696	1195.366429

For Condenser Section,

	Rel	hl	Xtt	F	ReTP	S	Hf-z	HTP
For Main Forward	200	235.3473587	0.537631007	4.018710884	1137.99001	0.990566214	302.4162501	1245.356312
For Side Forward	34	57.02541646	0.537631007	4.018710884	193.4583017	0.998803513	302.4162501	531.223075

Now for Evaporator Section forward flow,
$h_{tp} = 2957.3218 + 1195.366429 = 2962.811116$
Now for Condenser Section forward flow,
$h_{tp} = 1245.356312 + 531.223075 = 2060.715691$
There are total eight channel, So,
Overall Heat Transfer Coefficient, U= $(2962.811116 + 2060.715691)/8$ = 313.970 W/m^{2}°C
Absolute Error = $\left|\frac{U_{exp}-U}{U_{exp}}\right|$ % = $\left|\frac{487.309-313.970}{487.309}\right| = 24\%$